NOAA Technical Memorandum ERL NSSL-91

1980 SPRING PROGRAM SUMMARY

R. J. Doviak, Editor

Contributors:

W. Bumgarner
J. Carter
R. Davies-Jones
J. Dooley
S. Fredrickson
J. Lee
M. Maier
V. Mazur
S. Nelson
R. Rabin
D. Rust
L. Showell
D. Sirmans
B. Taylor
J. Weaver
D. Zrnic'

National Severe Storms Laboratory
Norman, Oklahoma
April 1981

UNITED STATES DEPARTMENT OF COMMERCE
Malcolm Baldrige, Secretary

NATIONAL OCEANIC AND ATMOSPHERIC ADMINISTRATION
James P. Walsh, Acting Administrator

Environmental Research Laboratories
Joseph O. Fletcher, Acting Director

NOTICE

The Environmental Research Laboratories do not approve, recommend, or endorse any proprietary product or proprietary material mentioned in this publication. No reference shall be made to the Environmental Research Laboratories or to this publication furnished by the Environmental Research Laboratories in any advertising or sales promotion which would indicate or imply that the Environmental Research Laboratories approve, recommend, or endorse any proprietary product or proprietary material mentioned herein, or which has as its purpose an intent to cause directly or indirectly the advertised product to be used or purchased because of this Environmental Research Laboratories publication.

TABLE OF CONTENTS

LIST OF SYMBOLS AND ABBREVIATIONS

ACCAS	Altocumulus Castellanus
ADC	Areas of Deeper Convection, also Analog-to-Digital Converter
AFB	Air Force Base
AGC	Automatic Gain Control
ΔAZ	Angular Distance Between Radials of Weather Radar Data
AZ	Azimuth Angle
BLM	Boundary Layer Model
CB	Citizen's Band
CDP	Computer and Data Processing Group
CG	Cloud to Ground
CNRZ	Recording Format for SAM System
CPU	Central Processing Unit
CRO	Coordinator of Radar Operators
CST	Central Standard Time
DI	Digital Integrator
DF	Direction Finders
DOD	Department of Defense
DR	Direct Record
ΔEL	Increment in Elevation
EL	Elevation Angle
ELmax	Maximum Elevation
ERT	Environmental Research and Technology, Inc.
FA	Fast Antenna for Electric Field Change Measurements
FAA	Federal Aviation Administration
F-106	Jet Aircraft used for Turbulence and Lightning Studies
ips	Inches Per Second
I	In-Phase Component of Complex Doppler Video
IRIG	Inter-Range Instrumentation Group used for Coding Time
LLWSAS	Low Level Wind Shear Alert System
M	PPP Sample Number
MEL	Mobile Electric Laboratory
MIT	Massachusetts Institute of Technology
MSL	Mean Sea Level
NASA	National Aeronautics and Space Administration
NCAR	National Center for Atmospheric Research
NHEML	National Hurricane and Experimental Meteorology Laboratory
NOSL	Nighttime/Daytime Optical Survey of Lightning
NRC	Nuclear Regulatory Commission
NRO	Doppler Radar at NSSL
NSSL	National Severe Storms Laboratory
N_s	Number of Time Series Samples Per Second
NWS	National Weather Service
ONR	Office of Naval Research
PA	Position Analyzer
PBL	Planetary Boundary Layer
PC	Program Coordinator
PPP	Pulse Pair Processor
PRF	Pulse Repetition Frequency
PRT	Pulse Repetition Time
Q	Quadrature Phase Component of Complex Doppler Video
R	Range
RAOB	Rawinsonde Observations

RHI	Range Height Indicator
SA	Slow Antenna for Electric Field Change
SAM	Stationary Automated Mesonetwork
SE	Storm Electricity
SEB	Storm Electricity Building
SWIMS	Surface Wind Monitoring System
T-28	Single engine propeller driven aircraft, armored for penetration of hailshafts
TAS	True Air Speed
TC	Time Constant of Digital Integrator
THI	Time Height Indicator
TIP	Tornado Intercept Project
TVS	Tornado Vortex Signature
U-2	High Altitude Jet Aircraft
VHF	Very High Frequency (20-80 Megahertz)
VHS	A Video Recording Format
Z	Radar Reflectivity Factor
Ω	Antenna rotation rate
ΔE	Electrostatic Field Change
τ_p	Measured Time Delay
τ_r	Total Radar Delay

1980 SPRING PROGRAM SUMMARY

1. INTRODUCTION

This program summary serves to inform data analysts, both inside and outside of NSSL, on experiments conducted, procedures used, and the date of experiments performed at NSSL during the 1980 spring observing period. Researchers interested in data sets for analysis and in specifics on the quality of each data set may contact J. T. Dooley, Data Dissemination Coordinator at NSSL, or the principal investigator of the experiment of interest. This summary records all experiment objectives with the procedures used to initiate and conduct experiments, and gives highlights of data collection.

The 1980 Spring Observation Program was substantially reduced from the SESAME program hosted by NSSL the previous year. Principal objectives of the 1980 observations were 1) to emphasize coordination of storm electricity measurements made by the recently formed Storm Electricity Group at NSSL, 2) to observe the prestorm environment with NSSL's Doppler radars modified for this purpose, 3) to support data collection for FAA and NASA experiments on storm hazards to aircraft, and 4) to support the hail collection experiment. Furthermore, severe thunderstorms of tornadic potential within the NSSL dual Doppler network are uncommon, and data collection in such events is always warranted. As a matter of fact, we have no dual Doppler data on tornadic storms since 1977.

Although the 1980 program was principally an in-house effort, it was nevertheless attractive to others who participated with their own equipment and support. The University of Oklahoma performed experiments for lightning echo studies using a recently installed 23-cm radar, and NASA flew an instrumented F106 jet aircraft to measure turbulence and storm electricity. Under FAA auspices, MIT's Lincoln Laboratory arranged to have South Dakota School of Mines and Technology fly its armored T-28 in thunderstorms so that researchers at Lincoln Lab and NSSL could obtain additional data for comparison of measurements of turbulence made in situ and remotely with NSSL's Doppler radars. NCAR arranged to have one of its hail collection vehicles and personnel to sample hail fall. Researchers from Purdue University were here to measure corona, and from the State University of New York at Albany and New Mexico Institute of Mining and Technology to measure optical emissions from lightning. The University of Mississippi participated by making in situ electrical measurements near tornado cyclones, and an investigator from the National Hurricane and Experimental Meteorology Laboratory in Miami operated lightning ground strike location equipment. The program was partially supported by the FAA, NASA, ONR, and NRC.

The program involved about 25 of NSSL's staff, and cost about $95,000 in addition to employee salaries; this sum may be compared with the $875,000 cost for the 1979 SESAME program. Eighteen experiments were planned in 1980, and all were attempted.

Figure 1.1 diagrams the equipment utilized during the 1980 observational period which extended from 15 April to 19 June. Figure 1.2 shows the location of the fixed surface observing network. There are three radars at NSSL in Norman, Oklahoma (NRO Doppler; WSR-57 and a 23-cm lightning echo radar); the nearby storm electricity building houses sensors for the electric field and other parameters, and a VHF lightning mapper. The second Doppler radar (CIM Doppler) and VHF mapper are located at Page Airfield (formerly Cimarron Airport) 40 km to the northwest of NSSL. The rawinsonde network was composed of 4 sites within commuting distance

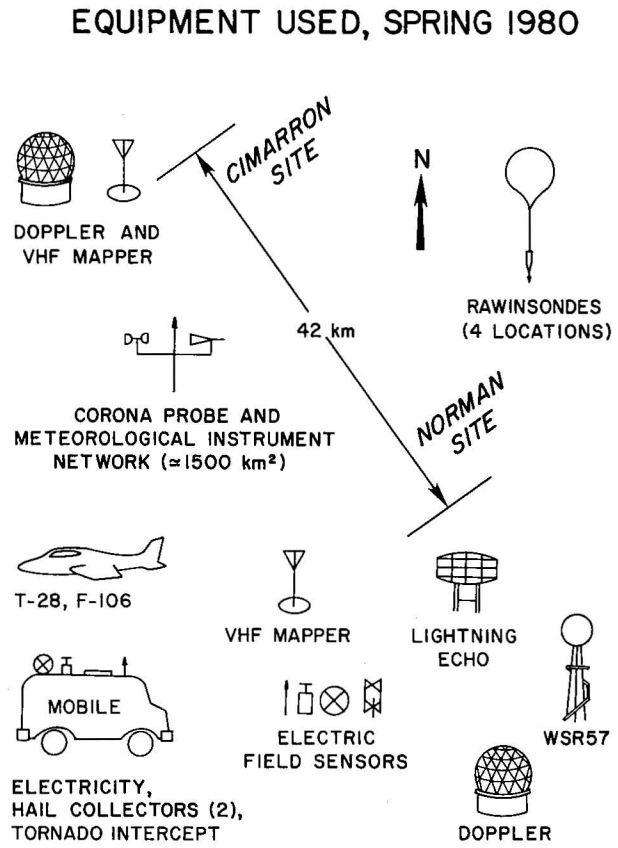

Figure 1.1 Equipment used.

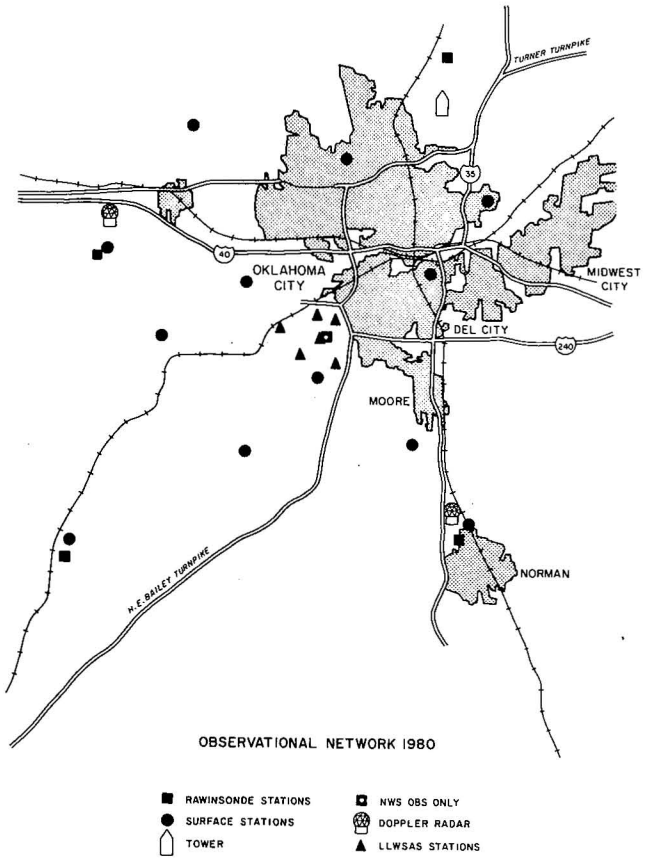

Figure 1.2 Location of surface instrumentation.

from Tinker AFB in order to minimize operational costs, but still provide soundings in gust fronts. These stations were manned by the U.S. Air Force Sixth Weather Squadron (Mobile) which kindly provided data at no cost to the program. The surface network, also deployed over a limited area (Fig. 1.2) to cut costs, consisted of 12 stations within commuting distance of NSSL. With the help of NWS and its cooperative observers, NSSL hygrothermographs recorded temperature and relative humidity at six sites around central Oklahoma. In addition, we recorded wind data at six LLWSAS stations maintained by the FAA for detection of wind shift lines along the approach path of aircraft flying into Will Rogers World Airport. The KTVY television tower was also instrumented by NSSL at seven levels.

Although there were abundant spring rains, Oklahoma had an unusually low incidence of severe weather. However, on six occasions (May 1, 11, 17-18, 29, and June 16 and 19) we did obtain data on severe thunderstorms in central Oklahoma.

2. LIST OF EXPERIMENTS, PRINCIPAL INVESTIGATORS OR COORDINATORS, OBJECTIVES, AND FIRST IMPRESSIONS ON DATA ACQUISITION

2.1 Prestorm and Areas of Deeper Convection (R. Rabin. R. Doviak) [3.6.1]*

Objectives:

To determine whether a single Doppler radar, measuring the structure of wind and/or reflectivity fields in clear air or in ADC's prior to storminess, can give useful clues to the onset and intensity of storms.

Doppler data were acquired in the prestorm mode (long pulse transmission and Hi-gain to detect weak echoes, typically below 15 dBZ) on 10 days (4/24, 5/12, 5/19, 5/30, 6/1, 6/11, 6/16, 6/17, 6/18, 6/19, six of which featured ADC's (4/24, 5/30, 6/11, 6/16, 6/17, 6/19. Out of these six days, showers developed within the dual Doppler-radar mapping area on only two days (4/24 and 6/19) and only on 6/19 did the showers become thunderstorms with severe weather. Prestorm data were collected on a dry line that passed through Norman on the morning of 5/12. Data on 5/19 showed what appeared to be a lowering of reflectivity of clear air targets in the PBL beneath a radar-detected cloud band at midlevel heights. Data collection on 5/30 started at 0930 and lasted for ten hours during which time a frontal boundary was evident on the radar displays. Although storms developed along this line, no storms developed within 100 km of Norman. The one day (6/19) during which thunderstorms developed within the dual Doppler area after prestorm data collection may be the most interesting one to analyze.

2.2 Dual Mapping and Storm Electricity Experiments (D. Burgess, W. Taylor, and D. Rust) [3.6.2]

Objectives:

1) To combine thunderstorm wind and precipitation fields (mapped from NSSL's dual Doppler-radar observations) with lightning-produced VHF emission source locations (mapped with NSSL's dual VHF receiving arrays colocated at the radar sites) and other electricity measurements in an effort to determine what relationships exist between thunderstorm's electrical processes, its dynamics, and its production of precipitation.

2) To locate lightning initiation areas and determine how storm structure influences the direction and progression speed of lightning.

3) To obtain four-dimensional data on severe thunderstorms to determine storm-produced mechanisms and organization that culminates in tornado occurrence.

Dual mapping (lightning and radar) data were collected on five days (5/11, 5/17, 5/20, 6/16, 6/19). Storms on 5/11 and 5/20 were quite far (>60 km) from Norman and hence data may be of marginal value. Data of marginal value were collected for 40 minutes on a storm to the north of Norman on the late evening of 6/16.

---

* Bracketed numerals refer to sections in which experimental procedures are outlined.

Strong storms appeared in the late evening of 5/17 and early morning of 5/18, and dual mapping data were collected for almost four hours. Because storms were aligned in at least three bands oriented N-S, we had difficulty in selecting the Doppler radar's PRT that would provide data without overlaid echoes from multiple trip storms. Operations were not planned for these storms, and personnel had to scramble quickly in order to catch the first line of thunderstorms before it moved off to the east out of the dual mapping area. As a consequence, coordinated data collection began on the second line of thunderstorms. Cimarron radar data of 5/17-18 have intermittent errors in the velocity field which will cause difficulty in synthesizing wind fields.

Dual mapping began at 2000 on 6/19 and lasted for four hours. Coordination went well, and a preliminary look at the data shows no serious problems. Data on 6/19 may be the best for Doppler radar analysis, but the storms were less active electrically. (This experiment was supported in part by NASA.)

2.3 High PRF Experiment (D. Zrnic') [3.6.3]

Objective:

To measure, with Doppler radar, maximum wind speeds of tornadoes within 100 km of the radar, and to compare these observations with in situ photogrammetric measurements of tornado winds.

Because of the low occurrence of severe thunderstorms in Central Oklahoma, high PRF data were collected on only one day (5/11). However, this tornadic storm occurred on a "down" day, and because there were no planned operations and because the storm began in Central Oklahoma and moved rapidly to the northeast, we were able to obtain data for only 20 minutes when the storm was at a range of 90 km and moving quickly away. Tornadoes were reported earlier and radar did detect a signature at the start of data collection. High PRF data were collected on this mesocyclone. At the time of data collection, there was not a significant tornado present. (This experiment was partially supported by NRC.)

2.4 Gust Front Experiment (Lee and Brandes) [3.6.2 A6]

Objective:

To determine whether Doppler radar can detect and assess the gust front hazards to aircraft landing and takeoff when the radar is displaced a considerable distance (≃40 km) from the airport. To determine whether it is possible (and how far in advance) to predict gust front formation and movement using single Doppler radar. Seek relationships between the formation of downdrafts, sensed with dual Doppler radars, and the subsequent gust front movement and single Doppler signatures of gust fronts.

Gust fronts were observed by radar on five days (5/11, 5/17, 5/29, 6/16, 6/19). A "roll vortex" was present on the Doppler radar velocity displays on 5/11 at 2125 CST and later from 2226-2316. The display showed shear and wind reversal over the band of echoes oriented SW to NE. On 5/17 a gust front was recorded on the tower instruments, and dual Doppler radar coverage was also provided. Gusts to 25 $m \cdot s^{-1}$ were reported.

Single Doppler radar (NRO) was collecting data from 0100-0200 on 5/29 when a front with gusts of 30 $m \cdot s^{-1}$ was recorded at the tower at about 0130. Only on 6/16 was data collection specialized for gust front observations. Twenty minutes observation commenced at 1042 with both radars operating. Gust front data acquisition was initiated by the two Doppler radars on 6/19 at 2217 when the front was 35 km NW of Norman and rawinsondes were released in the vicinity of this front. The gust front passed NRO Doppler at 2310. (This experiment was partially supported by FAA and NASA.)

2.5 Turbulence
(J. Lee and D. Zrnic') [3.6.2 A.7 or 3.6.4]

Objective:

To determine how well the Doppler measurement of turbulence (measured spectrum variance minus variance due to shear) relates to aircraft-measured turbulence.

There were nine days (5/18, 5/20, 6/3, 6/4, 6/6, 6/8, 6/9, 6/16, 6/17) of coordinated aircraft and Doppler radar measurements. None of the storms was severe and none occurred within the dual Doppler area. Nevertheless, there were single Doppler radar (NRO) observations during times (5/18, 5/20, 6/16, 6/17) when the aircraft experienced moderate to severe turbulence.

Good dual Doppler observations occurred on 6/19, and these data should be best for comparing turbulence measured by the two Doppler radars. (This work was partially supported by FAA and NASA; it was also a joint experiment between NASA, MIT's Lincoln Laboratory, South Dakota School of Mines, and NSSL.)

2.6 Storm Cluster and Tracking
(K. Wilk; R. Crane, Environmental Research and Technology, Inc.) [3.6.5]

Objective:

To use Doppler radar-inferred properties (e.g., peak reflectivities, cell size, intracell motion, top heights, etc.) of storm cell and cell clusters to determine thunderstorm severity and project its path in the immediate (next 10-20 minutes) future.

Processing algorithms developed by ERT automatically detect and track cells and clusters of cells that may delineate regions of potential turbulence hazards to aircraft. This experiment was the easiest to conduct. It required one radar to collect data on storms over a large area (200 km range) so the number of events was high, and required a minimum of coordination with mobile platforms providing in situ observations. This experiment was conducted on 4/24, 5/7, 5/11, 5/17, 5/20, 5/29, 5/30, 6/16, 6/17, 6/19. (This experiment was partially supported by FAA.)

2.7 10- and 23-cm Radar Echoes from Lightning
(D. Rust; V. Mazur, University of Oklahoma; D. Zrnic')
[3.6.8]

Objectives:

1) Correlate lightning echo progression with the apparent propagation of the locations of VHF emission sources.

2) Relate lightning echo location to severe storm phenomena (e.g., mesocyclones, hail, drafts, etc.)

3) Determine characteristics of lightning echoes and relate these to associated electric field changes.

4) Examine the Doppler spectrum of lightning echoes for evidence of explosive channel growth.

Simultaneous 23- and 10-cm lightning echo data were collected on 5/20, 5/28, and 6/16. In all cases, beams were fixed and lightning echoes were seen in real time. The 23-cm radar has been dedicated to lightning echo studies so there is a larger body of lightning echo reflectivity data from it. However, the 10-cm Doppler radar recorded time series data so Doppler spectra can be retrieved. (This experiment was supported by ONR.)

2.8 Radiation (10 cm) from Lightning
(D. Rust) [3.6.9]

Objectives:

1) Determine distribution of radiation along lightning discharge paths and continue earlier study showing characteristic burst of radiation prior to first stroke.

2) Examine streamer processes and compare with those deduced from VHF mapping. Owing to operational constraints, only one attempt was made to collect S-band radiation data. (This experiment was supported by ONR.)

2.9 Lifetime of Thunderstorm Features
(D. Zrnic') [3.6.6]

Objective:

To determine the scale size and time of thunderstorm reflectivity, velocity and spectrum width. Lifetime experiment was conducted on 4/24, 6/16, and 6/17. (This experiment was supported by FAA.)

2.10 Boundary Layer Experiment
(R. Doviak; P. Long, NWS) [3.6.7]

Objectives:

1) To observe the growth of the convective mixed layer in height and time using Doppler observations of wind and reflectivity.

2) To compare the divergence of the horizontal wind field computed from four simultaneous radiosonde releases with area-averaged values from the Doppler radar and also the BLM that is being developed by NWS.

3) Compare divergence computed by the small-scale rawinsonde network with values from the synoptic network.

This experiment was conducted on three days (5/23, 6/4, and 6/11). Rawinsondes were released simultaneously from all four sites between 0500 and 1200, with soundings spaced about two hours apart. Radar was able to measure wind speed from near the surface to a height of 4.0 km or more at all times during the experiments. However, it was difficult to measure the increase in height of the mixed layer because echoes, due either to insects or shear instabilities (intermittent turbulence), caused returns to exist almost at all levels resolved by the radar (radar resolution is about 200 m).

For the third experiment (6/11), we attempted to distinguish diffuse echoes, due to buoyant mixing, from shear-related layered echoes by using an RHI display. Layered echoes showed very well on this display. The success of this method was not immediately apparent during the course of the experiment, and thus a more careful examination of the recorded RHI data needs to be undertaken. Ground clutter prevents data collection much closer than 15 km in the RHI so resolution ($\simeq$200 m) may make pattern recognition difficult. Future experiments of this type should use the shielded 10-cm antenna pointed to the vertical, improve the radar resolution to 15-30 m, and use the newly developed THI, so that returns from insects and shear layers would be more easily distinguished from the buoyantly mixed layer.

2.11 NEXRAD Experiment
(K. Wilk; A. Hansen, NEXRAD Office)
[3.6.10]

Objective:

To determine, using VAD techniques, the wind field and divergence along a cross section of an advancing front and to compare these with dual Doppler measurements.

No data were collected in this mode although the prestorm data collected on 30 May 1980 does satisfy the NEXRAD objective by having a frontal boundary along which weak convection occurred. However, the front was one that remained relatively stationary. Nevertheless, VAD analyses on CIM and NRO data can be performed and results compared.

2.12 Drop Levitation
(W. Taylor and D. Zrnic') [3.6.11]

Objectives:

1) To determine whether a vertically pointed Doppler radar can sense the change in raindrop terminal velocity when the electric field above it is suddenly changed because of an electrical discharge.

2) To determine the vertical motion of discharge channels within the beam.

This experiment was conducted on 5/17. Although lightning discharges were occurring during the time the radar beam was pointed vertically, no rapid changes in the mean fall velocity of drops were revealed in the real-time displays that could be correlated with lightning. Recorded data are being examined for Doppler spectrum changes that might be correlated with lightning.

2.13 Hail Sampling
(S. Nelson; N. Knight, NCAR)
[3.6.2 and 3.6.12]

Objectives:

1) To determine the growth histories of hailstones that fall contemporaneously at the same and different locations within a hailstorm.

2) To relate crystalline structure of collected hailstones to their growth history determined from a numerical model using wind field obtained from Doppler analysis on the storm that produced the collected hailstones.

Twenty-eight quenched hail samples were collected on five days (4/24, 5/17, 5/29, 6/16, and 6/19) by the mobile hail collection vehicles with an additional 20 unquenched samples collected from various sources. The most promising days for analysis were 5/17 with seven samples from two locations collected by the mobile crews and 12 additional unquenched samples from the public; 6/19 with 11 samples collected by one vehicle on two separate storms. The potential for dual Doppler radar analysis exists for the storms on both these days even though the Cimarron data for 5/17 suffer from some problems. (This experiment was partially supported by NCAR.)

2.14 U-2 Lightning Study
(D. Rust; R. Orville and B. Vonnegut, State University of New York at Albany; M. Brook, New Mexico Institute of Mining and Technology)

Objectives:

1) To measure the time dependency of light emitted by lightning from above storm tops to provide data for development of satellite sensor for lightning location.

2) To compare airborne measurements of the above with those obtained at the ground.

3) To determine spectral characteristics of lightning in the wavelength region 300-1600 nanometers.

There were no U-2 data of lightning observed over Oklahoma. We did have good nighttime data over Arkansas, but there were almost no ground data for comparison. The flights were terminated ahead of schedule by NASA. (This experiment was partially supported by NASA.)

2.15 Lightning Ground Strike Location Experiment
(D. Rust; M. Maier, NHEML)

Objective:

To relate the location, frequency of occurrence, and time of occurrence of lightning ground strikes to storm structure measured with Doppler radar.

As with the storm cluster experiment, this one was also easy to conduct. Once set up, data acquisition was automatic and the equipment required the part time of one person to ensure that it was functioning. No coordination was necessary. This experiment, as with the cluster experiment, was conducted whenever storms were within 200 km of Norman. Data were collected on all storms from 4/12 to 6/1. (This experiment was supported by NRC.)

2.16 Corona Beneath Severe Storms
(D. Rust; C. Church, Purdue University)

Objectives:

1) To determine corona current over large areas beneath a severe storm.

2) To determine whether large thunderstorms can contribute anomalously high values of current to the earth-electrosphere system.

Data were obtained from all or most of the 11 instrumented sites, with the best days appearing to be 5/15, 17, 29, and possibly 6/4.

2.17 Storm Electricity Experiments with Mobile Laboratory
(D. Rust; R. Arnold, University of Mississippi)

Objectives:

1) To provide a mobile laboratory for storm electricity measurements and other observations, in particular, on tornadic storms.

2) To provide longer time-continuous data on a storm's electrical properties by tracking with the moving storm.

The mobile, storm electricity laboratory is a van that has been equipped with most of the instruments used at the SEB: slow antenna (two), fast antenna, 3-MHz sferics detector, electric field mill, optical detector, TV video system, microphones, and time code. The fundamental difference with the mobile laboratory is that it allows us to intercept and track with severe storms to observe electrical phenomena for periods significantly longer than possible with fixed-based sites.

Our first impressions of the 1980 data are very favorable. We successfully intercepted and made measurements on several severe and tornadic storms. The longest continuous data acquisition was ≃ three hours on a storm with a mesocylone (and one or two small tornadoes) in the Texas panhandle (6/19). Data on other storms also appear to be of good quality. (This experiment was partially supported by NASA.)

2.18 Tornado Intercept Project
(R. Davies-Jones and J. Weaver)

Objectives:

1) To obtain close-range movies of tornadic debris clouds for estimating wind speeds and correlation with measurements made by the Doppler radar in High PRF mode.

2) To photograph areas of deep convection to correlate with prestorm radar observations.

3) To acquire data using special sensors such as an optical system to detect luminosity (of electrical origin) in tornado funnels.

The team spent about 82 hours on the road and drove 2984 miles during 11 chase days, four of which were excursions to Texas. Slide photos of clouds and severe storm phenomena were taken on all chase days, and movies (time lapse and normal speed) were taken on 5/30, 6/3, 6/16, 6/17, and 6/19.

3. PROCEDURES FOR EXPERIMENTS

3.1 Procedures to Initiate Data Acquisition

3.1.1 When To Report for Work

Decision to work was based on forecasts. Most participants were on a "first forty" workweek. Equipment was not required for operation before 1100 CDT unless otherwise indicated, and thus in some cases, the workday began later than usual. Recorded telephone messages were the most frequently used method of communication. These messages were updated every morning at about 1130 CDT and on occasions in the late afternoon.

Monday. This day was, in all but the most unusual circumstances, a workday. It, in essence, reset our program by guaranteeing that everyone was available for meetings and discussion.

Tuesday-Friday. These were workdays unless there was a message not to work. A not-to-work message was recorded in the late afternoon of the preceding day.

Saturday-Sunday. These were not workdays unless a recorded message the afternoon of the previous day designated them as workdays or unless someone needed to complete a 40-hour work period. If the weather was such that no decision to work could be reached on the preceding day, the message indicated a call-in after 12 noon for the following day, This latter procedure was most commonly used.

Once a decision had been made to designate a day as a "no-work" day, most equipment and personnel were released for that day. In the event that weather conditions changed, we operated with whomever we could contact by radio-telephone pager.

3.2 Briefings with Project Coordinators

At 0930 each day, there was a meeting between the program manager (R. Doviak), an early morning prognosticator (D. Burgess), Storm Electricity program leaders (D. Rust and W. Taylor), Engineering Support manager (D. Sirmans), storm hazards to aircraft program leaders (J. Lee and D. Zrnic'), or their representatives. The prime purpose of this meeting was to review the status of the experiments and decide on a preliminary operational plan for the day.

3.3 Debriefings with Principal Investigators and Project Coordinators

There were debriefings at 1000 when there had been operations on the previous day. All program who were active in data acquisition attended. These debriefings were taped.

3.4 Daily Weather Briefing

A formal weather briefing was held at 1130 CDT each day except on occasions when it was clear that there was very little chance of storms on that day as

forecasted from the previous day. The weather situation was summarized and a forecast indicating location, movement, and time of formation of severe or non-severe storm was given and an outlook for the next day was presented. Operation plans for the day were then decided. Figure 3.1 shows, in block diagram, the decision process used.

3.5 Procedure for Gathering Personnel to Conduct Experiments on Days of Unexpected Storms

The following procedure (see Fig. 3.2) was used when data collection had not been arranged either in the morning briefing or through prearranged call-in:

1) The Program Coordinator (P.C.: R. Doviak; W. Taylor), after discussion with the forecaster (J. Weaver; D. Burgess), decided what experiments might be organized for imminent (1-6 hours) data collection.

2) The Program Coordinator contacted the Coordinator of Radar Operators (CRO: D. Sirmans; J. Carter). If there was no response, the P.C. assumed there was to be no radar support for experiments.

3) If a CRO was contacted, then the P.C. assumed that at least the Norman Doppler radar would be available for data operations and the P.C. then attempted to contact (a) the Coordinator for Storm Electricity (W. Taylor; D. Rust), (b) the Coordinator for Radar Data Acquisition (D. Zrnic'; D. Burgess), (c) the Coordinator for Aircraft Operations (J. Lee; K. Wilk), and (d) the Coordinator for Intercept Projects. If anyone was reached, we went into an operational mode. The forecaster was then contacted to put a message on the "call-in" phone, indicating expected time for initiation of data collection and requesting persons calling in to go to their data collection station.

4) The remainder of the data collection team was contacted by a telephone pager which indicated that they must call in.

Once operators had been collected, the type of experiment to be conducted depended upon who showed up. We did not expect anyone to feel obligated to report for duty on a weekend if the forecast messages on Friday or Saturday afternoon were for no operations on Saturday or Sunday, respectively. We conducted experiments with whoever was available. Participants able and willing to come to work on a day that was forecast to be a no-storm day kept their pagers on.

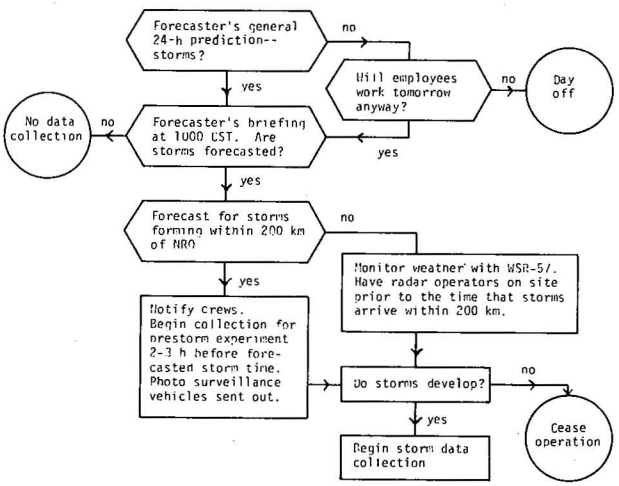

Figure 3.1 Block diagram of dicision process.

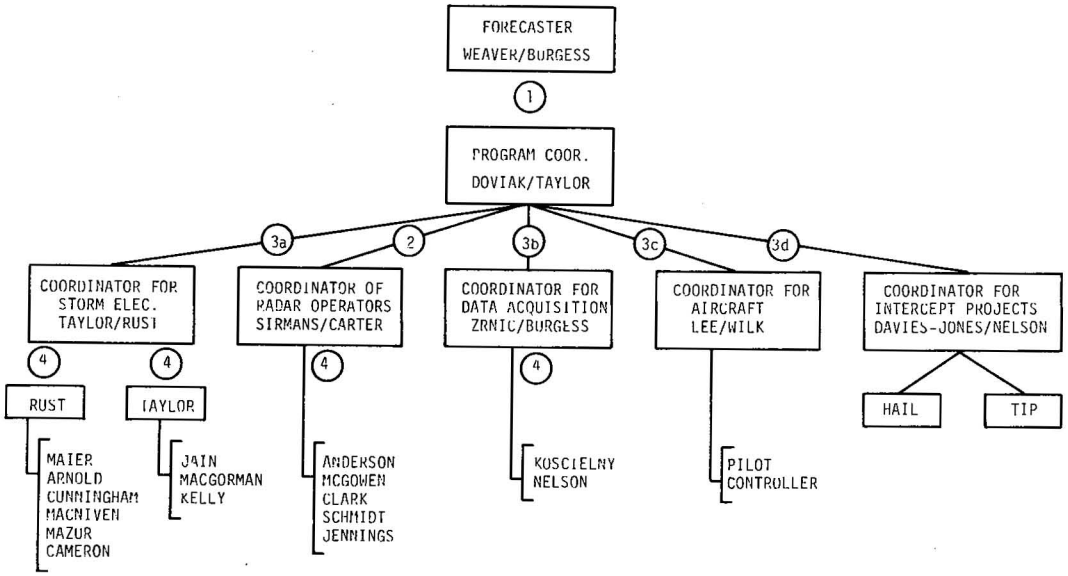

Figure 3.2 Procedure to gather personnel to collect data on storms that were not forecasted.

3.6 Data Acquisition Procedures

3.6.1 Prestorm and ADC's

1) Collection of data on wind and reflectivity began at least two hours before anticipated precipitating convection when forecasted for an area within 200 km of Norman.

2) Both Doppler radars operated on long PRT (2304 μs), used long pulse (e.g. 3 μs) width, and were required to make three 360° scans, one at 0.4°, the other two at 0.8° and 1.2°. NRO started at 180° and rotated clockwise, CIM at 270° and rotated counterclockwise. These three low-elevation scans were repeated twice before incrementing to higher elevation angles. Antenna rotation rate Ω was set to $6°s^{-1}$, pulse pair processor sample number, M, to 64 and DI time constant, TC, set to 32 PRT's.

Norman Doppler radar continued collection at angles 2°, 3°, etc., to 10° and presented the echo heights on the height contour display. This procedure (1-10) was repeated every 30 minutes, starting two hours before anticipated storms.

3) For the first (0.4°) scan, reflectivity, velocity and spectrum width were displayed. After the first scan, the height contour display was used.

4) If areas of deeper convection (ADC) or storms developed in the dual Doppler area, sector scan sequences at both radars were collected in support of the lightning and FAA programs. Storms were generally defined as echoes having vertical continuity to 8-10 km with a reflectivity factor $\geq$ 20 dBZ or clouds that produce electromagnetic emissions. When storms appeared within the dual Doppler area ($R \leq 115$ km), the radar was switched to low gain and interlaced sampling mode, antenna rotation increased to $8°s^{-1}$, PPP sample number decreased to M=32 and DI time constant to four PRT's. The PRT was selected to remove ground clutter away

from 2nd trip areas of interest. Sector scans were designed to have elevation steps corresponding to 1 km height increments, and azimuthal limits were chosen so as to complete a tilt sequence simultaneously with both radars.

5) If storms were outside the dual Doppler area, CIM sector scanned them and recorded continuously, following the procedure for storm cluster and tracking experiments. However, NRO and CIM radars coordinated low elevation scans (0.4°, 0.8° and 1.2°) every 30 minutes (only if PBL echoes were present to ranges of at least 60 km from NRO); otherwise NRO continued 360° surveillance scans, using height display, or it performed other experiments as requested by program coordinator. Data were recorded at NRO only if ADC echoes were seen inside 115 km and PBL echoes out to 60 km.

6) In order to support the ADC experiment, time lapse photography of cumulus clouds being sensed by radar was required. It was the purpose of this comparison to determine when radar senses the presence of clouds relative to the time it is optically sensed, and to compare the spatial extent of clouds detected optically with the spatial distribution measured by radar.

For this comparison, field photography commenced as soon as clouds formed in the area of forecasted convection. Information on the time of initiation of precipitation on the ground from the jointly observed clouds was also gathered by the intercept team. After cumulonimbi developed, the field team left its photographic position and moved to intercept the storms.

3.6.2 Dual Mapping and Storm Electricity Experiments

This experiment was performed when ADC's developed reflectivities greater than 20 dBZ, tops above 8-10 km, and a centroid range less than 100 km.

A. Radar Data Acquisition Parameters

1) Interlaced sampling:
PPP (M = 32); DI (TC = four PRT's); free run

2) Antenna rotation rate: $8°s^{-1}$; azimuth scan sector: ±35° about Z centroid. Azimuth limits were increased beyond ±35°in order to contain 25 dBZ area of storm cell (not anvil or other cells!).

a) If VHF mapper indicated lightning-generated VHF impulse centroids were outside sector being scanned, then azimuth sector limits were increased to encompass VHF impulse centroid.

b) Azimuth limits were set to include gust fronts.

3) Elevation steps: EL = 0.4°, 0.8°, 1.2°; then $\Delta EL = 60/R_c$ where R_c is range (km) to reflectivity centroid. Δ EL was always greater than 0.8°, but less than 6.0°.

a) EL angle topped 20 dBZ echo level above storm centroid by the addition of one more EL step above the last detected 20 dBZ echo. EL angle was then reset to 0.4°.

b) If the Storm Electricity Coordinator called for elevation angles that required more than 5 minutes for tilt sequence (with Δ AZ > 70°),

then the maximum elevation, EL_{max}, requested by the Storm Electricity Coordinator was divided by 15 and elevation incremented in steps Δ EL = $EL_{max}/15$ from 2° upward.

4) If cell was over radar (as indicated by other radar showing 30 dBZ region of cell over the radar site) then the radar discontinued sector scans and started to do continuous 360° cw or ccw scans with rotation rate increased to $12°s^{-1}$. Elevation increments Δ EL were kept at 6°. If azimuth sector limits indicated Δ AZ = 180°, then antenna was continuously rotated in azimuth at $12°s^{-1}$.

B. Gust Front

Time series data were requested when gust fronts passed over Will Rogers and Tinker airports. Both radars added time series data over sectors called for by the Program Coordinator; otherwise procedure was the same as in item 4 above. However, during time series data collection, the radar parameters were changed.

1) Radar collection parameters:

a) Uniform PRT, PPP (M = 64) and time series data recorded with 64 samples per record. Recorded on time marks spaced 0.2 s.

b) The 16 time series gates were spaced 4 μs in range-time, and DI (TC = 32 PRT's).

c) Time series data were collected only for 0.4°, 0.8°, and 1.2° elevations. (If there were overlaid echoes, then time series data were collected on tilt sequences alternating with interlaced sampling.)

d) Azimuthal sectors of prime interest and beginning range-time for this experiment are tabulated below:

TARGET AREA	NRO SECTOR	CIM SECTOR	
Will Rogers	305°-345°	100°-140°	Az
	100 μs *	106 μs*	Range delay
Tinker	10°-40°	90°-110°	Az
	110 μs *	300 μs *	Range delay

* Time delay measured on A-scope to 1st gate

C. Turbulence #1

If aircraft was penetrating a storm being observed with Doppler radar, then the following procedure was used to obtain Doppler spectral data along and/or in the vicinity of the flight path.

1) Uniform pulse trains were transmitted and time series data were collected at only the NRO radar. Time series data were collected on alternate tilt sequences. Otherwise procedure was the same as in A above.

2) Number of PPP samples M = 64; Digital Integrator TC = 32 PRT's.

3) 16 gates of time series were spaced 8 s to span the aircraft's intended path through the storm. Time series data records were initiated on time marks spaced 0.2 s.

D. Real-Time Displays

Thresholds were adjusted so that weak echoes of the gust front were displayed on, at least, the velocity display.

E. Storm Electricity

1) Storm Electricity (SE) Coordinator, located in the SEB, monitored remoted Doppler radar displays and lightning data displays, coordinated all radar and electricity measurements made at NRO, CIM, and SEB, informed SE personnel as to which experiment was being conducted, ascertained that correct data were being collected for the experiment in progress, oversaw data acquisition to conduct a crude form of real-time quality check of data being recorded, and helped where needed.

2) VHF Mapping Stations:

The NRO and CIM Operators brought the two stations up to a recording mode and checked for proper operation. They labeled and logged digital data tapes, video monitor tapes, and strip charts. Operators observed the arrival directions of VHF impulses and the number of impulses in each flash and continually coordinated the selection of azimuthal sectors and amplitude threshold levels to use at each station for optimum data acquisition. The NRO Operator reported the functioning of the equipment and the appearance of the data from both stations to the SE Coordinator.

3) The SA/FA Operator managed 2 slow antennas (SA), 1 fast antenna (FA), recorded gain settings on an 8-channel monitor, checked for coincidence of VHF mapping data and usable SA response (10%-100% full scale). SA #2 was kept 2 gain steps lower; FA kept 2 gain positions higher; all gain settings, as well as problems and trends in data, were recorded by live microphone in the SEB and reported to the SE Coordinator.

4) Cupola Observer:

Visual observations, primarily of lightning (e.g., CG and direction, thunder arrival) were recorded through a cupola microphone, and the event button was activated for CG flashes. The Cupola Observer informed the SE Coordinator of interesting changes or possible problems.

5) Tape Recorder Operator kept tapes loaded in all recorders, labeled tapes after removing from recorders, performed calibration at least once during each tape change as specified on the calibration chart, monitored all signals being recorded on all recorders, prepared next data tape to be used on each machine by removing packaging and degaussing (1" analog only), calibrated each video cassette recorder being used for analog data at least once during each storm or at end of data collection and recorded this on 8-channel strip chart, visually checked timing accuracy of all video time generators, and performed daily poststorm tape inventory.

6) Time Lapse Camera Operator adjusted the camera in the main building observatory to a scanning or stationary mode in collaboration with SE Coordinator, ascertained correct exposure or autoexposure operation, logged film on/off times, changed film, labeled all film immediately upon removal, and performed poststorm film inventory.

7) 23-cm Radar Operator managed the 23-cm radar to acquire lightning echoes by coordinating with other experiments in progress.

8) The operator of the cloud-to-ground lightning strike locator oversaw operation of recording devices and generated real-time lightning location plots. Both digital data on magnetic tape and hard copy paper for real-time observations were available.

F. Mobile Storm Electricity Laboratory

Many of the data acquisition procedures are similar to those at the SEB once a storm is intercepted. There is, however, a great deal of forecasting and logistical effort required to intercept a severe storm, position the mobile laboratory correctly in the storm environment, and maintain it there. (Details of storm intercept procedures are found in 3.6.13.) The crew was usually four people with these duties: 1) Driver--drove and provided verbal notations of storm features and lightning, 2) Meteorologist--forecast, nowcast, navigation, and photography informed SEB and NRO of status by communication with NSSL Nowcaster; 3) Instrument Rack Operator--kept all sensors set at correct sensitivities and documented the monitor and strip chart recorder; and 4) TV System Operator--operated TV system and all 4 magnetic tape recorders for data recording.

3.6.3 High PRF Experiment

This experiment was to be performed when a tornado vortex signature (TVS) was detected (or a tornado reported) in a storm within 90 km.

A. Procedure:

1) As soon as the decision was made to collect high PRF data, the Radar Computer Operator entered the azimuth and range of the circulation center.

2) Then the Radar Operator was informed to change transmitter to the high PRF channel.

3) The Radar Computer Operator reprogrammed the radar computer for the high PRF data acquisition and display.

4) Upon entering the range and azimuth of circulation, the computer printed out the azimuth sector and the beginning range gate for the high PRF time series data collection. Those parameters were immediately communicated to the Radar Operator. The computer kept a log of storm motion, range, azimuth, and time of circulation. This information helped real-time tornado tracking, and it also was used to direct the attention of the damage surveyors to those areas from which high PRF data were collected.

B. Data Collection:

1) Eighteen range gates (3 sets of 6) spaced 2 μs apart were collected covering a range of 5.4 km. The narrowband filter (3 dB width, 0.45 MHz), used in

the high PRF experiment, modified the received pulse to create an effective range-weighting function with a 10-dB width of about 300 m.

2) A 16° azimuth sector scan was used, and each radial data record was keyed on time.

3) One hundred twenty-eight complex time series samples were collected; PPP sample number was set to 128 samples; the AGC was turned off; and low gain was used.

4) The antenna rotation rate was set to 0.83°/s, and thus recorded data radials were 0.3 s apart.

5) Three scans of data (one minute) were collected at an elevation angle of 0.5°.

6) After each 1-min interval, an elevation scan (1° and 1.5° only) was obtained to check vertical continuity of the tornado.

7) The computer displayed and recorded 16 x 16 spectra in the polar format. An average of two contiguous spectral points and a four-spectra average were utilized for the display.

3.6.4 Turbulence #2

Turbulence #1 experimental procedure is presented in Section 3.6.2C. This turbulence experiment was conducted when the aircraft flew along the beam toward the radar at ranges less than 60 km.

A. Antenna beam was pointed in the direction of the aircraft, and the Radar Operator had manual position control of both EL and AZ. Uniformly spaced pulses were transmitted (PRT = 768 μs).

B. PPP sample number was set to M = 64.

C. The DI time constant was set to 32 PRT's.

D. Sixteen spectra were simultaneously displayed in real time.

E. Gate spacings were 2 s.

F. First gate delay was set so that the last 3 gates coincided with the aircraft position, as seen in the spectrum display.

When the aircraft reached the third gate, the antenna beam was elevated to keep the aircraft in the beam and range gates were moved inward by 20 s. Azimuth bearing was changed to keep radar beam on the aircraft.

3.6.5 Storm Cluster and Tracking

This experiment was performed when storms were at ranges R ($115 \leq R \leq 230$ km).

A. Radar Acquisition Parameters

1) CIM usually recorded data and its antenna rotation was set to $6°s^{-1}$. Elevation steps ΔEL were set to 0.8°. Elevation scan cycle was less than 5-6 min.

2) Interlaced sampling mode was used. PPP (M=32); DI (TC=four PRT's). Free run mode was used to maximize data throughput.

3) All storms were topped (i.e., reflectivity (Z) centroids were considered topped when Z above centroid was less than 20 dBZ).

4) Azimuthal sector was large enough to encompass all storms only if elevation scan cycle time was maintained. Otherwise sector limits were decreased to encompass the larger storms.

B. NRO Doppler radar performed surveillance, did other experiments, or was used as a backup to the Storm Cluster and Tracking Experiment.

C. This experiment was also used to support the Hail and Mobile Storm Electricity Experiments.

D. If storms were inside dual Doppler area, then experiment was terminated, and the Dual Mapping Experiment was initiated.

E. The WSR-57 radar's range resolution was set to 1.0 km, and time samples were averaged. The elevation tilt sequence was executed every 5 minutes. Digital data and film records were acquired.

3.6.6 Lifetime of Features

Radar acquisition parameters:

A. Antenna speed: 8°/s

B. Norman PRF mode, uniform PRT = 768 μs, and M = 64 samples. DI TC set at 32 PRT's.

C. NRO and CIM made 3 scans--one at 0.4°, the other two (EL 2; EL 3) depending on range r_c to storm core. EL2 = $300/r_c$, EL3 = $600/r_c$ where EL is in degrees and r_c in km.

D. Data were continuously recorded for 10 minutes.

3.6.7 Boundary Layer Experiment

A. Forecast for clear weather with (1 day) and without (2nd day) thermal advection needed to be known the afternoon before the day of the experiment.

B. Rawinsonde teams were notified the afternoon of the day preceding the experiments. Soundings were taken simultaneously at 4 sites at 0500, 0600, 0800, 1000, and 1200 CST. The Edmond site took soundings every hour starting at 0500 and ending at 1200 CST. Soundings were taken to 50 kP pressures.

C. Radar

1) Data collection was made every hour starting at 0500 CST until 1200 CST.

2) Real-time spectra were displayed (20 spectra averages).

3) Time series, set at M = 64 samples, DI, TC set to 32 PRT's. Uniform PRT and normal gain were used.

4) Beam elevation was in manual position control.

5) Azimuths selected were 0°, 50°, 90°, 125°, 170°, 235°, 260°, 320°.

6) Elevations were set to 0.4, 1.6..... in steps of 1.2° to top of PBL for each azimuth.

7) Minimum of 20 time series records were acquired for each data.

8) Sixteen gates were spaced 8 μs apart (R = 1.2 km).

9) Initial delay was set at 30 s (i.e., first gate at about 5 km).

10) Computer operator read and recorded, in real time, the height of echoes.

3.6.8 10-cm Radar Lightning Echoes

Principal coordination was between the SEB (D. Rust) and NRO (D. Zrnic')

NRO:

Antenna Control: Antenna stationary; AZ and EL coordinates were selected in real time by Principal Investigators. To obtain echoes from cloud-to-ground strokes the AZ angle of strokes were obtained from the observer in the cupola.

Transmitter: Uniform PRT, maximum PRT=1229 ms, DI TC = 32 PRT's.

Option: Long pulse, maximum PRT=3687 ms (for reflectivity data only).

Data Recording: Time series (I, Q) with long records (N_s=4096); gate to be decided in real time by Doppler Radar Coordinator.

CIM: Sector/tilt scanned the storm of interest.

SEB:

Experiment coordination was directed from the SEB utilizing electrical and radar (WSR-57) data in real time, and communication was by phone with headset.

Radar data were recorded on analog magnetic tape @ 60 ips for both log video (direct record wideband 2(WB2)) and I and Q (FM WB2). Video cassette recording of formatted video (IRIG B on audio track).

Electrical data recording: Several parameters including slow antenna, fast antenna, 30-80 MHz radiation, and time were recorded at the SEB. VHF lightning mapper at Norman operated if storm was within 80 km.

3.6.9 10-cm Radiation from Lightning

Principal coordination was between D. Rust at the SEB and D. Zrnic' at NRO.

NRO:

Antenna Control: Antenna was stationary; AZ and EL were selected in real time by Principal Investigators.

Transmitter was off (only during data acquisition period).

CIM: Sector/tilt scanned the storm of interest.

SEB:

Experiment coordination was directed by SEB Coordinator.

Radar receiver noise at log video output was recorded on analog magnetic tape at 60 ips. VHF Lightning Mapper at NRO operated if storm was within 80 km.

3.6.10 NEXRAD Experiment

A. When an approaching cold front was within 30 km of CIM, data collection was to begin. The CIM antenna rotation rate was to be approximately one RPM, requiring about six minutes to complete a six-degree tilt sequence. If a front passed CIM, NRO was to begin operations and dual-Doppler data was to be collected continuously until the front passed NRO (in about one hour, or ten tilt sequences). NRO was to begin antenna rotation so that both radar beams crossed the Will Rogers area at nearly the same time. If the front had passed NRO, operations at CIM were to end, but NRO was to continue until the front was beyond 30 km from NRO.

B. If the cold front was a nonprecipitating one (i.e., receiver not saturated by echoes for $R \leq 30$ km), then data were collected as in the prestorm experiment.

C. If cold front had precipitation, then data were to be collected in the interlaced sampling mode.

D. One tilt sequence every 15 minutes.

E. WSR-57: Data recording was planned for the duration of the experiment. Time constant = 16 PRT's; 0.5 km range resolution.

3.6.11 Drop Levitation

A. Uniform PRT = 768 μs record time series and PPP

B. Low gain/AGC on

C. Number of samples M = 128

D. DI TC = 64 PRT's

E. Time series on N_s = 128, gate spacing 4 μs, 0 steps

F. First gate range-time = 6 μs

G. Record on time = 0.2s

H. EL = 90°

3.6.12 Hail-Sampling Procedure

On the basis of forecasts, nowcasts, and WSR-57 radar information, the collection teams were dispatched from NSSL either directly to a storm or to a staging area in anticipation of storm formation. Barring unusual circumstances the vehicles did stray farther than 150 km from Norman. The teams were guided to locations on improved roads where one or more storm cores were expected to pass. Owing to storm development and uncertainties in storm and vehicle locations, last minute position adjustments were usually made by the vehicle crews. Storm selection and the orientation and distance between the two collection teams were determined by the Hail Project and TIP Coordinator at NSSL and based on the storm's radar characteristics.

Unfortunately, the most severe hailstorms in Oklahoma are often tornadic. Penetration of tornadic storms were attempted only if good real-time Doppler data were available to pinpoint the tornado vortex signature (TVS). In addition, the crews were positioned to remain far north of the TVS. Night intercepts were attempted only if storms were nontornadic.

3.6.13 Tornado Intercept Procedure

The TIP field team consisted of a team leader and three other members. The team leader had the final word on all in-vehicle decisions and was responsible for his team's safety and performance. He also chose the intercept route, based on the availability of roads, visual storm observations, and information received from base (NSSL). Team members were assigned driving, documentary, photographic, and navigational duties. Emphasis was placed on accurate entries of time, location, and records of photography and visual observations in a log (usually a tape recording).

The Nowcaster was the NSSL-based person who communicated with the team leaders. His duties involved monitoring the weather throughout the day when the potential for severe storm development existed. By keeping abreast of the latest developments, the Nowcaster sought understanding of the current state and tendency of the atmosphere. He relayed the latest nowcast and radar information to the field vehicles, obtained their opinions and current visual observations, and directed the vehicles to the most strategic locations. The Nowcaster was also the link between the Intercept teams and other participants in NSSL's Spring Program.

To maximize intercept chances, teams entered the field well before severe weather developed and often even before the formation of echoes on NSSL's WSR-57 radar scope. Immediately after the 1000 CST forecast (or even before when conditions warranted), the initial status of each team was resolved. Choices were (a) dismiss the teams, (b) place them on standby at NSSL, (c) dispatch them to a designated standby location in the field, or (d) vector them toward a target storm. Since the initial decision proved to be a vital one, much depended on the forecaster's ability to assess the probability of severe storms during the day, and the prime time and location for development. On potential or actual severe storm days, the status of each team was updated frequently until the mission was terminated, either because of darkness or because of lack of suitable target storms within range. When storms failed to form by the predicted time, the teams were tempted to drive home early. However, policy has been to remain in the field until dusk because of several instances of rapid storm development in regions just vacated by returning teams.

After storms had developed, the intercept strategy depended on vechicle positions in relation to storm locations and movements, and expected weather developments. Unless a decision was made to forego existing storms in favor of ones anticipated in a different region, a target storm was chosen for each vehicle on the basis of the storm's accessibility and its tornadic potential. As a field team approached a storm, it maneuvered around the precipitation core and took up a tracking position on the storm's right rear flank. Driving through the core was avoided whenever possible.

As target distance decreased, the intercept crew's own visual observations became increasingly important, and their reliance on relayed radar information diminished. This was fortunate since communication channels are often unavailable. Once a tornado or suspicious cloud feature had been spotted, the team positioned itself ahead and to the right of the extrapolated track (and left itself an escape route to the south or east). This vantage point generally offered the best visibility because the tornado is silhouetted against a light background, and there is least likelihood of intervening precipitation. Teams which have pursued tornadoes from behind have experienced poor photographic contrast and road obstacles due to fallen debris.

The Mobile Electric Laboratory operated in essentially the same manner as other intercept crews. Minor deviations occurred in an attempt to assure that high quality electrical data were obtained.

3.7 Communication Network

Coordination between the various elements was accomplished by voice telephone links, telephone data links, or radio telephone links. Figure 3.3 is a block diagram of the communication network.

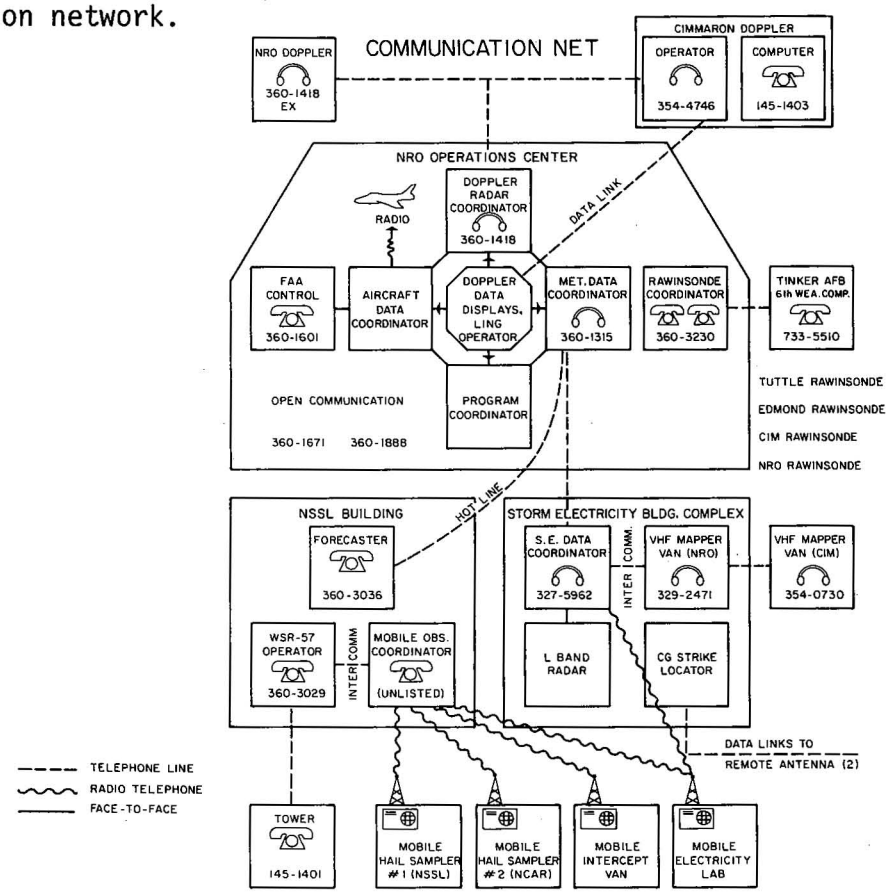

Figure 3.3

4. BRIEF DESCRIPTION OF EQUIPMENT USED
(see appendices for detailed specifications)

4.1 Radars

NSSL operates and maintains three 10-cm radars. Two are Dopplers spaced 41 km apart, one (NRO) located at NSSL and the second (CIM) at Page Field (formerly Cimarron Field). The third radar is an incoherent surveillance radar (WSR-57) located at NSSL.

4.1.1 Doppler Radars

The NRO and CIM radars are nearly a matched pair, and detailed specifications are given in Appendix A. Briefly, each radar records either or both of the three moments (power, mean velocity, and spectrum width) of the Doppler spectrum at all ranges and the time series samples of the Inphase I and Quadrature Q phase video signals sampled simultaneously at 16 range locations. There are several options in transmitting pulses: (a) a uniform train for Doppler spectral analysis, (b) an interlaced PRT (dual sampling mode) for automated range de-aliasing of multiple trip targets and logging of range overlaid echoes, (c) long transmitted pulse width (3-5 μs) for maximum sensitivity to detect clear air echoes, and (d) a high PRF mode (NRO only) for measuring tornadic speeds.

Typical antenna scan rates are 6°-10° s^{-1}; angular resolution is about 0.8°, and range resolution is as fine as 150 m but depends on transmitter mode used.

4.1.2 WSR-57

This incoherent radar has an angular resolution of about 2° and a range resolution of 1 km (for most experiments). It provides reflectivity estimates and scans at a rate of 18° s^{-1} in azimuth and automatically steps in elevation at increments selected by the WSR-57 operator. This radar is usually operated hands-off in a surveillance mode.

4.2 VHF Mapping System

A wide-band VHF system, employing time-difference-at-arrival techniques, provides azimuth and elevation angles to individual sources of electromagnetic impulses from lightning discharges. Acceptable elevation angles are limited to 45° above the horizon; azimuth angles are limited to a 60° sector, selectable in 30° increments. Angles are determined to 0.5° accuracy for lightning occurring within a nominal 60-km range. Maximum instantaneous rate of reception is 16,000 per second. Data are recorded on 9-track magnetic tape, and a real-time azimuth-elevation display is available to assist in detecting and tracking thunderstorms. Simultaneous observations are made near NSSL's Norman and Cimarron Doppler radars (see Appendix B for details).

4.3 Storm Electricity Building

The SEB serves as a central location for acquisition of storm electricity data and coordination with other areas of experimental data collection, e.g., Doppler facility, storm intercept control, etc. Instrumentation located at, and in the

field near, the SEB is used to measure various electrical phenomena such as electric field changes associated with lightning, optical transients from lightning, video documentation of lightning and storms. Data are recorded on analog magnetic tape with time code synchronized to WWV (see Appendix C for details).

4.4 The 23-cm Radar

A 23-cm radar is located at the SEB for acquisition of radar echoes from lightning. The lightning radar echoes are recorded on the same magnetic tape as the electricity phenomena and on a separate video cassette recorder. Because of its long-range capability for observing lightning (200 km), this radar is also used to acquire data on storms being studied with the Mobile Electric Laboratory (see Appendix D for detailed specifications).

4.5 The Stationary Automated Mesonetwork

A small number (12) of meteorologically instrumented stations was used in Spring 1980, and these were located close to NSSL so that they could be routinely serviced without additional manpower cost. Each site provided wind speed and direction, wet and dry bulb temperatures, pressure, rainfall, and corona current. One-second samples were averaged, and these were recorded on magnetic cassette tapes. Detailed description of recording ranges, quantization increments, and sensor types is given in Appendix E.

4.6 Rawinsondes

The 1980 spring mesometeorological rawinsonde network was established at four locations surrounding Oklahoma City (see Fig. 1.2). GMD-1 rawinsonde equipment was used to obtain soundings with a VIZ Manufacturing Company (ACCU-LOK) instrument. These instruments were factory calibrated (pre-baselined). Personnel from the U.S. Air Force Sixth Weather Squadron (Mobile) located at Tinker AFB in Oklahoma City manned and operated each of the four sites.

Specialized data acquisition and processing procedures were used to bring data to the laboratory in near-real time. Each site was equipped with a standard ASR-33 teletypewriter with paper tape punch and acoustic coupler, and standard commerical telephone. At Tinker AFB, Model 3610 computer system was used for processing the raw rawinsonde data. At NSSL an HP 9825A received the output data from the Model 3610 CPU and plotted the data in graphic form on a standard skew T, log p diagram.

Altogether, 176 soundings were taken during the period 1 May through 19 June 1980.

4.7 Aircraft

4.7.1 T-28

A T-28 aircraft was operated by the Institute of Atmospheric Sciences, South Dakota School of Mines and Technology, in support of the joint FAA-NSSL aircraft turbulence program. The Massachusetts Institute of Technology's Lincoln Laboratory was also a partner in the program.

The T-28 is an extensively modified single-engined propeller-driven military training aircraft. The structure of the aircraft is strengthened and all leading edges including the low-level wing and tail surfaces are armor plated to protect the aircraft from hail damage. The aircraft was instrumented as indicated in Appendix K. Penetration true airspeed was 90 to 95 $m \cdot s^{-1}$ with a flight duration 1-1/2 to 2 hours. The aircraft arrived in Norman on 12 May. The T-28 program was terminated on 20 May when, after a successful mission, the aircraft sustained damage to the nose wheel and engine caused by running off a taxiway onto soft turf.

4.7.2 F-106

The F-106 aircraft, supplied and flown by NASA, was part of the severe storm program of NASA, FAA, and NSSL. This single-engined jet fighter is instrumented as indicated in Appendix K, Table K.1. The objective of the program is to improve the state of the art of severe storm hazard protection, detection, avoidance, and design of aircraft for those hazards which cannot be reasonably avoided. The hazards include lightning, turbulence, wind shear, precipitation types (rain or hail), and precipitation rates, In this first phase of the program, turbulence and lightning were the major interest areas.

The F-106 arrived at Tinker AFB on 20 May and returned to Langley Research Center, Virginia, on 19 June. During this time, 9 flights were made to penetrate thunderstorms. The aircraft flew at a TAS near 195 $m \cdot s^{-1}$ and had just over a 1-hour flight duration. During these nine flights, the aircraft made 33 penetrations at altitudes indicated in Table 4.7.1.

Table 4.7.1 1980 F-106 Thunderstorm Penetration Altitude Distribution

Penetration Altitude (MSL)	No. of Penetrations
23,000 ft	2
22,000 ft	2
20,000 ft	8
16,000 ft	7
15,000 ft	9
14,000 ft	2
13,000 ft	3

4.7.3 U-2

The NASA U-2 is a single-engined jet aircraft designed for high altitude (above 60,000 ft MSL) flights. Crusing speed is around a true airspeed of 150 $m \cdot s^{-1}$. Besides the normal navigational and aircraft instrument recordings, three special systems for the lightning experiments were included as follows:

1) a slow antenna
2) an NOSL sensor
3) a TV spectrometer system

The U-2 was available for flights during the period May 10 through May 20. On May 15, the U-2 flew over a heavy rain-producing system in central and southwestern Oklahoma and later over more active thunderstorms in Texas. Several flashes were recorded.

4.8 Cloud-Ground Lightning Location System

The cloud-ground (CG) lightning location system was operated from April 12 until June 1. This instrumentation provides the time, location, peak field strength (current), and number of component strokes for each CG flash that lowers negative charge within about 200 km of Norman. The system consists of three remote direction finders (DF's) which independently determine the azimuth angle to the CG flash. These data are transmitted back to a central processing unit by leased phone lines. The central processing unit or position analyzer computes the intersection point of the azimuth angles and outputs the data on digital magnetic tape, hard-copy printer, and plotter in real time. These devices were located in the storm electricity building. A more detailed description of the system, network configuration, performance characteristics, and data format is given in Appendix F.

4.9 Meteorological Tower

The 461-m KTVY television antenna tower has been used as a multi-level boundary layer sensor facility since 1966. Currently, it is instrumented at seven levels--7, 26, 45, 89, 177, 266, and 444 m. Data are routinely recorded on magnetic tape. A 10-second sample interval is used during non-storm conditions and a 1.3-second interval during storm periods. Two gust front occurrences were recorded at the 1.3-s rate on 17 May and 16 June. Gusts over 25 $m \cdot s^{-1}$ were recorded several times during the season.

4.10 Low-Level Wind Shear Alert System (LLWSAS)

LLWSAS, initially called Surface Wind Monitoring System (SWIMS), is a real-time computer-controlled, surface-based wind sensor system using radio telemetry as a communication link. The system installed by the FAA at Will Rogers International Airport consists of six wind sensor sites located as shown in Figure 1.2. All sites use the vector vane-type sensor system mounted about 20 ft AGL. The wind speed and direction data are collected at 7-second intervals and processed by the computer for display in the airport air traffic control tower. Arrangements were made with the FAA to record the data before it was processed whenever severe weather was expected to cross the airport. Recording was sequentially accomplished using an AXIOM Corp. EX801 recorder. These data were then transferred to punched card for further analysis using developed computer programs. The LLWSAS provides a small mesoscale wind observation network nestled within the SAM network and, since airport-centered, provides ground truth for covering Doppler Radar Operations. Data were obtained for two gust front cases--17 May 1980 and 16 June 1980.

4.11 Mobile Equipment Platforms

4.11.1 Tornado Intercept

The Tornado Intercept Project operated only one chase van (NSSL 1) during the 1980 Spring Program. Emphasis was placed on obtaining verbal and photographic

documentation of cloud fields prior to storm development, and of thunderstorms features (especially tornadoes) after cumulonimbi had formed. Thus, the equipment carried into the field included three 16-mm movie cameras, two 35-mm slide cameras, tripods, lenses, various other photographic accessories and supplies, portable tape recorders for verbal commentaries, and maps. A "Vonnegut" camera (Vonnegut and Passarelli, 1978) was also taken along to detect luminosity (of electrical origin) in tornado funnels. The van was equipped with FM radio and a radio telephone. FM communications with the Nowcaster at NSSL were routed through a repeater located at the 440-m level on a tall television tower 40 km north of NSSL. Beyond the FM system's range (roughly 115 km from the repeater), the radio telephone was used whenever an open channel was available; otherwise, the Nowcaster was contacted by public telephone. Direct, short range, inter-vehicle communications, provided by a second FM radio channel, enabled the crew to exchange information with other field teams.

4.11.2 Hail

Time-resolved, sequential hailstone samples were collected by mesh funnels mounted on two radio-equipped vehicles (Hail 1, Hail 2). The funnels were mounted through the vehicle roofs with the hailstones being collected directly into containers of hexane at dry ice temperature (-78°C). This "quenching" in hexane, which preserves the hailstones' original crystalline texture, is necessary for later determination. Typically, the hail that falls on the sampling area (1 m^2) is collected for a one-minute interval before a second collection is begun. Hailstones collected and preserved by other methods may be used to determine embryo type but are not useful in structural studies because of the extensive recrystallization that occurs. At the end of the season, the hailstones were transported in dry ice to NCAR for detailed analysis.

4.11.3 Electric

In a joint program with Dr. Roy Arnold of the University of MIssissippi, a van has been equipped to function as a Mobile Electric Laboratory (MEL). Most of the instrumentation at the SEB is duplicated in the MEL. This provides the opportunity of making quantitative electrical measurements and video recordings of the storm in a position that is relatively fixed within the severe storm, in particular in the inflow region beneath the precipitation-free cloud base.

5. PERSONNEL ASSIGNMENTS

1) Program Coordinator:
   R. Doviak
   Alternate: W. Taylor

2) Forecaster
   J. Weaver
   Alternates: D. Burgess, R. Rabin
   Assistant: C. Kloth

3) Mobile Observations Coordinator and Nowcaster
   J. Weaver, S. Nelson
   Alternate: C. Kloth
   Assistant: C. Robertson

4) RAOB Control
   L. Showell
   Alternate: K. Wilk

5) Doppler Radar Coordinator
   D. Zrnic'
   Alternates: R. Brown, E. Brandes

6) Meteorological Data Coordinator
   D. Burgess
   Alternates: R. Rabin, E. Brandes

7) Cimarron Radar Operators
   M. Schmidt
   C. Clark (data acquisition coordinator)
   Alternates: J. Carter, M. Istok

8) Norman Doppler Radar Operators
   G. Anderson
   J. McGowen
   Alternate: D. Sirmans

9) Norman VHF Mapping Operator
   D. MacGorman
   Alternate: W. Taylor

10) Cimarron VHF Mapping Operator
   E. Kelly
   Alternate: D. MacGorman

11) WSR-57 Operator
   S. Nelson
   Alternate: D. Zittel

12) Aircraft Coordinator
   J. Lee
   Alternate: D. Zrnic'

13) Real-Time Display Computer Operator
    A. Koscielny (NRO)
    Alternate: A. Zahrai
    M. Schmidt (CIM)

14) In Situ Observations (mobile)
    a. Hail sampler (Hail 1): A. Adams, K. Kelleher
    b. Hail sampler (Hail 2): N. Knight, C. Kessinger
    c. Meteorological observations
       (Tornado Intercept): R. Davies-Jones,
       B. Smull, K. Drogemeier, C. Robertson
    d. Electricity observations
       (University of Mississippi): R. Arnold

15) Quality Control
    (Doppler, Tower, SAM, WSR-57, Soundings)
    J. Dooley
    Doppler: D. Sirmans, D. Rowlett, C. Clark
    WSR-57: E. Helm
    SAM: K. Johnson (cognizant meteorologist),
    D. Zittel
    Tower:. D. Zittel
    Soundings: L. Showell

16) Photography (WSR-57, NRO or CIM Doppler)
    a. C. Clark
    b. R. Goldsmith

17) Stationary Automated Mesonet
    a. J. Wardius, S. Fredrickson
    Alternate: J. Reece

18) Briefing Team (0930 CDT)
    a. R. Doviak
    b. J. Lee, D. Zrnic'
    c. W. Taylor, D. Rust
    d. D. Sirmans or J. Carter
    e. D. Burgess

19) Tower Operations
    L. Johnson
    Alternate: J. Reece

20) Equipment Status
    D. Sirmans
    Alternate: J. Carter

21) Electric Data Coordinator
    W. Taylor
    Alternate: D. Rust

22) SEB-Based Experiments
    D. Rust
    Alternates: M. MacNiven, L. Cunningham

23) Real-Time Dual Doppler Quality Control
    A. Zahrai (NRO)
    M. Schmidt (CIM)

6. OPERATIONAL PERIODS AND DAILY COLLECTION HIGHLIGHTS

The bar graphs that accompany the highlights of each operational day show time periods during which data were collected according to entries made in various observers' logs. There may be variance between these indicated data collection periods and the actual times during which data were recorded on either magnetic tape or film. For more accurate listings, one should refer to computer listings of times when recorders are on or to film data that have time recorded.

These highlights should serve the purpose of recouping the essence of the weather and operations for the day. For analysts not involved in the operations, this section provides a summary of the observer's first impressions on the type of data that were collected, quality, and problems. For the participants in the experiments, it gives the outlook of others who were making simultaneous measurements and observations with other instruments, while serving as a stimulus to recall other events of importance.

The following symbols on the bar graphs refer to type of experiment being conducted at the indicated times.

B = Boundary Layer (see Section 2.10)
C = Storm Cluster and Tracking (see Section 2.6)
D = Dual Doppler coordinated scans (see Sections 2.2, 2.5, 2.11, and 2.13)
E = Lightning Echo (see Section 2.7)
F = Coordinated Data Collection with F106 aircraft (see Section 2.5)
G = Gust Front Experiment (see Section 2.4)
H = High PRF Measurements (see Section 2.3)
I = Lifetime Experiment (see Section 2.9)
L = Levitation Experiment (see Section 2.12)
P = Prestorm (see Section 2.1)
R = Elevation Angle Scan Mode (RHI)
S = 360° Surveillance (usually in interlaced sampling mode)
T = Data Collection Coordinated with T-28 Aircraft (see Section 2.5)

6.1 24 April; Thursday

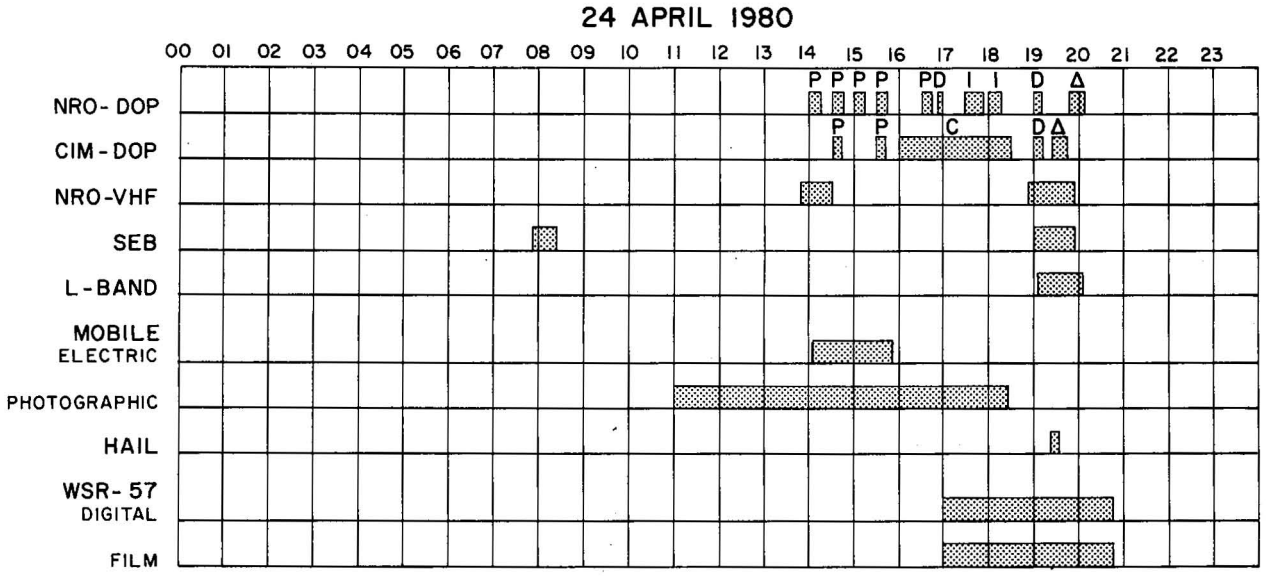

6.1.1 Forecasters' Outlook

Surface analysis on the morning of 24 April found a stationary front through southeastern Oklahoma. This front stretched northeastward from a low near Wichita Falls, Texas, through McAlester, Oklahoma. As the day progressed, the front pushed northward into central Oklahoma.

The 500 mb chart indicated strong, southwesterly flow over Oklahoma and northern Texas. An intense shortwave was approaching the area from New Mexico and, by midmorning, dry surface air began pushing eastward behind this wave.

Thunderstorms formed at about 1200 CST ahead of the shortwave, along the surface dry push boundary, and moved into western Oklahoma by 1530 CST.

6.1.2 Radar Observation Highlights

Radars recorded data in the long pulse mode during early afternoon when a surface warm front was in the area. There was no evidence of a frontal boundary seen on radar. However, winds in the lowest 0.5 km appeared to veer from ENE in the morning to SE in the afternoon. Clear air returns were mostly limited to the southern sector out to 50-km range where the sky had cleared. Two small ~35 dBz cells developed to the east and southwest at 50-km range. The latter was associated with an area of deeper convection (ADC) and radial velocity convergence. CIM acquired storm cluster tracking data on approaching thunderstorms about 200 km to the SW during the afternoon. There was some indication of a right-moving, splitting cell during this time. NRO collected lifetime data on a newly formed storm 75 km to the west. Single Doppler data were recorded in support of hail collection 85 km to NW (on base line).

6.1.3 Storm Electricity Observations

Norman VHF mapping, SEB observations, and 23-cm radar indicated storms were not very active electrically. The Mobile Electric Laboratory operated on storms near Graham and Snyder, Texas.

6.1.4 Aircraft Operations

None.

6.1.5 Mobile Ground Vehicle Observations

The NSSL 1 chase vehicle proceeded to the Wichita Falls, Vernon, Seymour area of Texas where a dryline bulge developed. At 1507 CST, they saw a small funnel emanating from a high based cumulus near Dundee, Texas. Ten minutes later, near Mabelle, Texas, the team observed a more threatening funnel pendant from an ill-defined wall cloud. The team penetrated a precipitation shaft near Lake Kemp at 1543 CST, and encountered heavy rain and pea-size hail. By 1600 CST, they were in the clear air on the west side of the line and saw a magnificent panorama of storms to the north, east, and south. Traveling east once more, NSSL 1 observed the effects of a recent hailfall at 1700 CST; small hail was completely covering the ground. The crew then headed north for a storm near Lawton which weakened as they approached it. However, around 1830 CST from 15 miles west of Lawton, they photographed a distant storm, which produced golf ball-size hail at Sayre at 1825 CST and a tornado near Elk City at 1850 CST. This storm was on the warm front. The chase was then called off because of ensuing darkness.

6.2 30 April; Wednesday

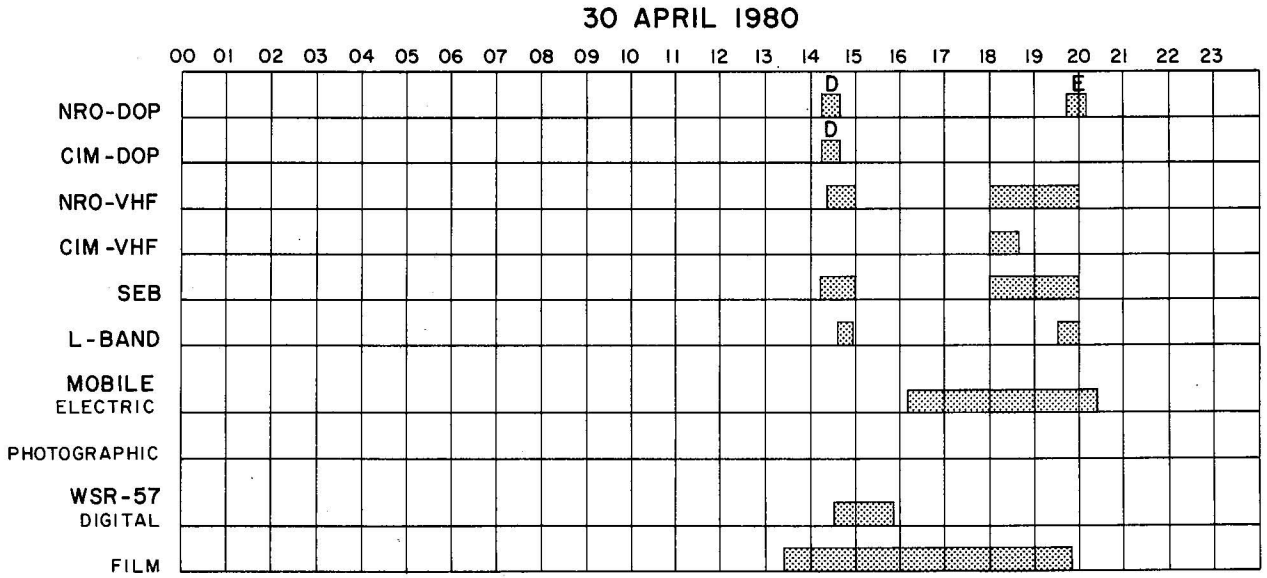

6.2.1 Forecasters' Outlook

A 300-500 mb closed low over eastern Arizona kept Oklahoma and Texas in southwesterly flow aloft. Diffluence was strongest over the Texas Panhandle and most of Oklahoma. A shortwave trough was moving northeastward out of southeastern New Mexico.

Early morning surface analysis showed a warm front along the Red River tied to a low pressure region south of Childress, Texas. During the morning and early afternoon, the warm front moved northward into central Oklahoma.

Moderately strong, but nonsevere, thunderstorms formed in western Oklahoma at approximately 1330 CST as the leading edge of the shortwave trough entered the state.

6.2.2 Radar Observation Highlights

Dual radar mapping data were recorded in support of a Storm Electricity experiment on a small 55-dBZ storm to the southwest until it rapidly reached the baseline. In the evening, lightning echo data were recorded from NRO in the vicinity of the Mobile Electric Laboratory (MEL).

6.2.3 Storm Electricity Highlights

Dual VHF mapper, SEB and L-band radar recorded data during two storm periods. There was good data correlation between Norman and Cimarron mappers. The MEL tracked storms for three hours from north of Wichita Falls to near Ada, obtaining good electrical data under wall cloud coincident with a radar "notch".

6.2.4 Aircraft Operations

None

6.2.5 Mobile Ground Vehicle Observations

None

6.3 1 May; Thursday

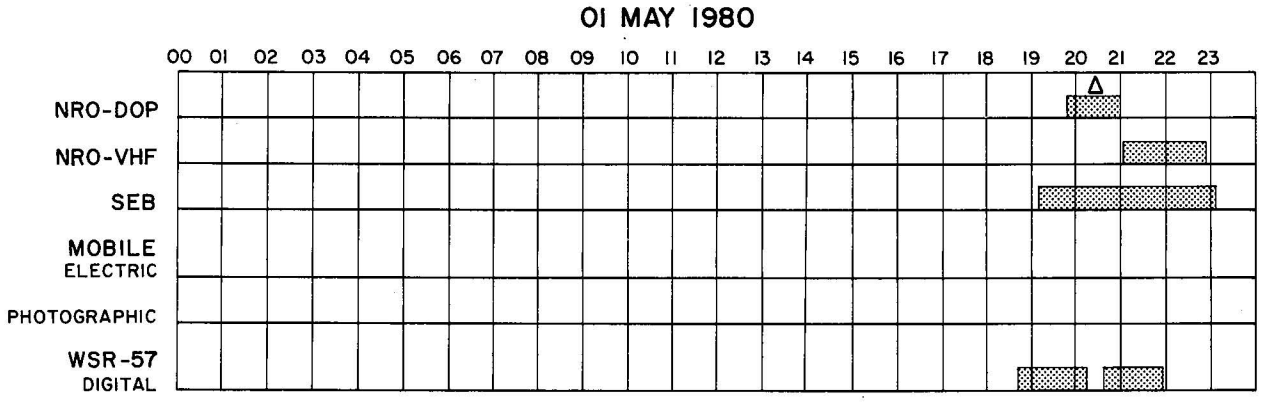

6.3.1 Forecasters' Outlook

Morning weather in central Oklahoma was characterized by overcast skies and cool temperatures. The region was situated north of a warm front running along the Red River. This front connected with a surface low just south of Dallas, Texas.

At upper levels, a weak-to-moderate low was moving eastward through New Mexico toward the Texas panhandle. Around the base of this low, an intense shortwave trough (in extreme southwestern Texas) was traveling northeastward.

Throughout most of the afternoon, thunderstorm activity confined itself to the warm front. However, at approximately 1800 CST, a short, north-south line of storms formed in central Oklahoma. Subsequent reports of large hail and funnel clouds were received from Ardmore, Oklahoma, and many areas of the Oklahoma City metroplex. No feature within the resolution of available data could be found to coincide with this line. At first, it was felt that unexpectedly rapid heating might have been the culprit, but study of the data shows that no particularly significant rapid heating occurred. Furthermore, the heating that did occur was widespread and covered most portions of central and eastern Oklahoma. No single surface or upper air feature clearly indicated a favored line where the storms actually formed.

6.3.2 Radar Observation Highlights

NRO sector scans covered evening storms some time after their unexpected development in support of an unsuccessful hail collection attempt. Because of the unexpected situation, CIM did not participate in data collection.

6.3.3 Storm Electricity Highlights

Only Norman VHF mapping and SEB instrumentation operated, but data seemed very good.

6.3.4 Aircraft Operations

None.

6.3.5 Mobile Ground Vehicle Observations

None.

6.4 7 May; Wednesday

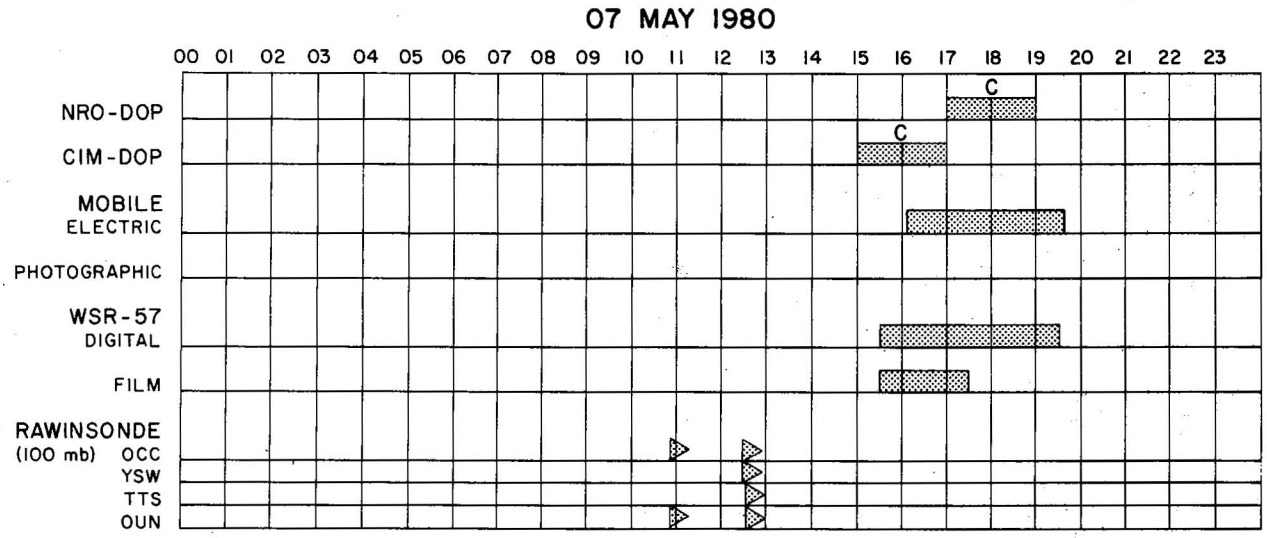

6.4.1 Forecasters' Outlook

A surface cold front pushed southward across Oklahoma during the morning and by noon was situated just north of the Red River. Oklahoma spent the remainder of the day in cool northeasterly surface flow.

Three shortwave troughs in a very complex upper flow pattern became evident during the morning hours over the region of interest. The first two brought early morning thundershowers to northwestern Oklahoma and eastern Texas. The third showed up only as a field of enhanced cirrus on satellite and strong pressure falls at the surface in eastern New Mexico and western Texas during this period.

Afternoon thunderstorms first formed in western Texas, but quickly built northeastward into north central Texas along the Red River. Several of these storms reached severe limits. Two tornadoes were reported, one of which the MEL crew documented.

6.4.2. Radar Observations Highlights

CIM began recording data for the storm cluster experiment in midafternoon on storms 300 km to the SW. These storms appeared to grow ENE along a line; however, their individual movement was to the ESE. NRO continued the tracking experiment as the storms passed 250 km to the south.

6.4.3 Storm Electricity Highlights

Only MEL operated. A tornado was observed near Vera, Texas, at 1620.

6.4.4 Aircraft Operations

None.

6.4.5 Mobile Ground Vehicle Observations

None.

6.5 11 May; Sunday

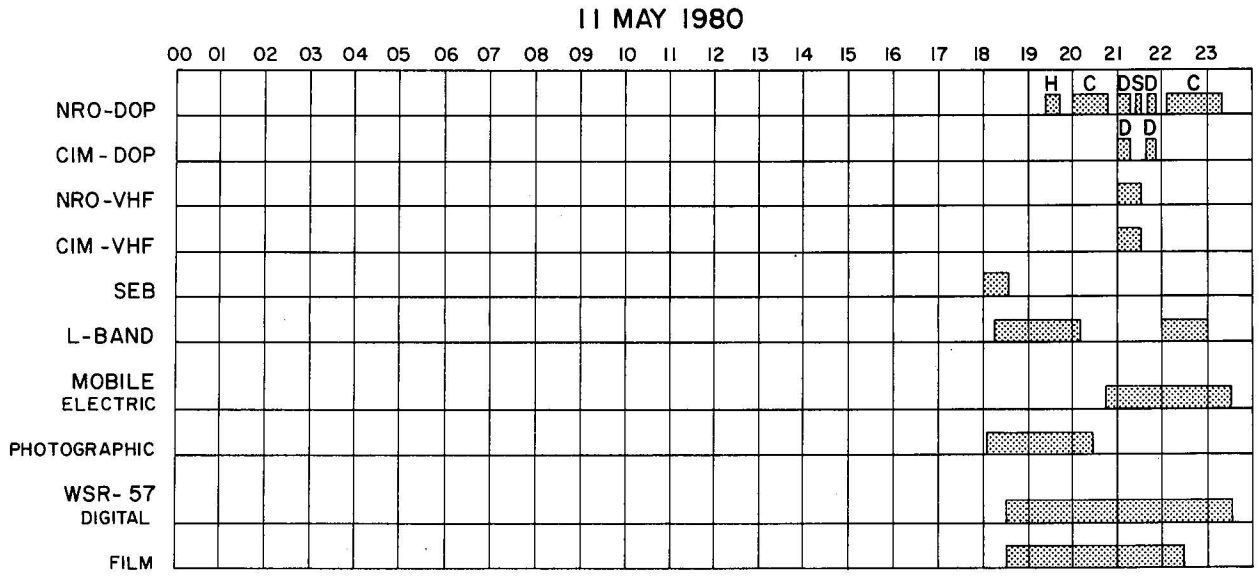

6.5.1 Forecasters' Outlook

Morning data were not very encouraging for the later development of severe thunderstorms. Even though the upper flow was southwesterly and strong, the nearest significant shortwave trough was far to the west in Arizona. Numerical forecast guidance suggested that only a very weak wave would affect Oklahoma by evening. Furthermore, morning radiosonde data from Oklahoma City showed an extremely shallow layer of moist air (~30 mb deep), with a 100 mb mixed layer value of only about 7.5 g kg^{-1}. 850 mb analysis indicated that even drier air was to be found at all upwind stations. A surface dryline in western Oklahoma was expected to mix rapidly eastward by afternoon and a triple point, i.e., dryline intersection with a cold front (in northern Oklahoma on morning analyses) was anticipated over Tulsa.

By midafternoon the dryline had still not moved eastward and was found on a line from Stillwater to Hobart. Dewpoints to the east of the boundary remained in the low 70's (°F). An unidentified moisture source was apparent. Evening sounding data showed more than 14 g kg^{-1} of moisture in the deepened Oklahoma City boundary layer. Moreover, at approximately 1700 CST, a large field of very well-defined altocumulus castellanus (ACCAS) moved rapidly into central Oklahoma, indicating the presence of a shortwave trough aloft of a much greater intensity than expected.

Shortly after the appearance of the ACCAS field, very intense storms formed in central Oklahoma along the dryline. The activity produced several severe reports and three tornadoes. A radar echo "thin line" was detected at about 2130 CST, and the Doppler velocity field showed evidence of a horizontal roll vortex.

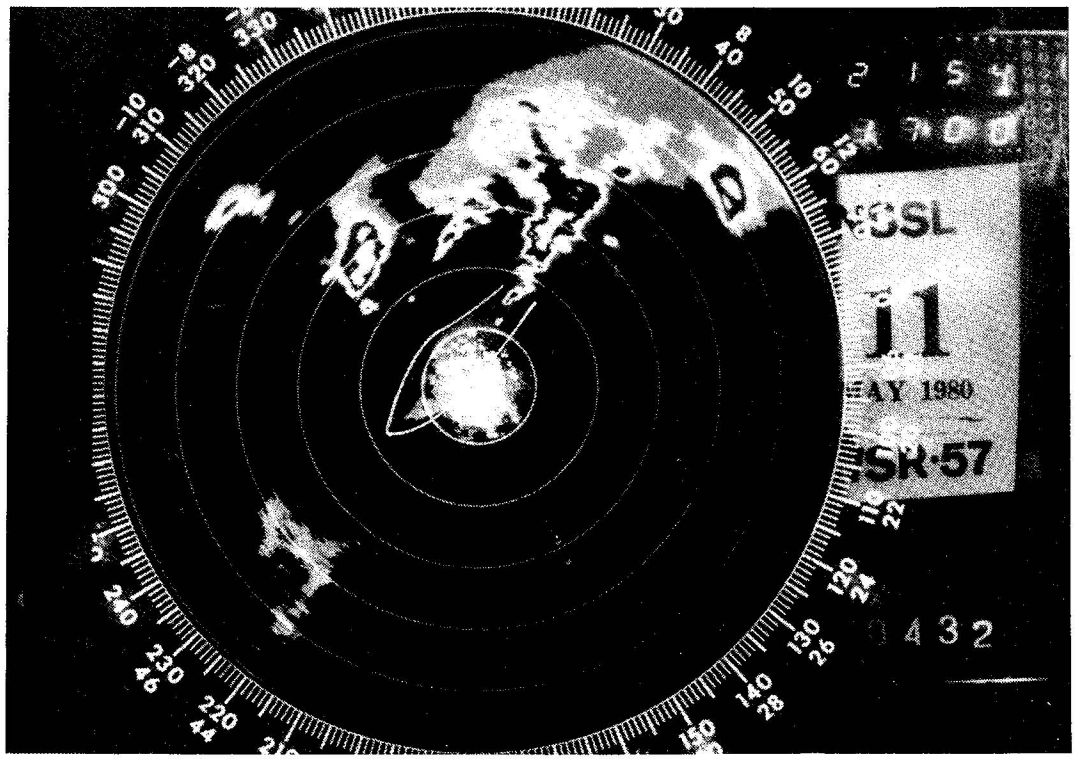

a. 2154 CST

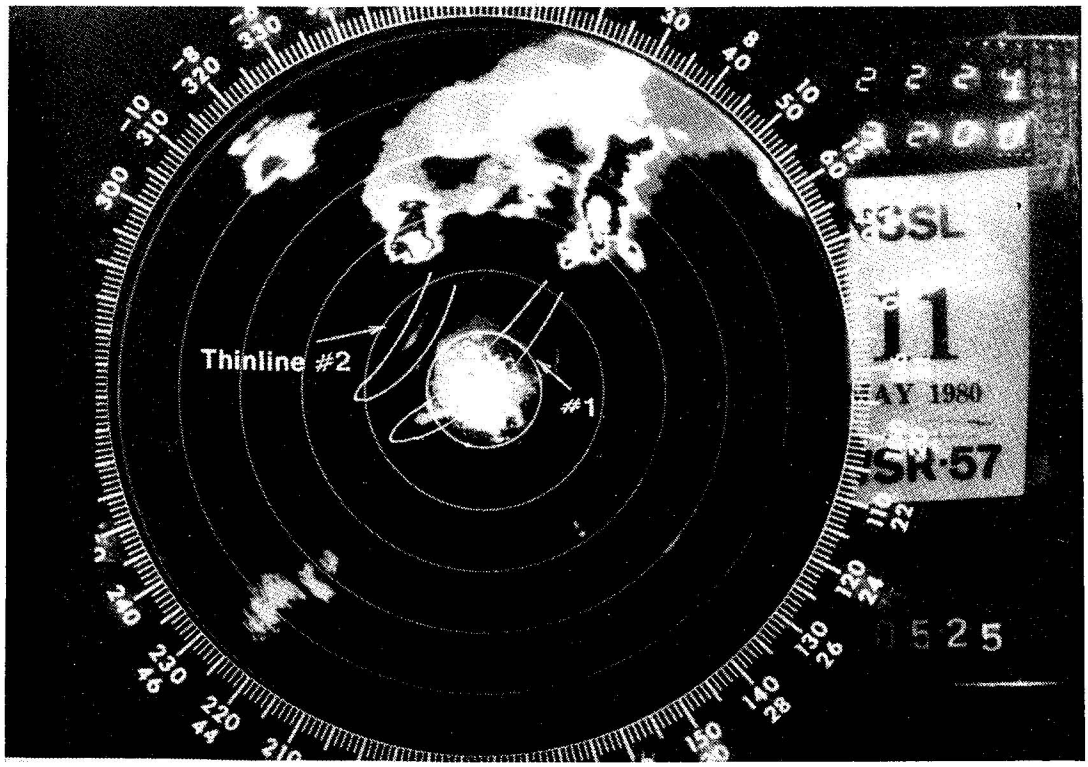

b. 2224 CST

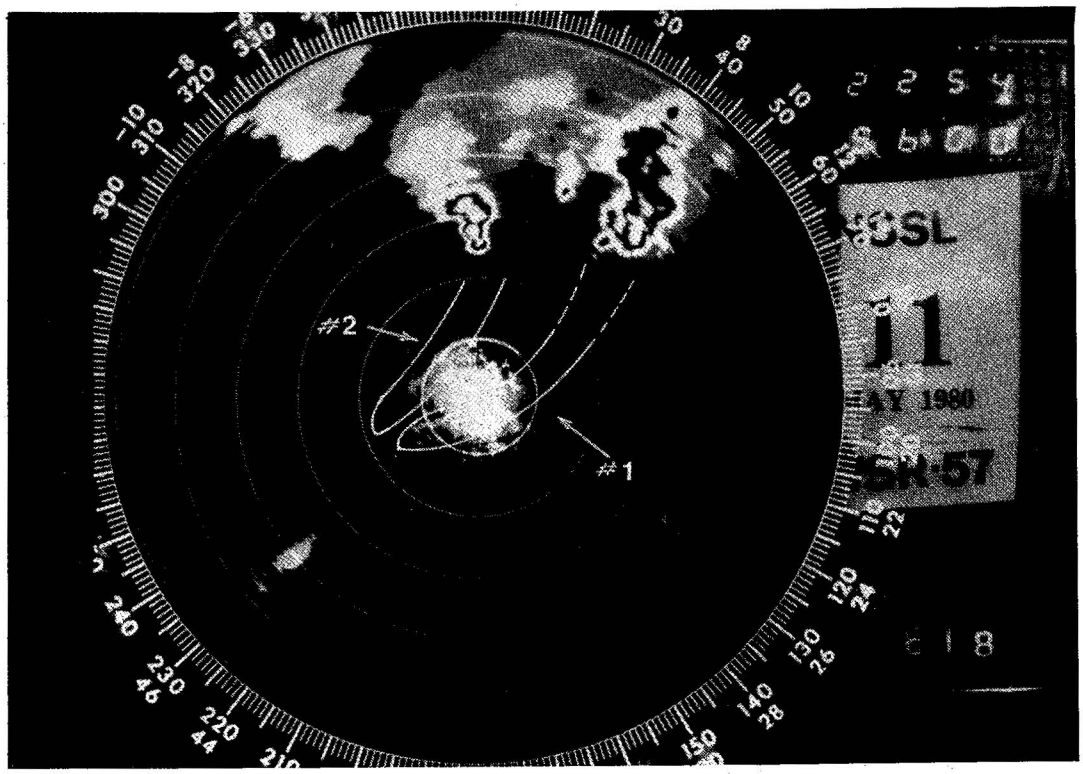

c. 2254 CST

Figure 6.1 WSR-57 radar photos for 11 May 1980 depicting two thin lines (gust fronts) associated with thunderstorm outflows. Range marks are every 40 kms.

6.5.2 Radar Observation Highlights

NRO was ready for data collection one hour after these Sunday evening storms developed. High PRF data were collected on a mesocyclone signature and possible tornado 90 km to the northeast. After a short period of storm cluster data collection in a broad sector to the north, CIM and NRO began coordinated sector scans on a north-south line of storms which extended to within 50 km north of NSSL. Hail chase was in this area, but encountered no hail. Some of the Doppler data appeared to be contaminated by overlaid echoes from stronger storms farther north. NRO began storm tracking on additional storms 100 km northwest which appeared to build southward. A gust front with northwesterly winds appeared to be imbedded in southerly flow well to the south of these storms.

6.5.3 Storm Electricity Highlights

Dual VHF mapping, SEB and 23-cm radar all operated but VHF data appeared to be uncorrelated because of the large range (75 km) of the storms. MEL intercepted a storm at Beggs, Oklahoma, about 2030 CST and observed two probable tornadoes between 2032 and 2058 CST.

6.5.4 Aircraft Operations

None

6.5.5 Mobile Ground Vehicle Observations

The NSSL 1 chase vehicle left NSSL at 1809 CST in pursuit of rapidly developing storms north of Oklahoma City. A flanking line funnel was seen briefly near Meeker, Oklahoma, at 1913. NSSL 1 was located three miles south of Junction 177/62 on 62. However, the chase team was never able to catch up with a mesocyclone to their ENE.

6.6 12 May; Monday

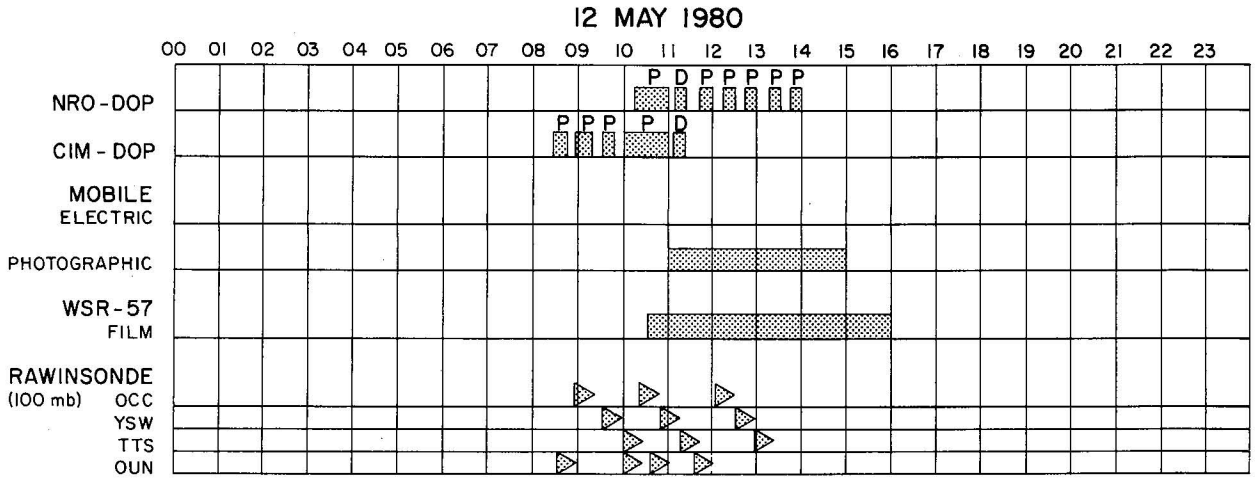

6.6.1 Forecasters' Outlook

Morning surface features included a cold front along the OK-KS border, a low near Ponca City and, in western Oklahoma, a dryline that moved into central Oklahoma by late morning. As on the previous day (see 5/11/80), morning rawinsonde data showed a very shallow layer of moisture in the boundary layer (60 mb depth of moisture at Oklahoma City).

Aloft, the flow was again southwesterly and strong. The leading edge of a very intense shortwave trough had already moved into western Texas by 0600 CST. The timing of this wave represented a problem for the later development of severe thunderstorms, i.e., the dynamic support seemed to be arriving before the time of best diurnal heating.

Towering cumulus began to develop along the dryline in central Oklahoma during the late morning hours. However, subsidence behind the shortwave, combined with mixing of the strong southwesterly flow at 850 mb, forced the dryline rapidly eastward. The event was observed by Doppler radar. The towers failed to build into strong Cb's until they had moved into much deeper moisture in northeastern Oklahoma, well out of the primary study area.

6.6.2 Radar Observation Highlights

CIM began a sequence of long pulse scans before passage of the dryline. NRO was temporarily delayed, but joined CIM in data collection while the dryline was close to Norman. The dryline appeared in the reflectivity field from 2-4 km height. A few showers developed and quickly weakened along the line as it passed over Norman. A general change in wind direction was clearly visible on radar from east to west. Speed shear and divergence were apparent after the dryline passed to the east.

6.6.3 Storm Electricity Highlights

None.

6.6.4 Aircraft Operations

None.

6.6.5 Mobile Ground Vehicle Observations

The chase team left NSSL at 1100 CST in pursuit of storms that developed just east of Moore, Oklahoma. However, these storms died rapidly. A line of towering cumulus was observed; however, these towers also dissipated. Storms to the northeast moved too rapidly to catch. Discouraged, the team returned to NSSL at 1500 CST.

6.7 15 May; Thursday

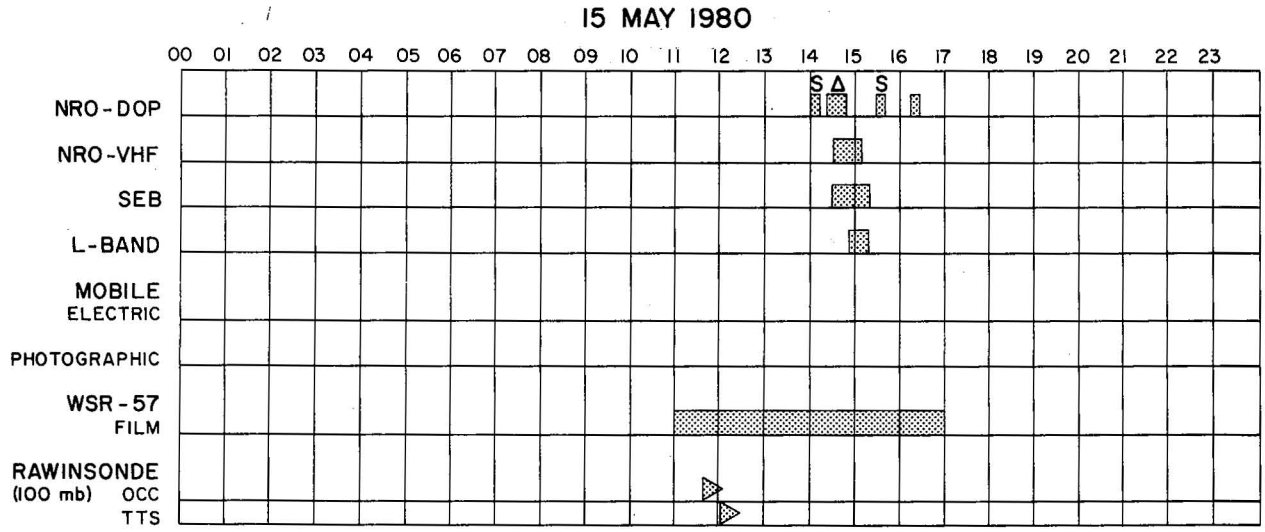

6.7.1 Forecasters' Outlook

On the morning of 15 May, an upper low was situated over central Arizona with a strong shortwave trough over northern Mexico. A surface low, over southwest Texas at 12Z, was forecast to deepen and move eastward along a stationary front stretching across central Texas. Severe thunderstorms were predicted for Texas, but not as far north as Oklahoma. During the day, rain and thundershowers were common across Oklahoma in the area of lifting north of the surface low. The only severe weather reported was in southern Texas.

6.7.2 Radar Observation Highlights

Single Doppler (NRO) data showed no exciting storm activities.

6.7.3 Storm Electricity Highlights

Norman VHF mapping, SEB, and L-band operated for a short period, but activity was minimal.

6.7.4 Aircraft Operations

U-2 flew an afternoon mission, arriving in the Oklahoma area near 1515 CST. Some thunderstorm activity was in the state, but lightning activity was very low. Thunderstorm activity was better developed far to the south so the aircraft left the area to intercept thunderstorms in the Austin, Texas, area.

6.7.5 Mobile Ground Vehicle Observations

None.

6.8 17 May; Saturday and
18 May; Sunday, a.m.

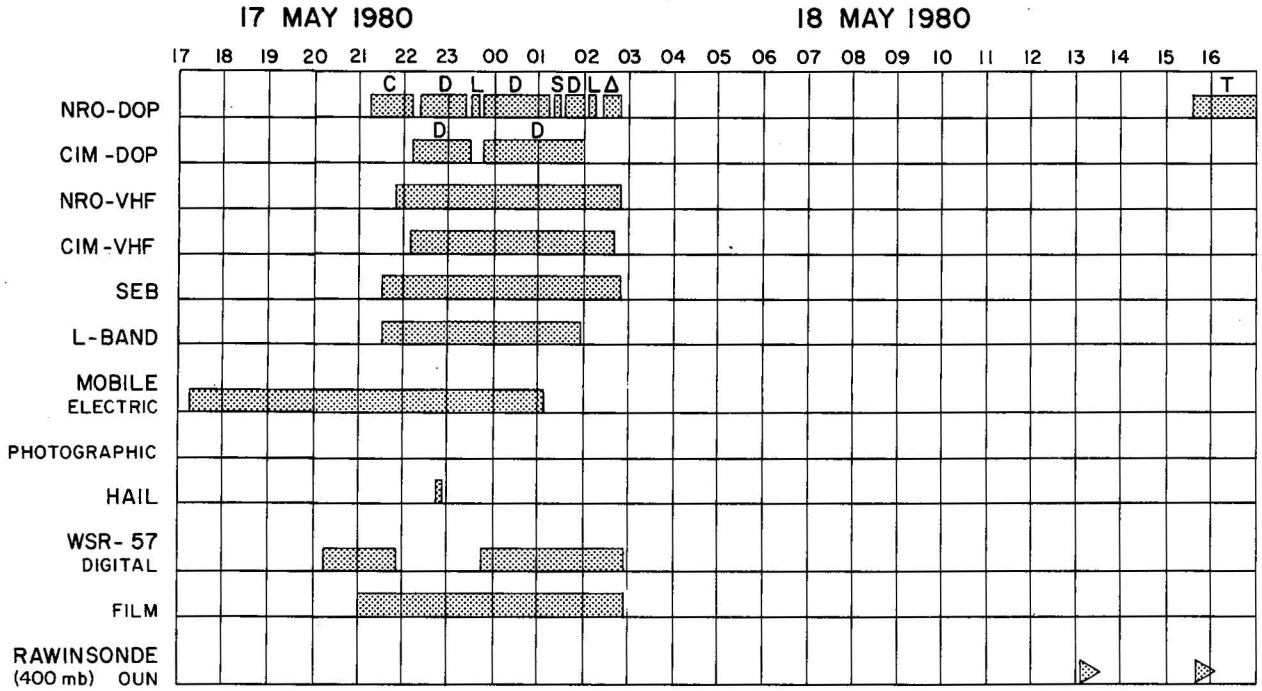

6.8.1 Forecasters' Outlook

Morning upper air charts found a strong upper disturbance moving toward Oklahoma from northwestern Colorado. Numerical guidance indicated that this system would be entering northwestern Oklahoma by 1800 CST.

A surface low, which had been in central Colorado in the morning, dropped into the northeastern corner of New Mexico, then began tracking slowly eastward. Meanwhile, an E-W oriented convergence boundary formed from the low eastward across western and central Oklahoma. Late afternoon found a low east of Dalhart, Texas, with a quasi-stationary front stretching eastward to Gage, Oklahoma, and on to Fort Smith, Arkansas.

By 1700 CST, when thunderstorms had not yet formed in the area of interest, it was decided to shut down with only informal monitoring of the situation. At approximately 2000 CST, a student assistant phoned the nowcaster to report a very intense storm entering western Oklahoma and traveling to the ESE. This meant the storm was apparently moving along the front and would probably remain intense.

Operations began at about 2115 CST. Several lines of storms moved rapidly eastward. The activity produced wind damage near Hammon, Oklahoma, and numerous other reports of severe weather. A gust front passed through Will Rogers World Airport and was monitored by the FAA's LLWSAS and meteorological instrumentation on the KTVY tower. Gusts to 50 knots were reported. Hail chase 1 and 2 successfully collected simultaneous hail samples (maximum diameter, 2 cm) at two locations from a storm near Union City, Oklahoma.

6.8.2 Radar Observation Highlights

NRO collected storm cluster data on storms 140 km to west. Dual Doppler-radar data began as storms produced hail (collection by two vehicles at 2241), but storms were near baseline. Reflectivity was greater than 67 dBZ, and a pronounced gust front was noted with velocity >23 m/s. As the storm system passed Norman, an attempt was made to record lightning overhead (Drop Levitation Experiment). Dual Doppler-radar data were recorded on two subsequent storm systems, which passed through the northern lobe of the acquisition area. No hail was collected with these storms; however, they were accompanied by vivid cloud-to-ground lightning activity. Drop levitation data were recorded as the final storm system passed overhead.

6.8.3 Storm Electricity Highlights

Good data were recorded on several storms with dual VHF mapper, SEB equipment, and 23-cm radar. Levitation and 10-cm echo experiments were conducted with apparently good correlation between the radar and VHF mapping. Some of the storms that moved through the observation area were initially tracked by the MEL as they formed in the Texas Panhandle. Some lightning optical transient data were obtained with the NOSL system (space shuttle instrumentation).

6.8.4 Aircraft Operations

None

6.8.5 Mobile Ground Vehicle Observations

Hail chase observations detailed above.

6.8.6 Other Comments

Will Rogers World Airport wind system (LLWSAS) recorded and KTVY tower system recorded at a 1-second sample rate to observe a 2300 CST gust front passage.

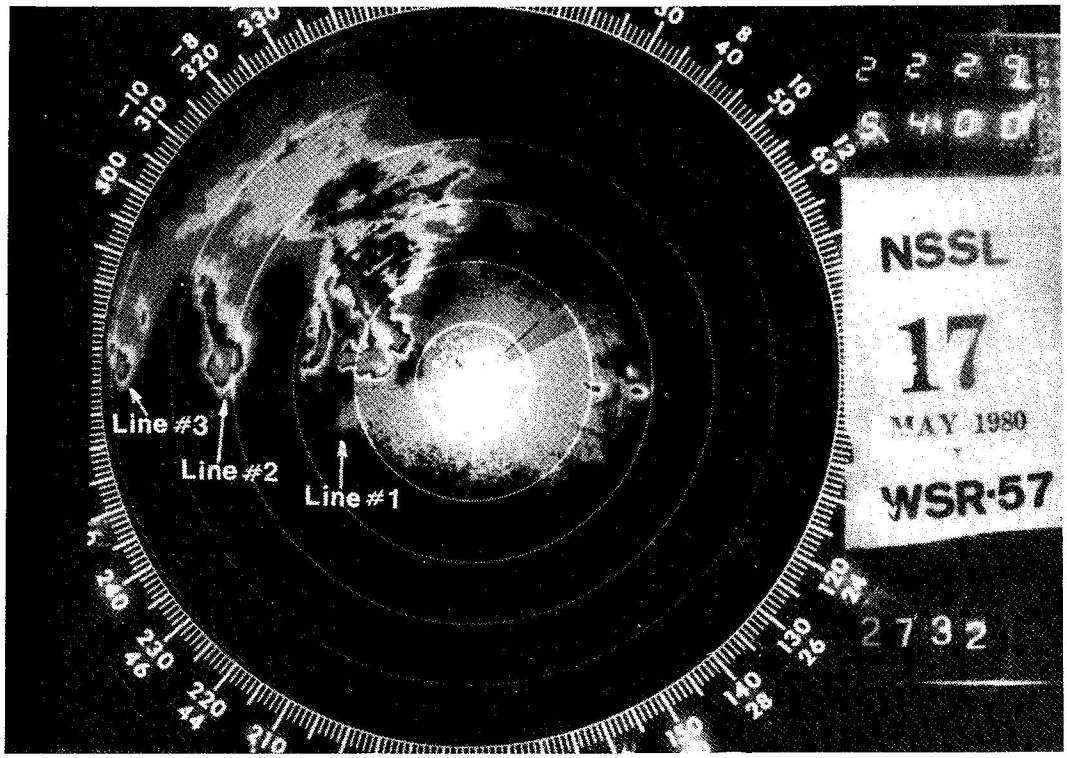

a. 2229 CST

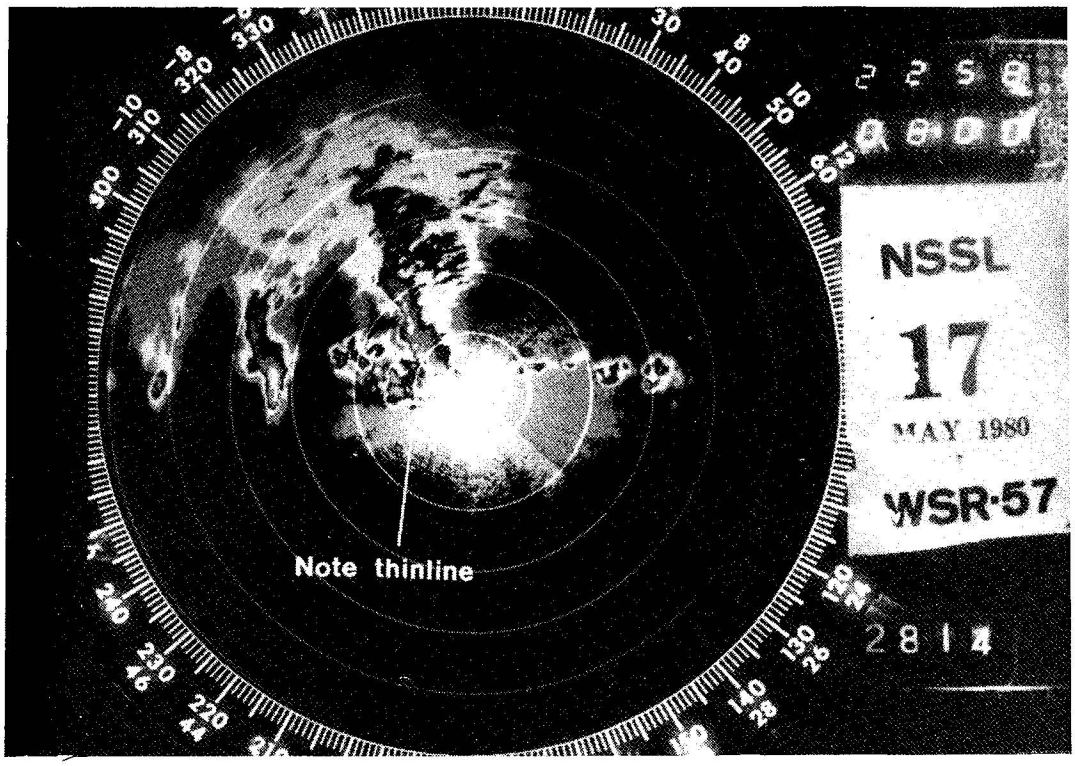

b. 2258 CST

Figure 6.2 WSR-57 radar photos for 17 May 1980 showing three equally spaced lines of thunderstorms which moved rapidly (≈ 70 km/hr) eastward. Range marks are every 40 kms.

6.9 18 May; Sunday, p.m.

6.9.1 Forecasters' Outlook

Mild positive vorticity advection aloft interacting with a southeastward moving cold front kept weak-to-moderately strong thundershowers alive throughout the day. The front (and shower activity) at dawn was situated on a Tulsa-Norman-Fort Sill, Oklahoma, line and moved to a Fort Smith, Arkansas - Ardmore, Oklahoma, line by nightfall. There was no severe weather reported in Oklahoma during the period.

6.9.2 Radar Observation Highlights

NRO recorded tilt sequences on moderate storms 150 km to the south in support of the T-28 aircraft penetrations.

6.9.3 Storm Electricity Highlights

None.

6.9.4 Aircraft Operations

The T-28 took off at 1524 CST and proceeded south of Norman to a group of thunderstorms about 130 km away. The first penetration was aborted as the cell intensity in the flight path increased to more than 50 dBZ. The T-28, then flying at 10,000 ft MSL, made two north-south penetrations just west of the maximum reflectivity associated with the storm complex's westernmost cell. Light-to-moderate turbulence was reported. A second series of penetrations was made just to the east of the maximum reflectivity. On these two north-south penetrations, the aircraft also experienced moderate turbulence.

6.9.5 Mobile Ground Vehicle Observations

None.

6.10 19 May; Monday

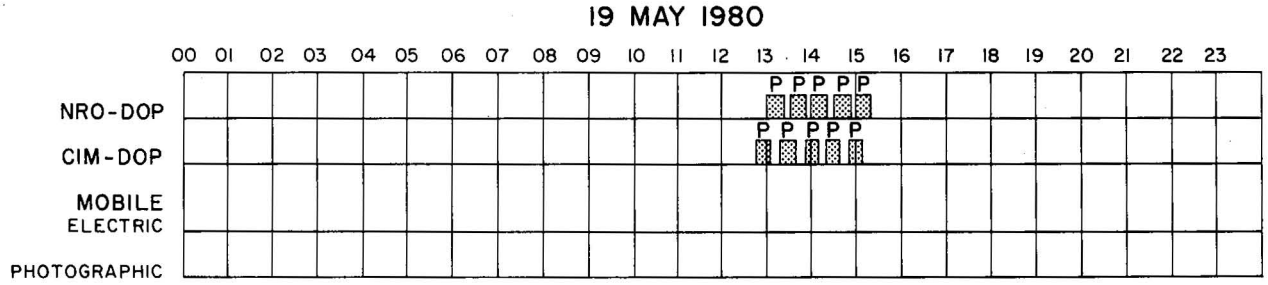

6.10.1 Forecasters' Outlook

Weather in the southern plains was dominated by northwesterly flow aloft following the passage of a significant shortwave during the night of 18 May. A surface high pressure area, initially in Colorado, was forecast to move to central Oklahoma by evening. The surface high provided relatively cool and dry air to the area of interest. Thus, a stable airmass and subsidence aloft prohibited storms or significant cloud activity.

6.10.2 Radar Observation Highlight

Long pulse data were collected; however, no storms developed. A band of minimum reflectivity near ground seemed to correspond with an area of restricted heating caused by high level cloud.

6.10.3 Storm Electricity Highlights

None.

6.10.4 Aircraft Operations

None.

6.10.5 Mobile Ground Vehicle Observations

None.

6.11 20 May; Tuesday

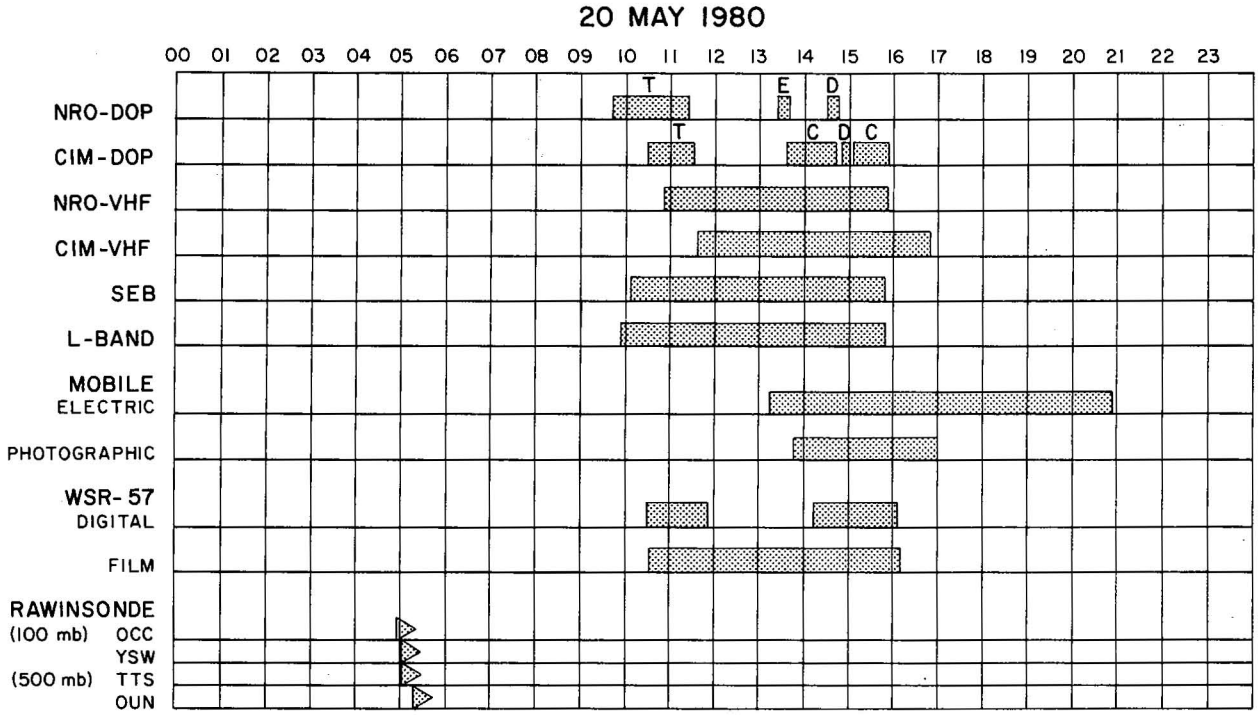

6.11.1 Forecasters' Outlook

The previous day's data had suggested that central Oklahoma would be between two moderately intense shortwaves on the morning of the 20th, one in eastern Oklahoma and the other in southern Nebraska. Furthermore, a surface front had swept through the state (into southern Texas) leaving Oklahoma beneath surface high pressure. Thus, a clear-air PBL experiment was planned.

The morning of the 20th did find a surface high over the region. However, the upper air pattern did not occur as expected. Instead, a strong shortwave trough entered western Oklahoma near dawn, bringing a round of early morning thundershowers. The activity forced cancellation of the PBL experiment.

6.11.2 Radar Observation Highlights

Data collection included both NRO and CIM on light thunderstorm activity probed by aircraft. Lightning echo data were recorded later with these storms.

CIM did a Storm Cluster Experiment on precipitation 250 km to the west. The data collection was interrupted for dual Doppler-radar support of the Hail Collection Experiment at 100 km SW (hail was not collected).

6.11.3 Storm Electricity Highlights

Very good dual VHF mapping correlation with good SEB and 23 cm radar data. MEL in SW Oklahoma observed positive cloud-to-ground lightning out of the anvil part of a storm.

6.11.4 Aircraft Operations

The T-28 took off at 0945 CST to intercept thunderstorms 80 km west of Norman. The first penetration was at 12,000 ft MSL through a storm with 45 dBZ maximum reflectivity. Light to moderate turbulence was encountered and one-half inch of ice built up on the wings. A penetration on a return heading resulted in a similar report. The aircraft was then placed at 14,000 ft MSL, and the penetration at this altitude was characterized as having moderate turbulence and 6 $m \cdot s^{-1}$ updrafts and downdrafts. Icing was still a problem, and the aircraft altitude was lowered to 10,000 ft MSL to allow the ice to melt. The fourth and last penetration for the day also encountered moderate turbulence.

6.11.5 Mobile Ground Vehicle Observations

The Intercept Team left NSSL at 1346 CST, arrived at Hinton at 1502 CST, and returned to the laboratory at 1700 CST. Storms weakened as they moved into a "bubble high", and nothing of note was observed.

6.12 23 May; Friday

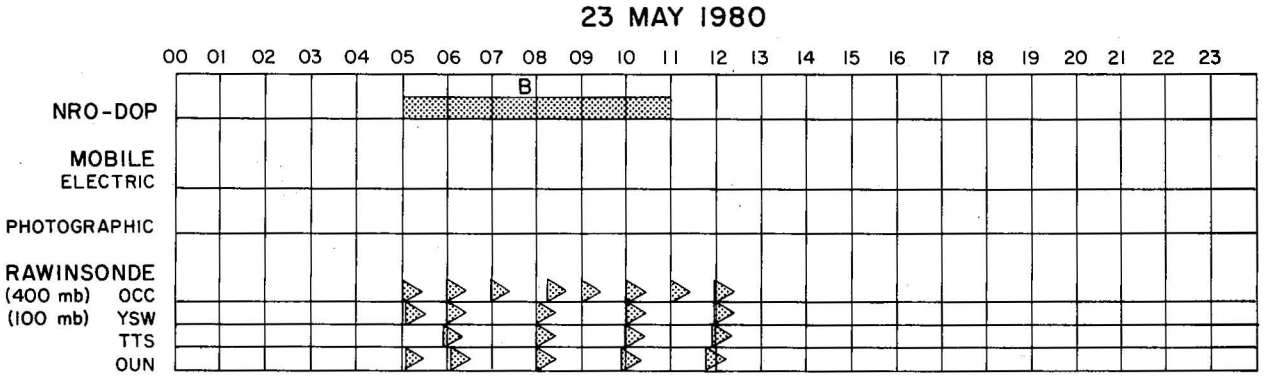

6.12.1 Forecasters' Outlook

Oklahoma lay beneath generally subsiding air to the west of a northeastward moving, upper, low-pressure center. High pressure dominated at the surface. A PBL Experiment was begun, but had to be terminated early (~1000 CST) because of the appearance of a midlevel cloud deck and a few very light rain showers over a small portion of central Oklahoma. No explanation for the small cloud patch could be found within the resolution of available data.

6.12.2 Radar Observation Highlights

Data were collected at NRO for the PBL Experiment. Unfortunately, middle cloud reduced the heating rate, perhaps limiting the growth of the PBL. In any case, the height of the mixed layer could not be ascertained from real-time data.

6.12.3 Storm Electricity Highlights

None.

6.12.4 Aircraft Operations

None.

6.12.5 Mobile Ground Vehicle Observations

None.

6.13 28 May; Wednesday

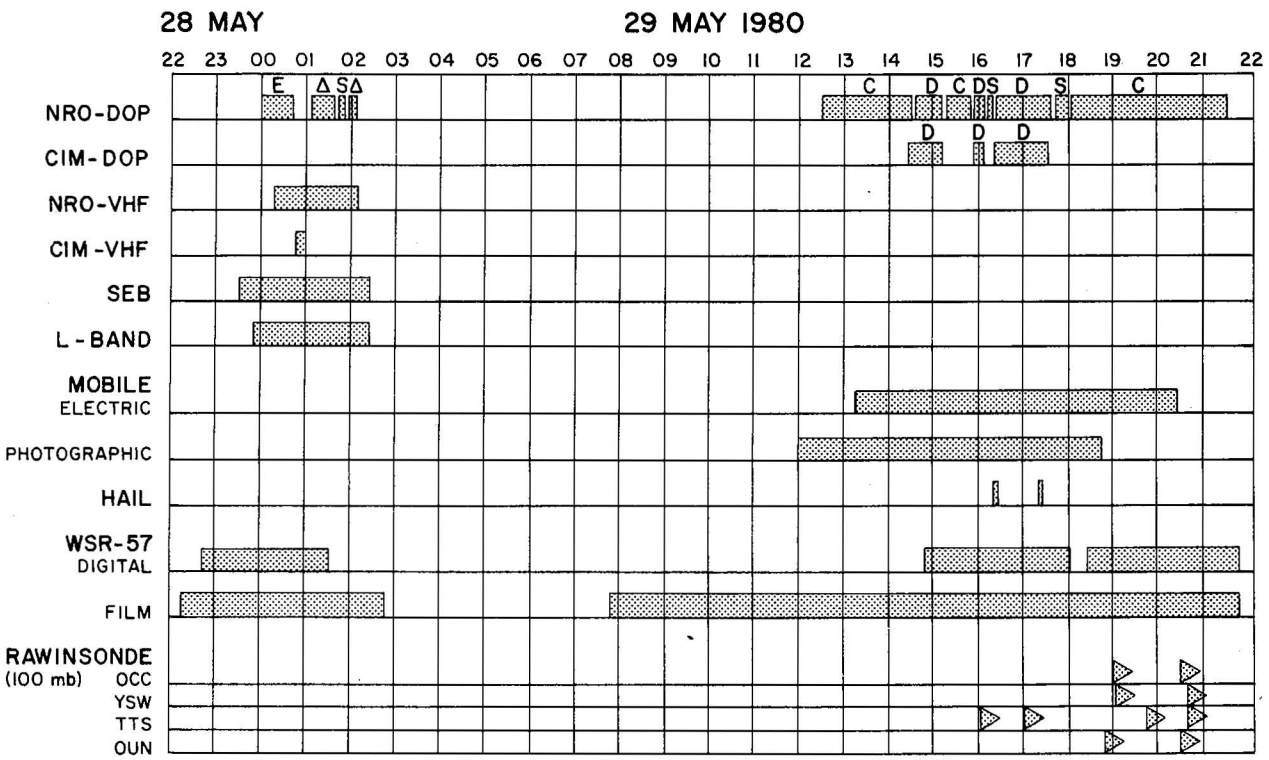

6.13.1 Forecasters' Outlook

A shortwave trough aloft was passing through Oklahoma during the early morning of 28 May with weak thundershowers. An apparently weak upper air disturbance was upstream, but far to the west (12Z position over Arizona and northern Mexico).

The low-level flow was southerly ahead of a dryline in eastern New Mexico, and moist air advection was expected during the day in west Texas and Oklahoma. Although conditional instability of the airmass was present (lifted index of -9 at Amarillo and -7 at Oklahoma City), subsidence aloft during the afternoon was forecast to prevent storm formation over the data collection region. Severe thunderstorms were probable, however, in the western Texas Panhandle near the afternoon position of the dryline.

There was no afternoon activity in Oklahoma, and severe thunderstorms did form along the Texas-New Mexico border by midafternoon. The activity was quite strong during the late afternoon in the Texas Panhandle with severe tornadoes reported.

Evening analyses revealed that the upstream shortwave was farther northeast and stronger than expected. The forecast was revised to include potentially severe thunderstorms moving into western Oklahoma by 2100 CST, and employees were put on standby.

Surveillance indicated tornadic storms entering western Oklahoma at 2030 CST, and the decision was made to call data collection personnel to work. Doppler radar operations began after midnight (a.m. of 29 May) as thunderstorm activity affected the central part of the state. Some of these storms produced very strong straightline winds and hail southwest of Norman.

6.13.2 Radar Observation Highlights (28 May - 29 May a.m.)

Collection began on early morning storms 90 km to the west. Lightning echo data were followed by single Doppler-radar scans at NRO of approaching storms and gust front.

6.13.3 Storm Electricity Highlights (28 May, p.m. - 29 May, a.m.)

None.

6.13.4 Aircraft Operations

None.

6.13.5 Mobile Ground Vehicle Observations

None.

6.13.6 Other Comments

KTVY tower recorder set for 1-second data rate at 0630 CST. Thunderstorm passage at Oklahoma City occurred at 0700 CST.

6.14 29 May; Thursday

6.14.1 Forecasters' Outlook

Morning 500 mb analysis found strong southwesterly flow aloft with two significant shortwave troughs embedded in the flow. The first wave extended from western Nebraska into central Oklahoma and helped produce strong thunderstorms in eastern Oklahoma during the morning. The second wave, situated from eastern Utah into southwestern New Mexico, was tracking ENE at 20 $m \cdot s^{-1}$ and forecast to trigger afternoon convection in western Oklahoma.

At the surface, a low in northeastern Colorado was moving slowly eastward. A dryline stretched southward from the low across western Texas. Winds ahead of the trough were southeasterly, those behind westerly-southwesterly. The morning convection had left most of Oklahoma affected by a thunderstorm meso-high. By noon, winds had veered back to the SSE in western Oklahoma, while those in the remainder of the state were from the north and east. The result was a region of surface convergence in western Oklahoma and the eastern Texas Panhandle.

Rawinsonde data from Oklahoma City were thunderstorm affected, but data from Amarillo and Stephenville, Texas, suggested a great deal of instability was present in the atmosphere (Lifted Index of -9 and -6, respectively).

Thunderstorms formed just before noon near Childress, Texas, and by mid-afternoon a complex covered large portions of southwestern Oklahoma. The activity produced several severe-weather reports during the afternoon across southwest and southern Oklahoma. A second storm complex formed in late afternoon along the stationary dryline in the eastern Texas Panhandle. As it moved eastward, the second complex became even more severe than the previous one with tornadoes striking Wellington, Texas, at 1640 CST, Altus, Oklahoma, at 1928 CST and near Vernon, Texas, at 2300 CST.

6.14.2 Radar Observation Highlights

NRO performed the cluster experiment on storms 250 km to the west shortly after noon. Dual Doppler-radar data were collected on a small storm that formed 60 km NW. More storm cluster experiments were performed on storms 100 km to SW, one of which had a mesocyclone. Later, these storms were covered by dual Doppler-radar scans while the storms passed to the south (hail was collected on two occasions). Finally, strong storms farther to the SW (200 km) were tracked as they moved SE. Mesocyclone signatures were noted on three storms.

6.14.3 Storm Electricity Highlights

Some reasonably good data were obtained from SEB equipment and 23-cm radar. Possible good dual VHF mapping (Cimarron) station could not record elevation angles), SEB and 23 cm radar data were obtained on 29 May. MEL observed Altus storm on 29 May.

6.14.4 Aircraft Operations

None.

6.14.5 Mobile Ground Vehicle Observations

The crew intercepted the southern end of a line of thunderstorms near Randlett, Oklahoma, and saw a tilted, needle-like funnel emanating from a shelf cloud at 1516 CST (14 miles south of Walters Exit on H.E. Bailey Turnpike). NSSL 1 followed this line, which appeared to be weakening rapidly, as it moved eastward. Their impressions were confirmed by a phone call to NSSL from Waurika at 1619 CST. However, on the way home, the chase team had a surprise encounter with a mesocylone (1745-1757 CST) about 8 miles NNW of Davis as they were leaving the Arbuckle mountains. Owing to limited visibility, NSSL 1 did not see a wall cloud to their northwest until they were just about to enter a precipitation shaft to their north. They experienced 30-45 knot westerly winds, which shifted to strong easterlies as they traversed the mesocyclone (7 miles N to 12 miles N of the Davis Exit on I-35). The mesocyclone core contained no hail, but extremely heavy rain; the visibility was so poor that vehicles were crawling along the Interstate at 5 mph. Near the mesocyclone's edge, the rain was striated and atomized by the strong winds. Because of flash flooding, the team decided to stay on the elevated interstate highway rather than pursue the mesocyclone. A new and intense storm had developed in the Wellington, Texas, vicinity, but since this could not be intercepted before dark, the team came home.

6.15 30 May; Friday

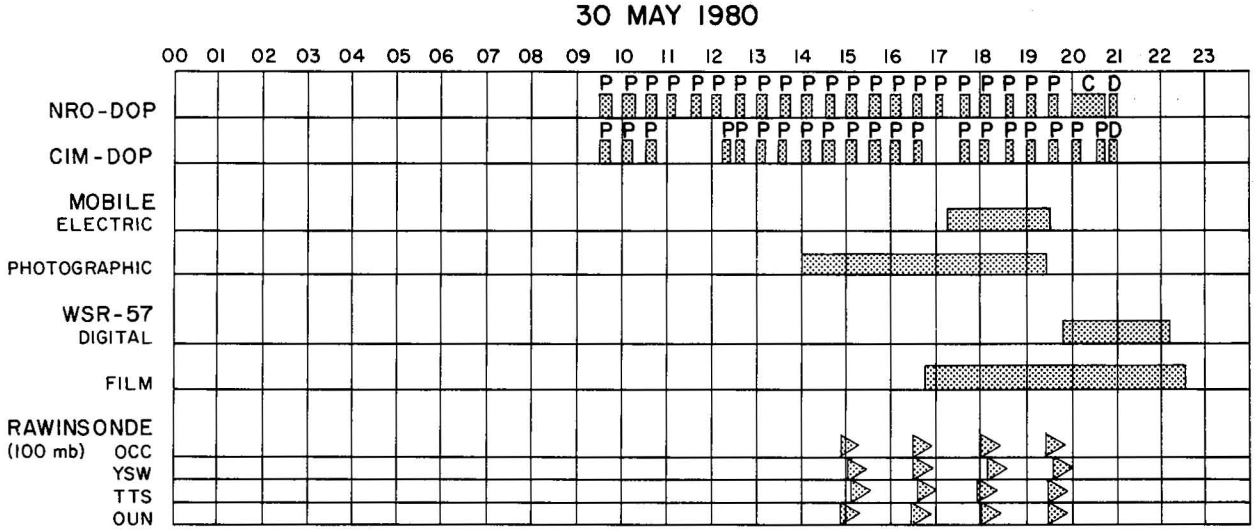

6.15.1 Forecasters' Outlook

A warm front stretched northeastward across central Oklahoma from a weak surface low in southwestern portions of the state. Morning sounding data revealed a conditionally unstable air mass, with a lifted index of (-9) given an afternoon temperature of 88°F. Aloft, a weak-moderate shortwave trough was approaching the state from the west. The morning data made it seem an ideal prestorm case with echoes expected to form in central Oklahoma by midafternoon.

Unfortunately, the expected strong development did not occur. Convergence along the surface front reduced with time as the front "washed-out" during the afternoon, the weak surface low disappeared, and 1°-2°C warming occurred between 700 and 500 mb. The only strong storms in Oklahoma formed in eastern and southwestern portions of the state. Convection was not initiated in central Oklahoma and storms that formed in southwest Oklahoma were isolated and died as they advected into the area of interest.

6.15.2 Radar Observation Highlights

Long-pulse data collection began in the morning. A warm front was discernible as an east-west line of weak echoes (~0 dBZ) 400 km long. Areas of deep convection were noted in the afternoon. Subsequent thundershowers developed to the NE, moved east and intensified. NRO began the storm cluster experiment as strong storms moved into SW Oklahoma. Some dual Doppler-radar scans were recorded as storms weakened.

6.15.3 Storm Electricity Highlights

MEL went to near Vernon, Texas, with L-band data for support.

6.15.4 Aircraft Operations

None.

6.15.5 Mobile Ground Vehicle Observations

NSSL 1 stopped near Elgin, Oklahoma, from 1520 to 1625 CST and saw abnormally rapid west-to-east motion of the cirrus and altocumulus overhead (the movement readily apparent to the naked eye). The team passed some towering cumulus near Faxon at 1740 CST. These clouds were being torn apart by the winds before they could develop into a thunderstorm. NSSL 1 finally intercepted a storm near Vernon, Texas, at around 1900 CST. They passed a flanking line on the storm's north side, but decided to penetrate the core and take a look at the storm's southwest flank. This turned out to be a poor decision since they were not in position to see the storm split. The left-mover proceeded toward Frederick, Oklahoma, and produced funnel reports, while the right-mover dissipated in the Vernon area as the crew watched.

6.16 3 June; Tuesday

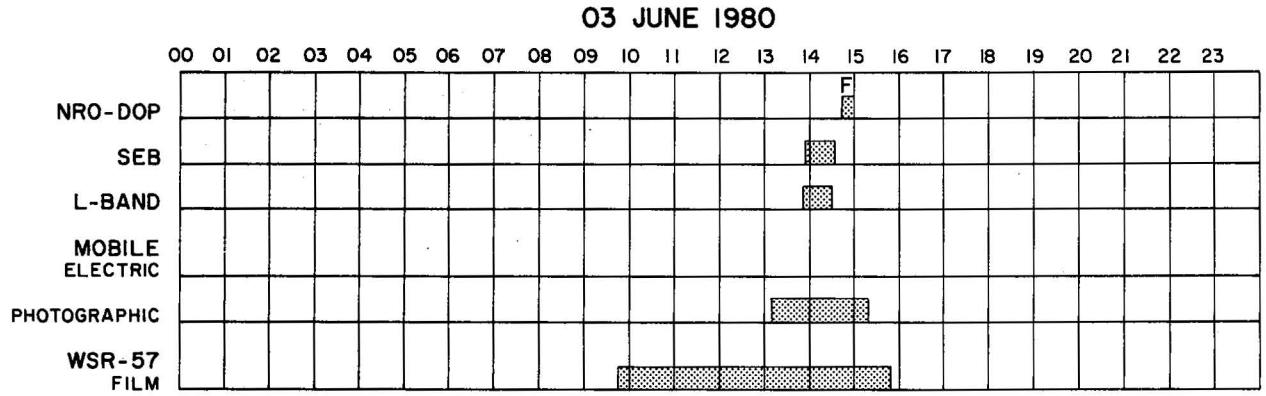

6.16.1 Forecasters' Outlook

Surface flow in Oklahoma and northward was mildly convergent as low-level air moved toward a lee trough stretching from eastern Colorado to southwestern Canada. Winds aloft were southwesterly over the western United States with several short-waves identifiable on morning analyses.

Thunderstorms formed from Oklahoma to North Dakota. The activity in Oklahoma was weak and high-based because of a developing temperature inversion between 850 and 700 mb.

6.16.2 Radar Observation Highlights

A WSW-ENE line of midlevel-based convection with reflectivity less than 47 dBZ was penetrated by the F-106. NRO collected time series data in the vicinity of the aircraft.

6.16.3 Storm Electricity Highlights

Short observations were made with SEB and 23-cm radar only.

6.16.4 Aircraft Operations

An F-106 flew two penetrations at 22,000 ft MSL through a weak (25 dBZ) storm 40-50 km east of Norman during the period 1420-1520 CST. Only light turbulence was reported, and no lightning was sighted.

6.16.5 Mobile Ground Vehicle Observations

The air mass in central Oklahoma was not conducive to convection. Nevertheless, the chase team went out to practice taking movies. Their time lapse film (from near Lindsay from 1407 to 1422 CST) of a shallow, laminar, midlevel cloud with a partly cumuliform top revealed progressive wave motion visible in the rising and sinking of individual cloud turrets along the cloud line.

6.17 4 June; Wednesday

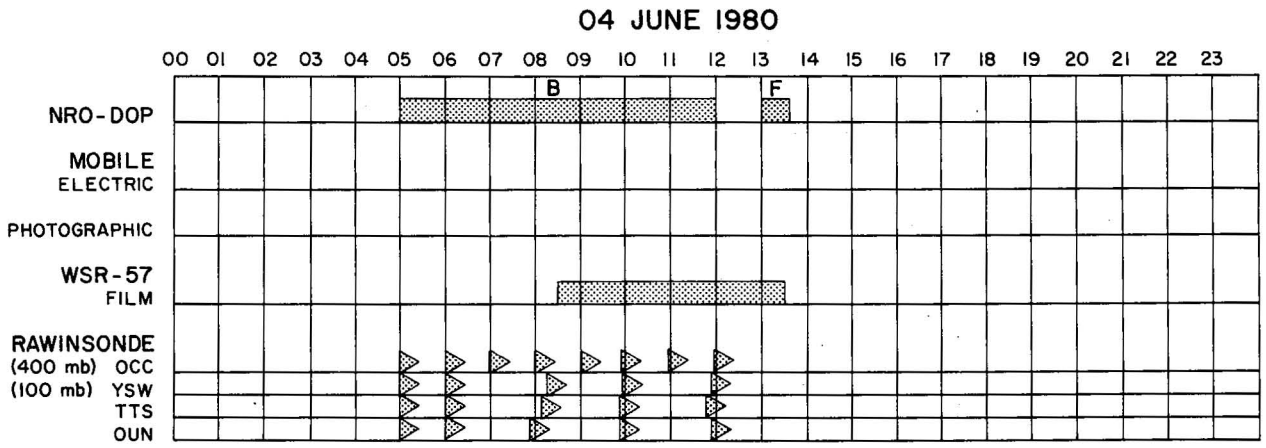

6.17.1 Forecasters' Outlook

Upper air ridging at lower latitudes was becoming stronger by the day. Morning sounding data from Oklahoma City indicated that a capping inversion between 800 and 600 mb would not mix out during the day. Shortwaves were mostly passing north of the state, but Oklahoma continued to be "brushed" by the southern end of stronger waves.

The operational day began early with a PBL experiment. The early portion of the experiment was marked by clear skies (except for scattered thin cirrus), but by the end of the morning, midlevel-based convection developed in central Oklahoma. However, the activity remained small scale and very scattered and, thus, solar heating did not appear to be significantly reduced.

Data collection continued into the early afternoon in support of aircraft operations.

6.17.2 Radar Observation Highlights

Normal pulse data were recorded at NRO for the PBL study. Scattered midlevel convection appeared before noon. One cell that developed over the surface network was accompanied by cloud-to-ground lightning and virga. As it moved east, the aircraft made some penetrations where reflectivity was 36 dBZ and shear was highest. NRO collected time series data.

6.17.3 Storm Electricity Highlights

None.

6.17.4 Aircraft Operations

The F-106 flew between 1300 and 1400 CST and made five penetrations at 20,000 ft MSL through storms 50 km NE of Norman. Only light turbulence was encountered, and lightning did not strike the aircraft.

6.17.5 Mobile Ground Vehicle Observations

None.

6.18 6 June; Friday

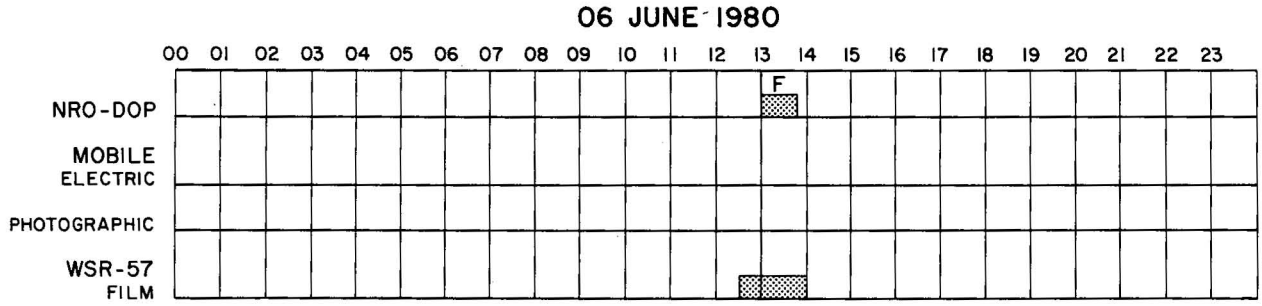

6.18.1 Forecasters' Outlook

As the westerlies receded northward, they left Oklahoma to the south of the subtropical jet stream, a region of subsiding air. The 500 mb jet ran from southern California to Iowa. Severe thunderstorms were forecast with the passage of shortwaves in the central plains and upper Mississippi Valley. Although low-level moisture was abundant over Oklahoma, no triggering mechanism was available as the upper subsidence produced a strong capping inversion (OKC 700 mb temperature at 12Z was 17°C). Clear skies and warm temperatures were forecast and verified).

6.18.2 Radar Observation Highlights

None.

6.18.3 Storm Electricity Highlights

None.

6.18.4 Aircraft Operations

The F-106 was flown on an instrument check flight, which included a coordinated 5000-ft MSL flight along a radial toward the Doppler radar for comparison of Doppler and aircraft winds (i.e., Turbulence #2 Experiment). The aircraft made three runs by the KTVY-TV tower at top-of-tower height to compare aircraft temperature and wind observations with those recorded at 1-second intervals at the tower.

6.18.5 Mobile Ground Vehicle Observations

None.

6.19 8 June, Sunday

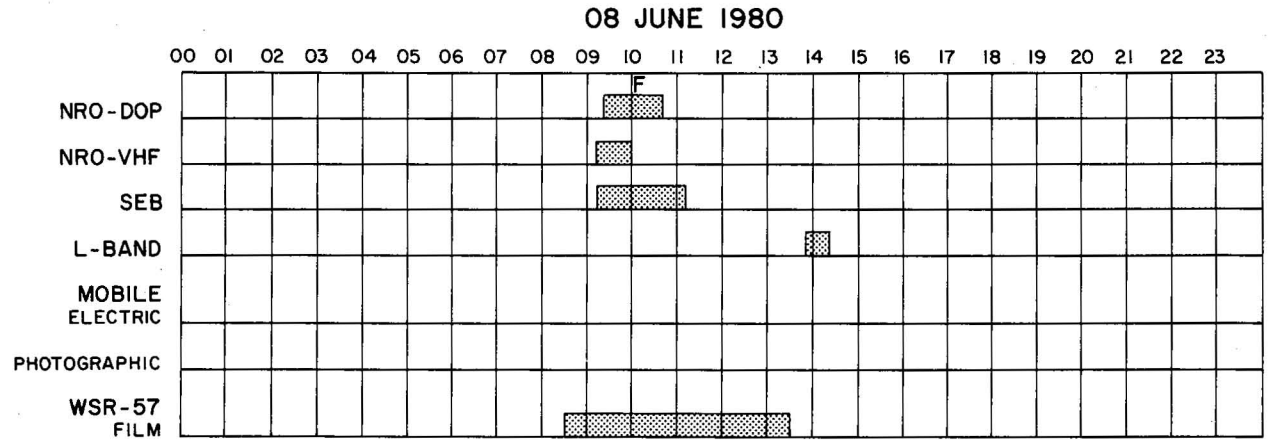

6.19.1 Forecasters' Outlook

A cold front had pushed through Oklahoma on the previous evening and by the morning of the 8th was south of the Red River. A small shortwave, sweeping around the west side of the upper ridge brought a round of early morning showers and thundershowers. Operations were conducted until about midmorning in support of aircraft experiments.

6.19.2 Radar Observation Highlights

A NW-SE line of thundershowers (46 dBZ maximum) was monitored to the south. NRO sector scans covered the area of best lightning at 80 km SE. Time series data were recorded in vicinity of aircraft penetrations.

6.19.3 Storm Electricity Highlights

Norman VHF mapper SEB equipment and 23-cm radar were operated, but data are poor.

6.19.4 Aircraft Operations

The F-106 made one flight from 0945 to 1000 CST. The first penetration of a storm at 120°/50 km, made at an altitude of 20,000 ft MSL, reported moderate turbulence. The second penetration was made at 23,000 ft MSL with only light turbulence encountered. The remaining two penetrations were made at 20,000 ft MSL. Light turbulence characterized these runs and there were no lightning strikes to the aircraft.

6.19.5 Mobile Ground Vehicle Observations

None.

6.20 9 June; Monday

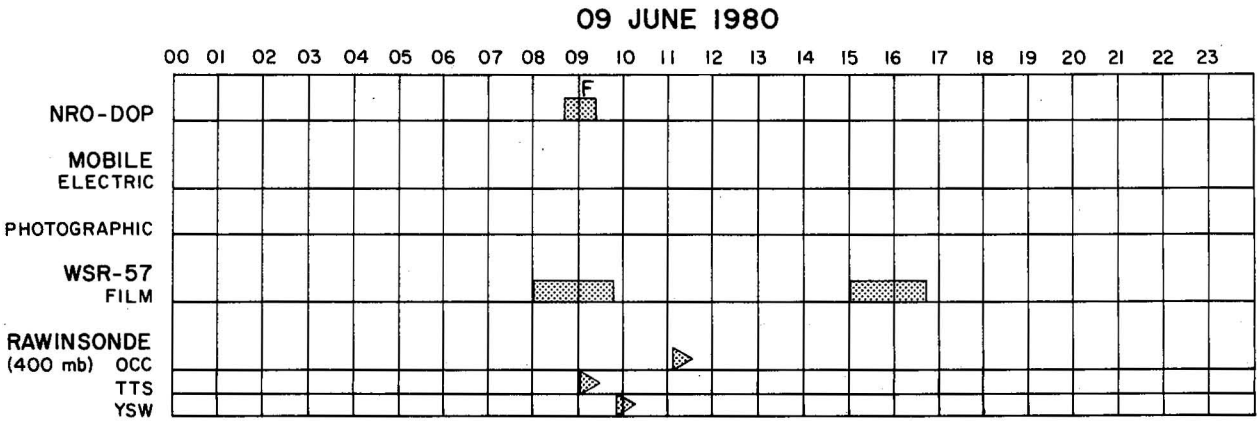

6.20.1 Forecasters' Outlook

Another round of exceptionally weak overrunning showers occurred in central Oklahoma at dawn. The activity moved into southeastern Oklahoma by 0900 CST.

6.20.2 Radar Observation Highlights

Light precipitation (generally less than 36 dBZ) was penetrated by aircraft about 150 km to the southeast of Norman. NRO collected time series data.

6.20.3 Storm Electricity Highlights

None.

6.20.4 Aircraft Operations

Two F-106 flights were made; one at 0835-0935 CST and the second at 1530-1630 CST. The pilot was seeking storm locations where lightning strikes to aircraft would be likely. On the first flight, two penetrations were made at 13,000 ft MSL on a storm 130°/70 km. Turbulence and lightning were not encountered, and the aircraft returned to base station. The second flight intercepted a thunderstorm at 285°/70 km. One penetration was made at 13,000, two at 14,000, and one at 23,000 ft. No lightning strike occurred, and turbulence was only light.

6.20.5 Mobile Ground Vehicle Observations

None.

6.21 11 June; Wednesday

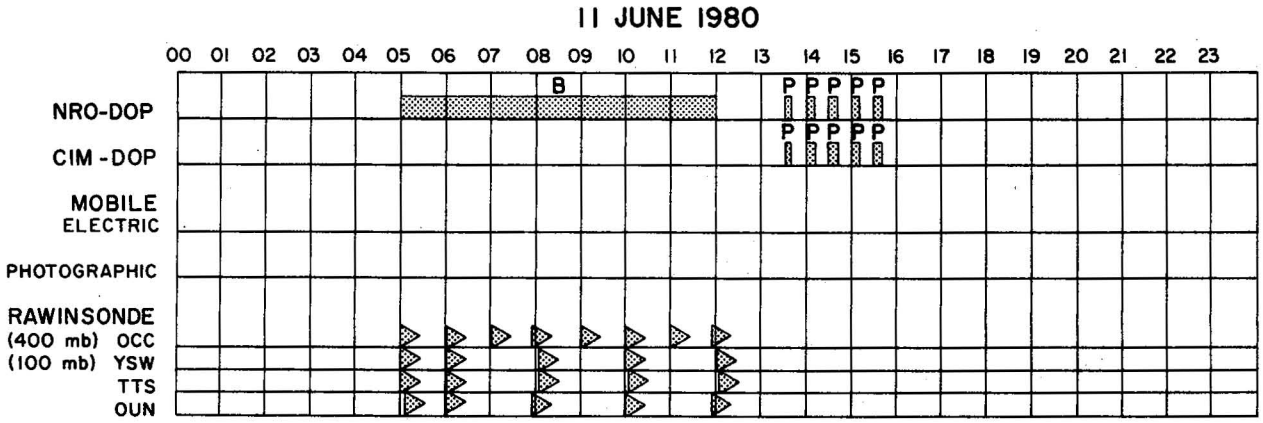

6.21.1 Forecasters' Outlook

An upper ridge continued to dominate Oklahoma weather. Shortwave disturbances that survived the effects of the ridge were unable to support precipitation of any sort and, instead, revealed themselves over the region only as patches of cirrus clouds.

On the early morning of the 11th, a broken-to-overcast deck of cirrus clouds threatened to interfere with a PBL experiment in progress, but the clouds moved off by 0800 CST and the experiment continued.

6.21.2 Radar Observation Highlights

PBL experiment data were collected in the morning. The RHI mode was employed. Some long-pulse data collected in the afternoon revealed some areas of deeper convection, but no precipitation was reported.

6.21.3 Storm Electricity Highlights

None.

6.21.4 Aircraft Operations

None.

6.21.5 Mobile Ground Vehicle Observations

None.

6.22 12 June; Thursday

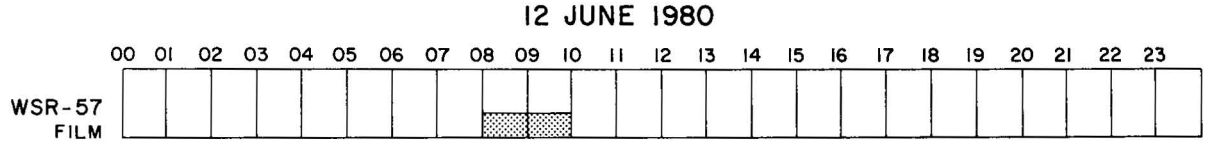

6.22.1 Forecasters' Outlook

The ridge-high pressure aloft still was acting as an effective inhibitor of convection in Oklahoma. Morning thunderstorms occurred in Kansas in association with shortwave passage across the central plains. Clear skies and warm temperatures for the area of interest were forecast and verified.

6.22.2 Radar Observation Highlights

None.

6.22.3 Storm Electricity Highlights

None.

6.22.4 Aircraft Operations

An early morning F-106 flight from 0830 to 0930 CST made three penetrations at 15,000 ft MSL on a 30-35 dBZ storm located 320°/160 km from Norman. The pilot reported only light turbulence and no lightning strikes.

6.22.5 Mobile Ground Vehicle Observations

None.

6.23 16 June; Monday

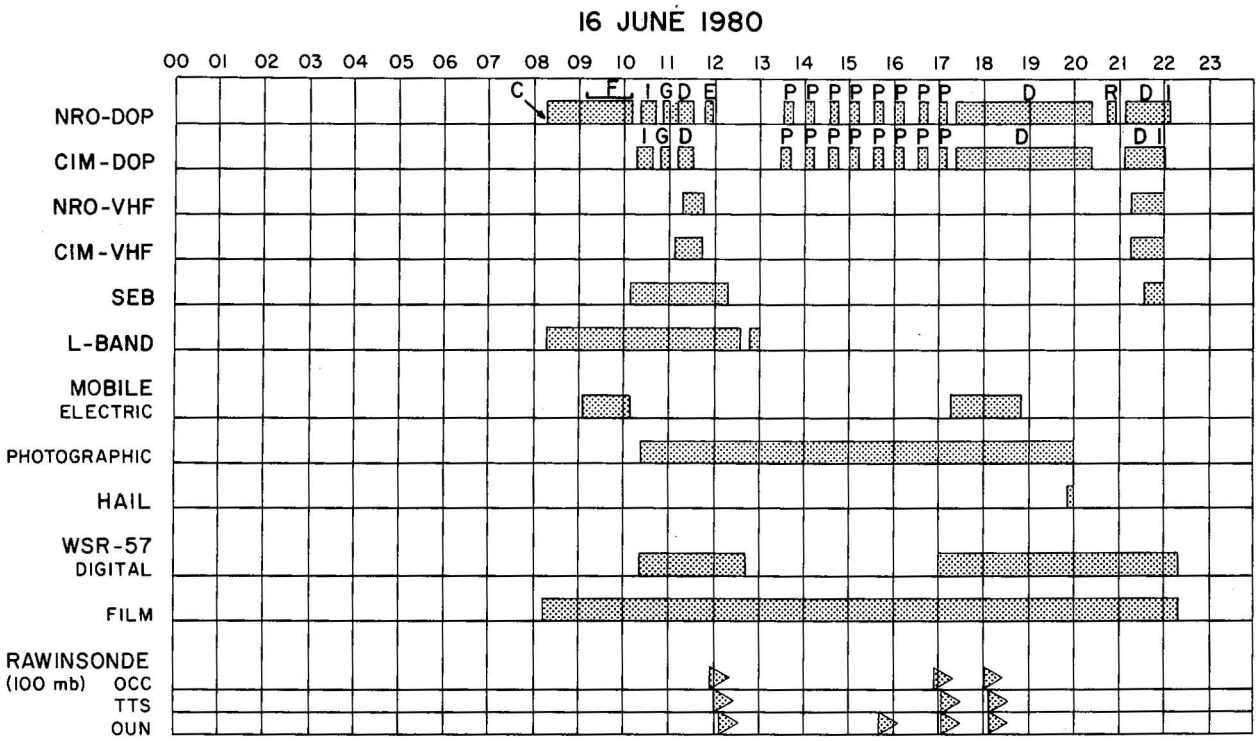

6.23.1 Forecasters' Outlook

The upper air pattern had changed from that of the previous two weeks (i.e., strong ridging over the central United States). By the morning of the 16th, a closed upper low had moved into Wyoming, suppressing the ridge and leaving Oklahoma in zonal flow. A moderately intense shortwave trough was entering northern Oklahoma from the west.

A cold front had pushed into central Oklahoma and at 0600 CST was on a Hobart-to-Oklahoma City-to-Tulsa, Oklahoma, line.

Thunderstorm activity associated with the morning wave intensified dramatically just after dawn (which was somewhat surprising, considering the time of day and the fact that the storms were about 60 miles north of the front) and produced extensive hail damage in northern Oklahoma. Storm cluster data were collected beginning ~ 0905 CST. Morning operations continued until noon.

During the early-to-midafternoon, the cool front, reinforced by thunderstorm outflow, pushed slightly farther south. A region of lower pressure in southwestern Oklahoma deepened, and by late afternoon a significant frontal wave was situated in the Altus-Hobart area. At 1630 CST, four thunderstorm cells developed very rapidly in the vicinity of the low.

6.23.2 Radar Observation Highlights

NRO cluster experiment began on strong morning storms 120 km to the northwest. Initially greater than 67 dBZ, they moved SE and gradually weakened. Aircraft

data were recorded, followed by a short lifetime experiment by both NRO and CIM. A thin line on the WSR-57 marked a SW-NE oriented gust front 40 km to the NW of NRO (1045 CST). Dual Doppler-radar data were recorded for about 20 minutes as the gust front moved SE. Another 30 minutes of dual Doppler-radar data to the north was acquired in support of hail chase. Data on lightning echoes to the NE were recorded by NRO.

Long-pulse data were recorded during the afternoon at both NRO and CIM. The front was seen clearly to the south as a thin line with a wind shift. RHI's were collected across the front. By late afternoon (1600-1700 CST), a cluster of thunderstorms developed 190 km to the WSW with weaker cells 90 km to the NW. Both NRO and CIM coordinated sector scans on the storms as they moved ESE. An RHI scan on a storm 80 km to the north revealed well developed structure. Dual sector scans were recorded on this storm. NWS issued tornado warnings, although single Doppler velocity fields did not indicate significant rotation. No tornado was reported.

6.23.3 Storm Electricity Highlights

During the morning, the dual VHF mapper and SEB equipment made simultaneous observations with the 23-cm and 10-cm radars. Lightning activity was very low. During the afternoon and evening, dual VHF mapping and SEB data were recorded. Excellent correlation between NRO and CIM mapping was observed. MEL tracked four storms west of NSSL and sighted one tornado. Continuous electrical data were obtained on the severe storm that produced the tornado.

6.23.4 Aircraft Operations

The F-106 flew during 0900-1010 CST, making 6 penetrations at 15,000 ft on a storm system 340°/30 km from Norman. Moderate-to-severe turbulence was encountered on all penetrations and, despite frequent lightning in the vicinity of the aircraft, the aircraft was not struck. Upon return to Tinker AFB, it was discovered that the turbulence had caused a leak in the secondary hydraulic system and the aircraft was grounded for the remainder of the day.

6.23.5 Mobile Ground Vehicle Observations

NSSL 1 left the Laboratory at 1020 CST and headed north to intercept storms north of Oklahoma City. These storms had extensive gust fronts, but no signs of rotation. At 1109 CST, NSSL 1 found pea-sized hail just west of Jct. 77/I-35 (south side of Guthrie). The team then headed west, anticipating storm development either along a west-to-east front or along the bubble boundary created by the morning convection. Distant isolated towering cumulus were photographed from Gracemont, Oklahoma, looking SW through NW between 1546 and 1632 CST. Around 1645 CST, a cumulonimbus grew from a cluster of towering cumuli, and NSSL 1 headed west to close in on the new storm. As they approached, they saw three rapidly developing storms in close proximity, #1 to their northwest, #2 to their southwest, and #3 to their west. These storms had extremely "hard-looking" towers. The NSSL Nowcaster advised NSSL 1 to intercept the west storm as this had the largest radar echo. This intercept was made at Cordell at 1720 CST. During a phone call to the lab (1720-1733 CST), a hard rain began falling on the road, yet the sidewalk remained out of the rain for twenty seconds. The sharp gradient to this precipitation shaft was very impressive. The Nowcaster advised the crew to head south out of Cordell in pursuit of a fourth storm, which had developed on the south flank of the one they were under. At 1736 CST, NSSL 1,

at Jct. 183/152, saw a laminar funnel pendant from a high base of storm #2 which was now to the east-southeast. However, the fourth storm rapidly became the dominant one as it moved to the south, and later to the southeast. By 1728 CST, it had developed a rotating wall cloud and, at 1756 CST, a tail cloud was also observed. Intense cloud-to-ground lightning bolts from the anvil concerned the crew. Funnels were seen at 1753 CST (3 miles west of Rocky, Okla., on a county road) at 1759 and 1801 CST (2 miles north of Hobart on Highway 183), and at 1812 CST (in Hobart, Oklahoma). In Hobart at 1814 CST, the wall cloud dissipated as rain-cooled air swept underneath it. However, a new wall cloud quickly formed to the south at the edge of this outflow boundary. At 1823 CST, with NSSL 1 just north of Roosevelt on Highway 19, a mini-tornado, visible as a dust whirl on the ground, formed from the north side of the wall cloud. Near Cooperton, the chase team heard the roar of a hailshaft between 1840 and 1852 CST and twice was caught briefly in hail up to golf ball-size. We learned later that this hailstorm did extensive crop damage, with reports of baseball hail. This was especially tragic since the harvesters were in the fields. At 1855 golf ball-size hail was found 7 miles north of Jct. 54/49 on 54, and at 1903 CST an impression hailshaft was still visible north of the vehicle which was at 1 mile north of Jct. 54/49 on 54. By 1913 CST the wall cloud had dissipated, but the storm still had an intense-looking hailshaft. The chase was broken off southeast of Snyder around 1950 CST.

Figure 6.3 Wall cloud with hail shaft extreme right (discernable only as bright area); photograph taken looking west at 1831 CST on 16 June 1980 from 3 miles N of Cooperton, Oklahoma.

6.24 17 June; Tuesday

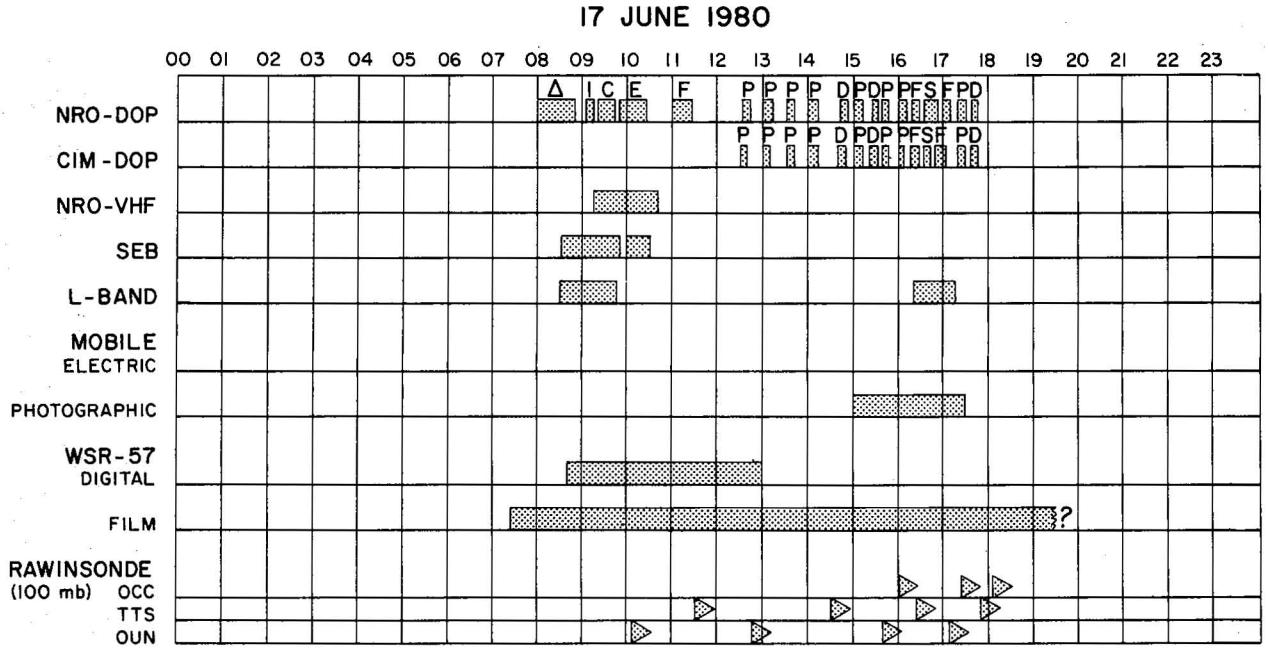

6.24.1 Forecasters' Outlook

As on the previous day, Oklahoma awoke to a round of early morning thunderstorms. The storms were intense just after dawn (similar to the day before), but on this day the activity weakened by 0900 CST.

Synoptically, Oklahoma remained beneath moderately strong zonal flow as an eastward-moving disturbance over central Nebraska suppressed the central United States long wave ridge. On the surface, the cold front had weakened considerably. Analysis of 0500 CST surface data found no well-defined front, but rather an inverted pressure trough through the state from a low in extreme southwestern Texas.

By noon, surface features had clarified somewhat. A stationary front was located on a line from Plainview, Texas, to Muskogee, Oklahoma. A cool region of air generated by the morning storms covered southeastern Oklahoma.

Because of the formation of these boundaries and a very unstable air mass over the state (lifted index of -6 at Oklahoma City given an afternoon maximum temperature of 91°F), prestorm operations began in the early afternoon. However, the only activity in the Doppler area was a short, E-W line of small thundershowers north of Oklahoma City. Post-storm analysis found several reasons for the failure of convection to develop. First, the afternoon temperature reached only 84°F instead of 91°F. Furthermore, there was a 2°C warming at all levels between 700 and 500 mb. Finally, the evening upper-air analysis indicated that central Oklahoma had been under negative vorticity advection throughout the afternoon.

6.24.2 Radar Observation Highlights

At 0800 CST, NRO began collecting sector scan data on storms 70 km to the northwest. Lifetime data were then recorded since the storms were 40 km to the north and had weakened considerably. A short period of storm tracking was followed by lightning echo data. Data were next collected in support of aircraft penetrations to the northeast.

Long-pulse data were collected in the afternoon. The RHI display revealed a possible boundary about 50 km SW. A weak echo developed (25 dBZ) 40 km to the SSW and was scanned by both NRO and CIM. A large area of deep convection developed to the NW with a brief 25 dBZ echo. Later, a line of rapidly growing echoes formed in this area, appearing to the west of larger storms already present to the east. Coordinated sector scans were recorded. Long-pulse data acquisition was interrupted for aircraft data collected to the northeast.

6.24.3 Storm Electricity Highlights

Good Norman VHF mapping, SEB, and 23-cm radar data were recorded. Twenty-three-cm radar observations were used to help vector the F-106 aircraft into regions of high lightning activity.

6.24.4 Aircraft Operations

Two flights were accomplished by the F-106. The first, from 1052 to 1200 CST, penetrated two storms, one at 360°/100 km and a second at 90°/120 km from Norman. On the first pass at 16,000 ft MSL, only light precipitation and light turbulence were encountered so attention was shifted to the second storm. Two penetrations at 16,000 ft MSL were made. Light to moderate turbulence was reported, and on the last run the aircraft received a direct lightning strike which hit the boom, traveled along the left side of the fuselage and left wing, and exited near the left wing tip.

The second flight for the day was made from 1600-1715 CST on storms 45°/160 km from Norman. Again the penetration altitude was 16,000 ft MSL. Light to moderate turbulence was encountered, and very frequent lightning activity was reported. In the first penetration the lightning struck near the nose boom and split down both sides of the aircraft. On the second penetration lightning again struck the aircraft.

Light to moderate turbulence was reported. While lightning activity was present on the third and fourth penetrations, no strikes were recorded.

6.24.5 Mobile Ground Vehicle Observations

The chase team took time lapse movies of "bubbling towers" and small cumulonimbi from Purcell, Oklahoma, between 1537 and 1729 CST.

6.25 19 June; Thursday

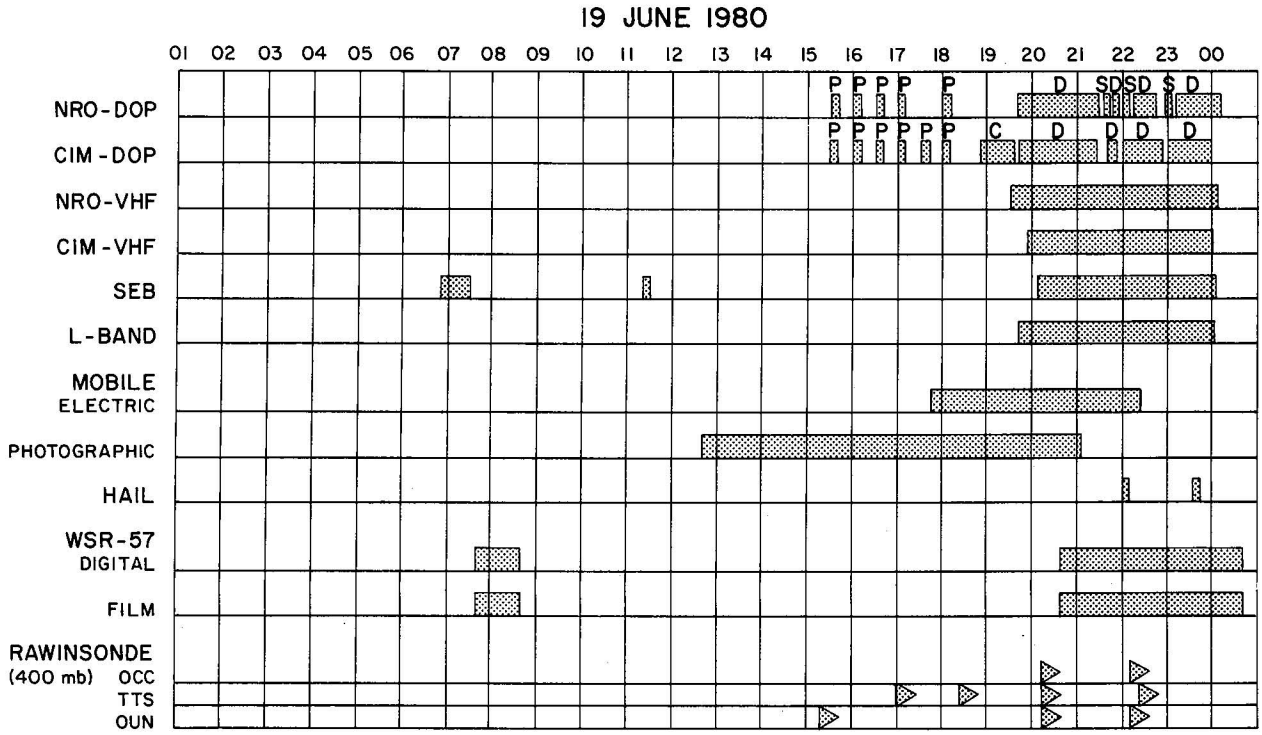

6.25.1 Forecasters' Outlook

A round of nonsevere thundershowers, which moved across Oklahoma during the night, pushed cooler air into northern Texas. By midmorning the boundary separating the cooler air in Oklahoma and northern Texas from the warmer air in southern and central Texas had become a warm front and was pushing slowly north.

Upper-air analyses revealed northwesterly flow aloft with a shortwave trough from Colorado to north-central New Mexico. The actual strength of this wave was masked considerably because it was within the peak of the upper ridge at 0600 CST. However, since the wave was exhibiting moderate strength in a synoptically unfavorable region, it was considered likely that as it moved east of the ridge line, it would reveal itself to be quite intense. The timing on eastward motion of the disturbance suggested arrival in western Oklahoma by early evening.

Prestorm operations began at ~1530 CST. A portion of the returning warm front, identified by the NRO Doppler radar, stretched from 271°/75 km to 180°/74 km. At 1900 CST, visual observations of a zone of layered clouds, extending ESE-WNW over Norman, confirmed the presence of the boundary in the area. The thin line of echoes seen earlier on Doppler reduced considerably by 1800 and because NSSL Storm Intercept teams were observing severe thunderstorms in the eastern Texas Panhandle, the prestorm operations were discontinued and CIM Doppler began collecting storm cluster data on storms far to the west for about 40 min. During the same period, NRO Doppler was down while repairs to the real-time displays were being made.

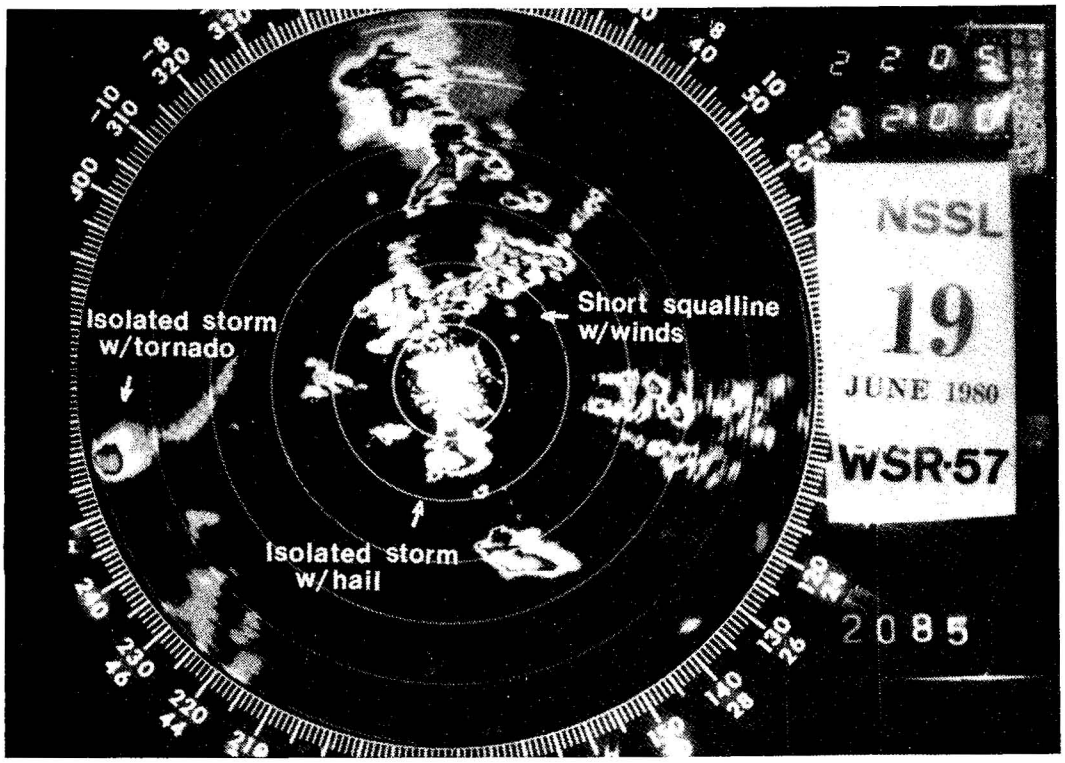

a. 2205 CST

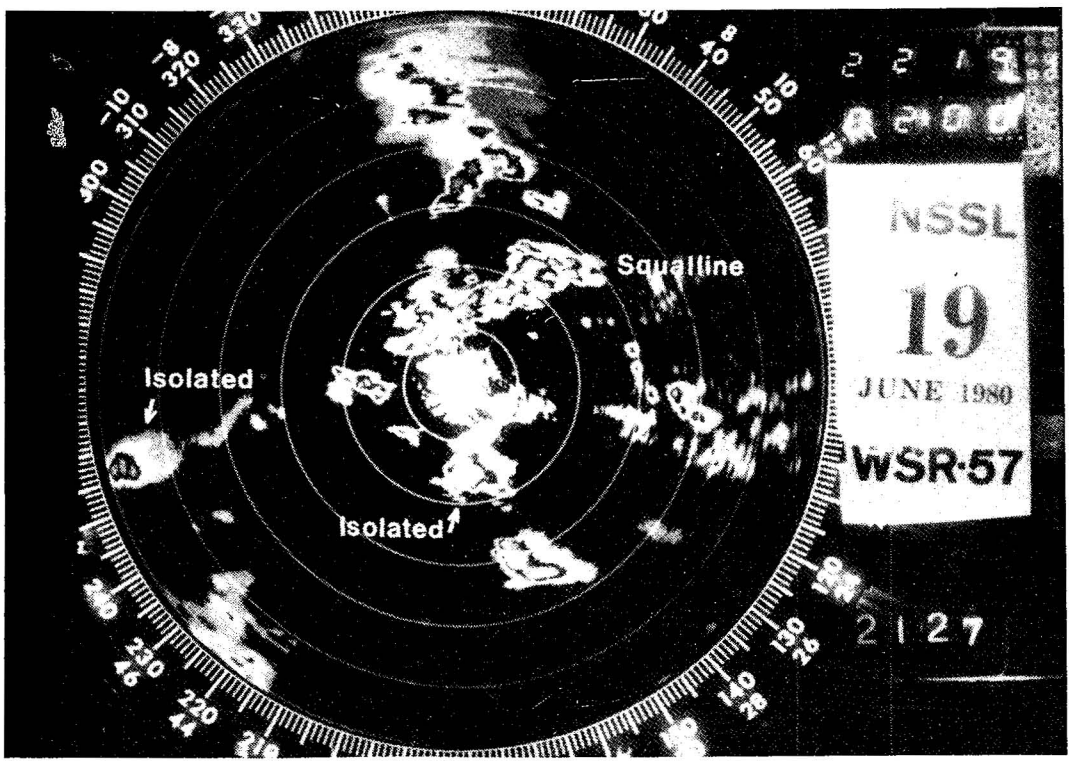

b. 2219 CST

Figure 6.4 WSR-57 radar photos depicting the storms on 19 June 1980. Range marks are every 40 kms. (b) Dual Doppler data were acquired on an isolated storm while hail was gathered by the Hail Sampler.

Figure 6.5 Wall cloud with cloud-to ground lightning in background between wall cloud and precipitation shaft. Photograph from 16 miles NW of Miami, Texas, looking N at 1829 CST on 19 June 1980.

Deep convection began developing to the southwest of Norman, Oklahoma, at ~1925 CST. The Dopplers started data collection at ~1935 CST. The activity became severe, producing many reports of large hail and damaging winds throughout the night, although no tornadoes were confirmed in Oklahoma.

6.25.2 Radar Observation Highlights

NRO and CIM began prestorm data collection in late afternoon. The single Doppler (NRO) radial wind pattern over a 100 km diameter circle appeared diffluent (incoming winds in the SW, outgoing in the NW and NE). Thunderstorms developed 150 and 300 km to the SE and 300 km to the west. CIM recorded 45 minutes of tracking data on the western storms while NRO was not recording. A cluster of cells developed 60 km to the west which were scanned by both NRO and CIM in the interlaced sampling mode after reaching reflectivity values of 25 dBZ. An intense storm developed within 2 hours and moved through the southern lobe of the dual Doppler-radar area. Coordinated scans then covered a developing line of storms 50 km to the north accompanied by a gust front. The strongest cells (60 dBZ) passed to the north while development occurred on the SW part of the line. Both Doppler radars were operating as hail was collected from two strong storms in the southern lobe of the dual Doppler area. Radar operations ceased about midnight although storms continued all night.

6.25.3 Storm Electricity Highlights

Four hours of good to very good data were collected from the dual VHF mapper, SEB, and 23-cm radar. Correlation of lightning between Norman and Cimarron was only fair. MEL tracked mesocyclone of a storm moving southeast from Miami, Texas, that produced a short-lived tornado.

6.25.4 Aircraft Operations

None.

6.25.5 Mobile Ground Vehicle Observations

NSSL 1 and the Storm Electricity vehicle stayed close together throughout this chase. A southeastward moving storm about 20 miles NW of Miami, Texas, was intercepted around 1745 CST. This storm was impressive visually with a banded inflow cloud (5 to 7 bands visible) flowing into the main storm tower from the east, massive towers on its flank, and striations on the sides and base of the main tower. A wall cloud formed at 1814 CST. Short duration but intense cloud-to-ground bolts out of the anvil gave rise to safety concerns. By 1830 CST, the wall cloud was rotating rapidly and the inflow winds at the crew's location were gusting to 40 knots. Small funnels were seen at 1831 and 1849 CST, and 2.5 cm hail was encountered 16 miles NW of Miami at 1837 and 1848 CST. Wall cloud rotation decreased at 1835 CST but reintensified around 1900 CST. Lightning for photography was poor throughout the observation period. Around 1915 CST, 2 miles NW of Miami, rapid inflow, upward, and circular motions were seen in the wall cloud and tail cloud. The roar of a tornado was heard at this time but, if there was indeed a tornado, it must have been obscured by the striated rain curtain. At 1920 CST, golf ball hail overtook the vehicle briefly in Miami, Texas, as it waited for a train to clear a crossing. The storm never appeared as threatening after this time but a short-lived mini-tornado, visible as an intense dust whirl, was seen at 2026 CST just north of Shamrock, Texas. Lightning was intense until 2100 CST, at which time the team gave up attempts at lightning photography and

headed home. At 2107 CST they penetrated a hail shaft with 2.5 cm hail six miles south of Shamrock.

6.25.6 Other Comments

0253 CST - 53-kt. wind at NSSL, minor wind damage to trees.
2210 CST - 1" hail ~ 3 mi. S of Lindsay in Garvin County.
2334 CST - Golf ball hail at Middleberg in Grady County.
0305 CST (20 June) - 57 kt. wind at NSSL, moderate wind damage to trees, power lines and outbuildings. (No radar data were collected on this storm; program ended on the 20th of June.)

7. QUALITY CONTROL SUMMARY

7.1 Doppler Radar

This summary for 1980 is again similar to those of previous years in that it includes a brief description of the NSSL Doppler radar systems and graphically depicts the results of routine calibrations that were performed throughout the spring and includes only abbreviated results of extensive experiments that were made for equipment evaluation purposes, which are published elsewhere. Thus, once again the data user is encouraged to refer to the previous summaries and supplemental references for interpretation and better understanding of this year's report. The 1975 and 1976 Summaries[1,2] establish the format and define the parameters used in the Quality Control Summary.

A summary of the basic parameters pertaining to the logarithmic receiver calibration is depicted in Figures 7.1 and 7.2 for normal and high gain modes. Collectively, these parameters provide an index of calibration stability and performance. The logging constant is the slope of the log receiver chain power transfer characteristics. The noise digit is the digital integrator output for noise alone. Noise power is derived by a technique described in the 1975 summary and is not measured directly.

A brief explanation of labels at the figure top is as follows:

PRT X768Y

768 = PRT in μ s. Routine calibration was at this PRT.
If (X=N), integrator gate spacing is 150 meters.
If (Y=L), receiver gain is normal.
If (Y=H), receiver gain is high.

Graphs for the interlaced sampling mode (X=E) are nearly identical to the mode (X=N) for simultaneous samples from the digital integrator and pulse pair processor so these are not presented here.

Receiver noise, with its well-behaved statistical properties, is useful for testing parts of the signal processing and recording chain, particularly the hardwired mean velocity and spectrum width calculation. During the "noise-alone" test, the receiver is disconnected from the signal generator used for calibration and is switched to face the antenna port. If the parametric amplifier is working well, the noise level measured looking toward the antenna port should be less than the noise measured when the signal generator is attached even though the signal generator is turned off. Thus, the noise digit in Fig. 7.1a should be larger than the mean digital integrator value if Fig. 7.3a. If it is not larger, this could either signify a poorly operating parametric amplifier or faulty setup. This can be further checked by examining the standard deviation of the

---

[1]Wilk, K., K. Gray, C. Clark, D. Sirmans, J. Dooley, J. Carter, and W. Bumgarner: 1976: Objectives and accomplishments of the NSSL 1975 spring program. NOAA Tech. Memo. ERL NSSL-78, 107 pp.

[2]Alberty, R., J. Weaver, D. Sirmans, J. Dooley, and B. Bumgarner, 1977: Spring Program '76. NOAA Tech. Memo ERL NSSL-83, 130 pp.

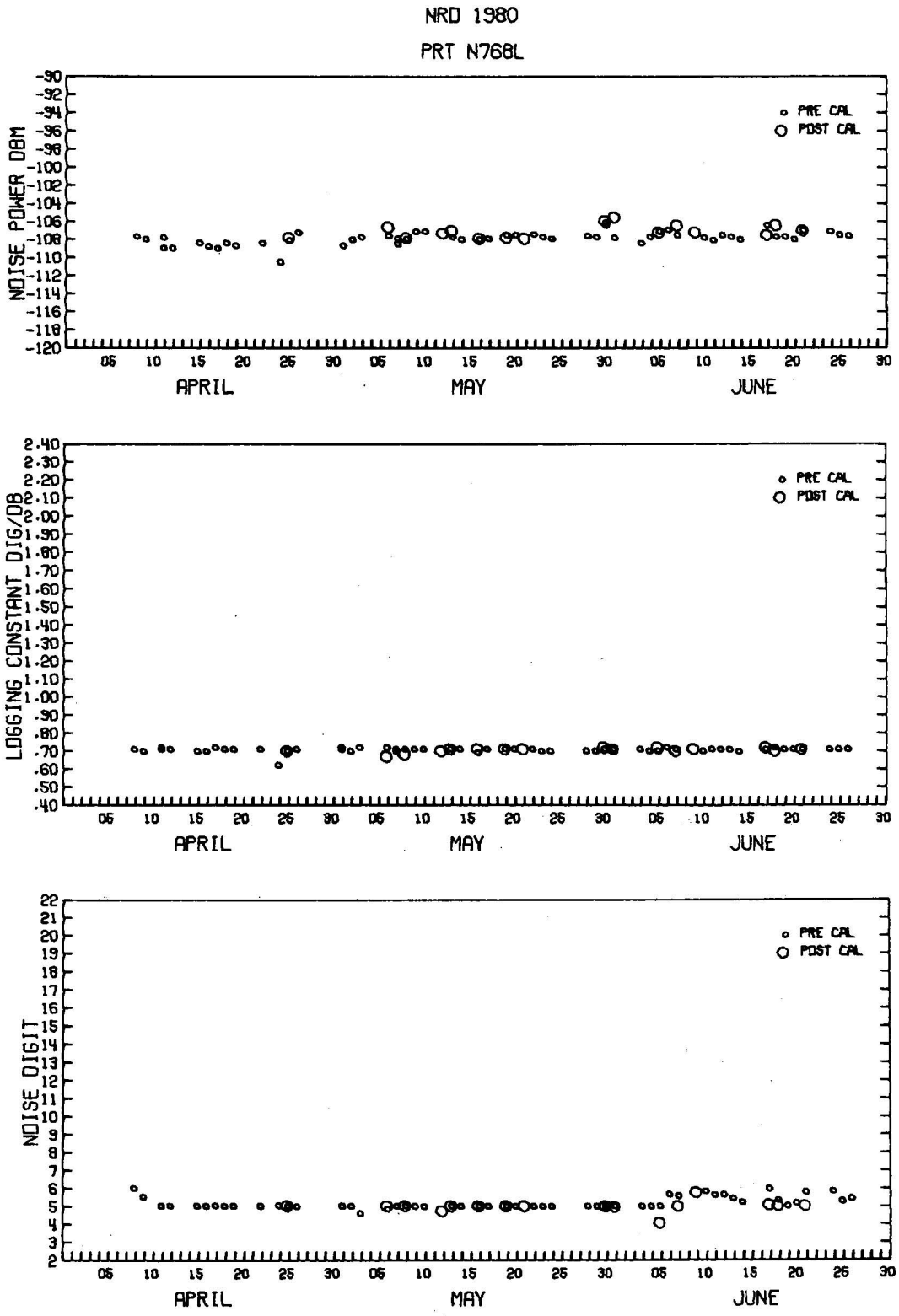

Figure 7.1a. Parameters monitoring logarithmic receiver performance and the constancy of the intensity calibrations at the Norman Doppler radar in low gain.

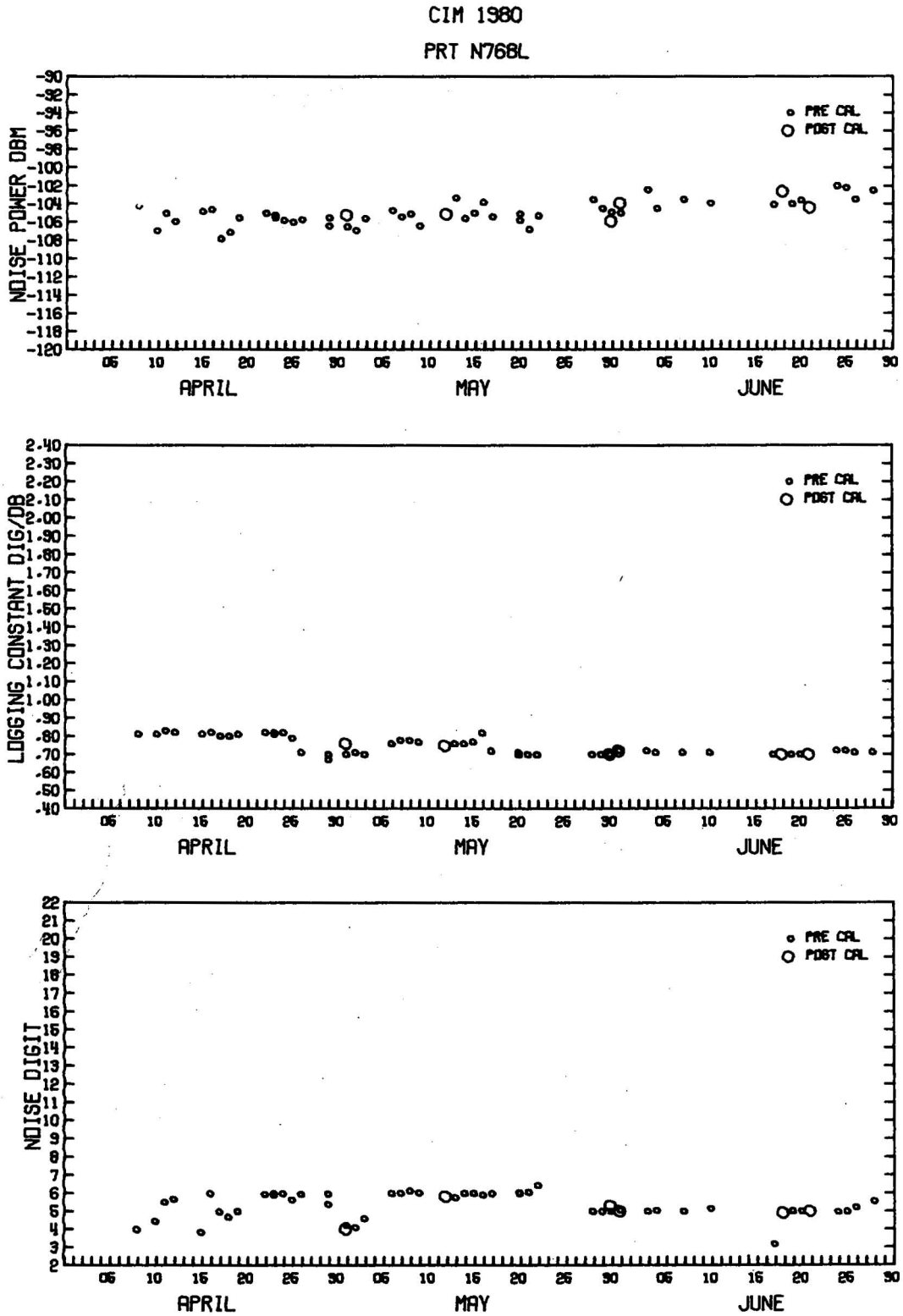

Figure 7.1b. Parameters monitoring logarithmic receiver performance and the constancy of the intensity calibrations at the Cimarron Doppler radar in low gain.

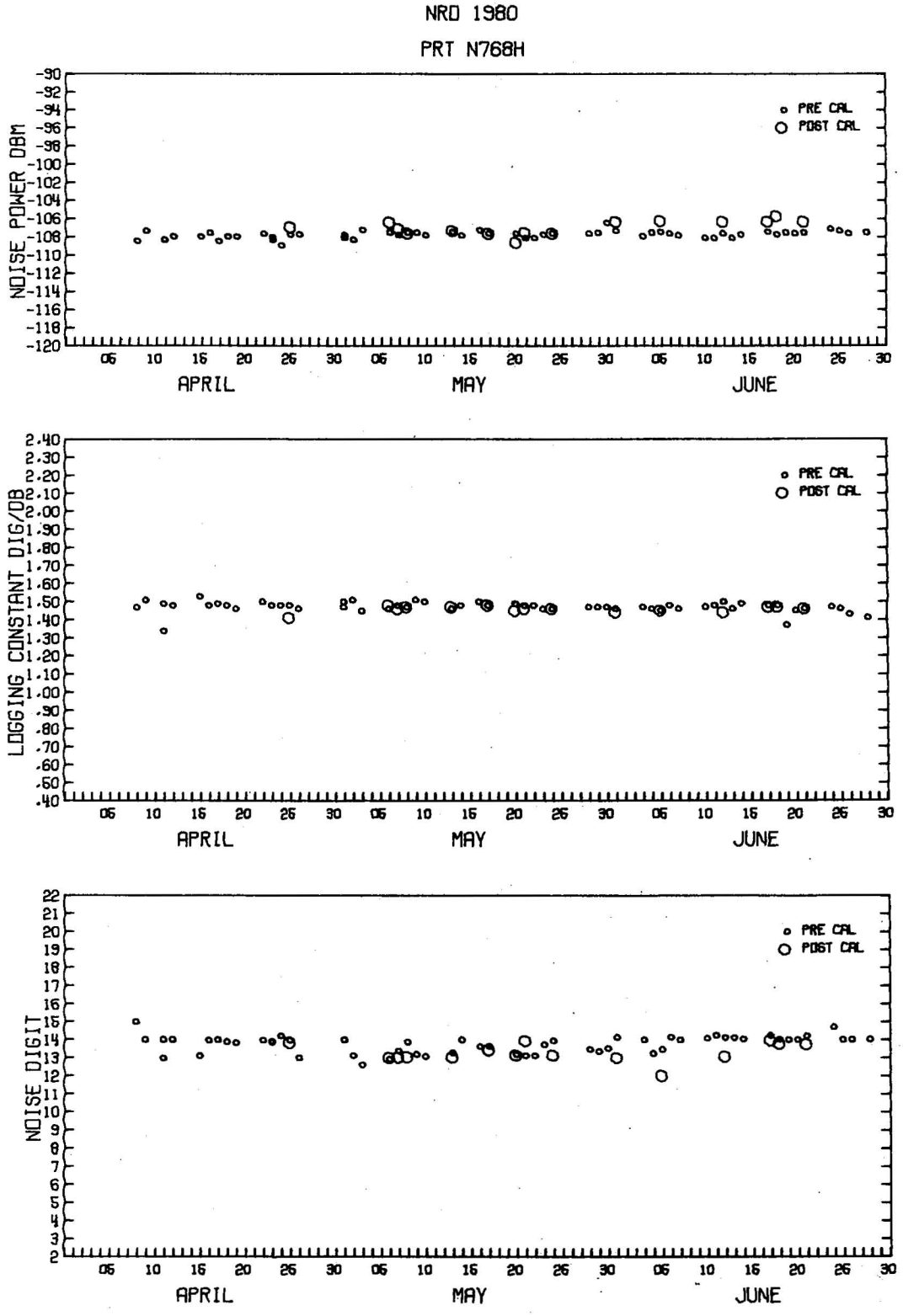

Figure 7.2a. Parameters monitoring logarithmic receiver performance and the constancy of the intensity calibrations for high gain at NRO.

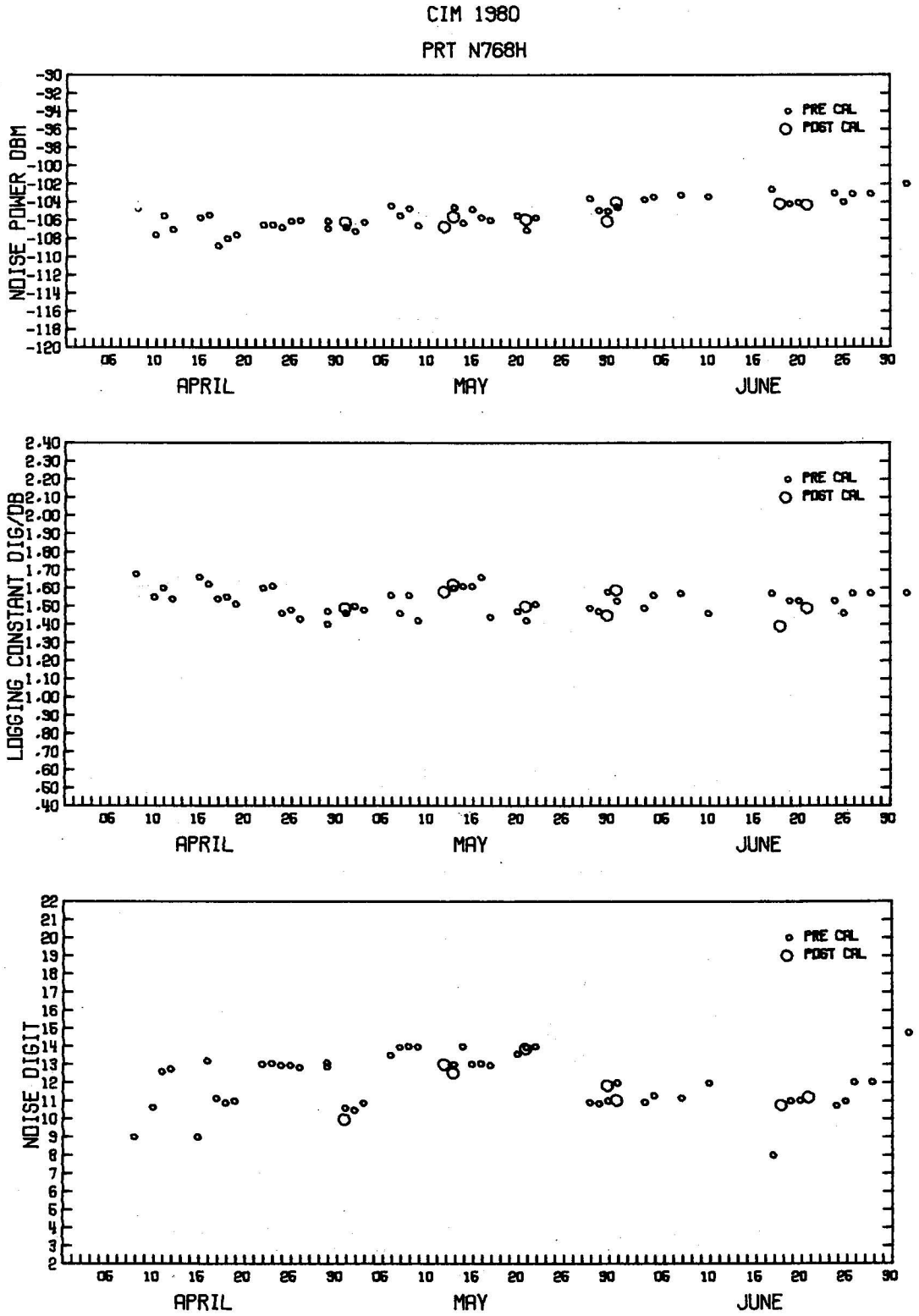

Figure 7.2b. Parameters monitoring logarithmic receiver performance and the constancy of the intensity calibrations for high gain at CIM.

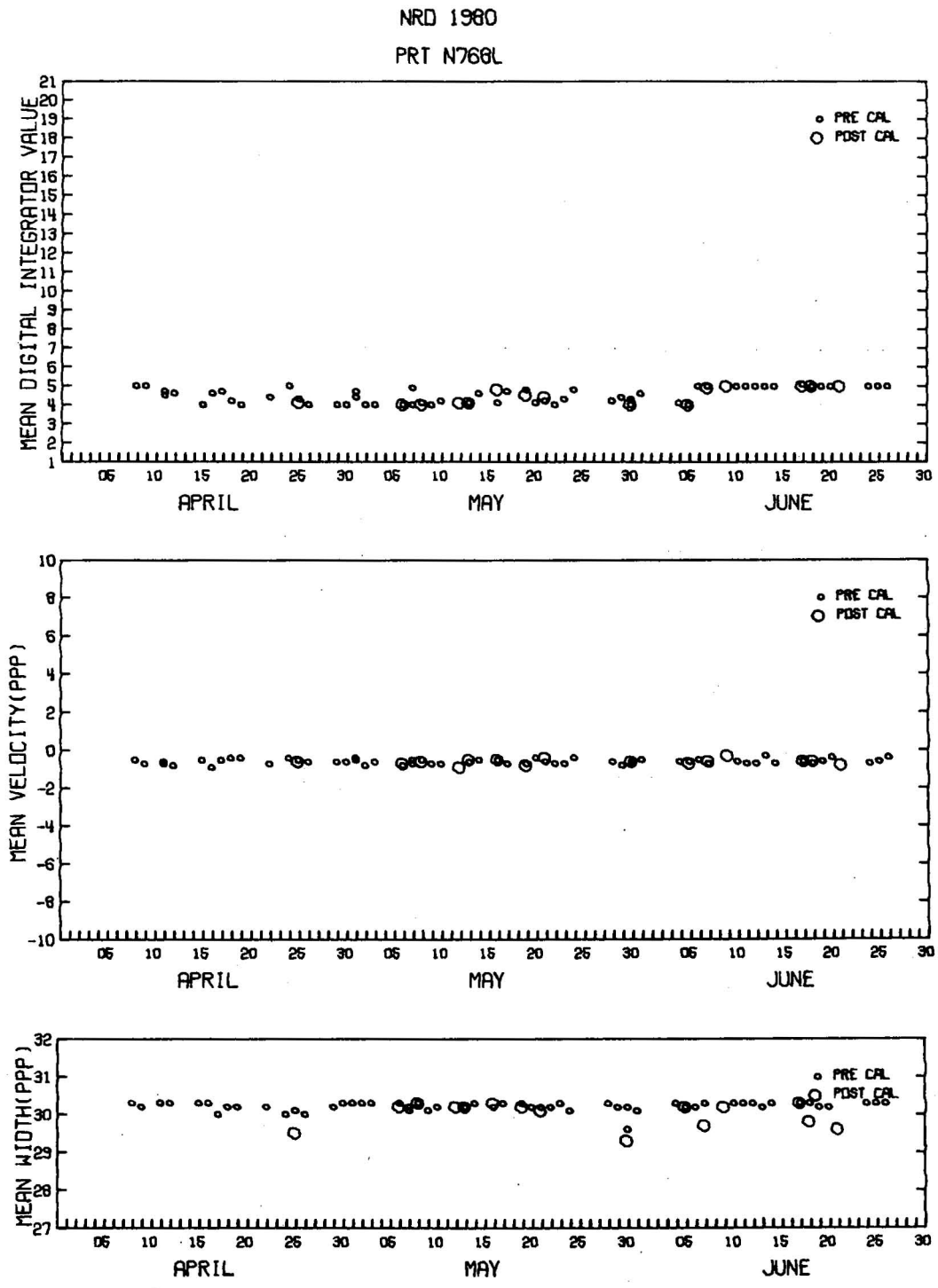

Figure 7.3a. Mean estimates of intensity from the digital integrator, and velocity and width from the pulse pair processor for noise alone at the NRO radar in normal gain.

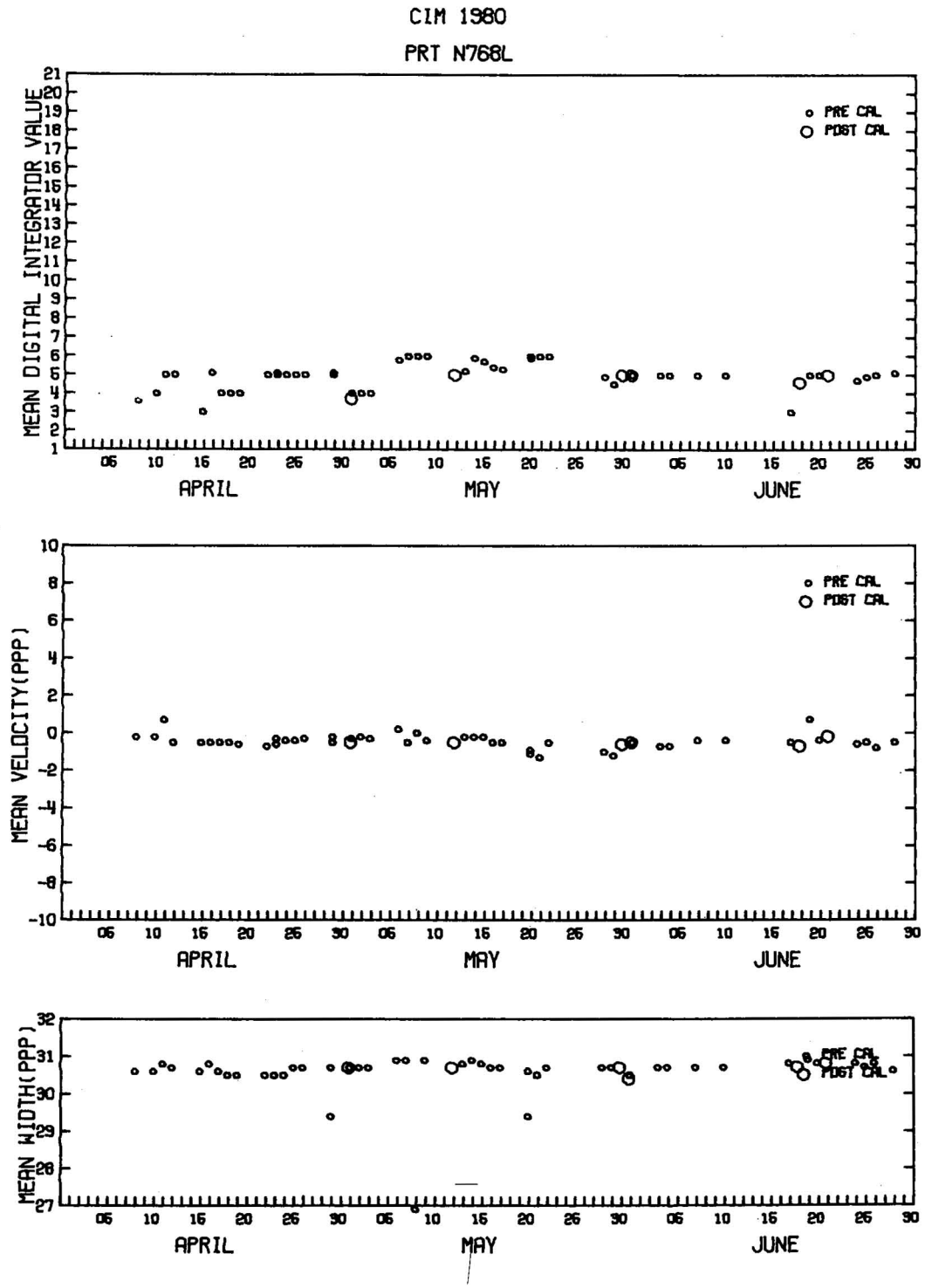

Figure 7.3b. Mean estimates of intensity from the digital integrator, and velocity and width from the pulse pair processor for noise alone at the CIM radar in normal gain.

integrator value for noise alone (Fig. 7.5, 7.6) which should have a non-zero value that depends only upon the time constant of the digital integrator.[3]

During "noise-alone" testing, the pulse pair velocity estimates should have a uniform distribution across the Nyquist interval. Thus the mean velocity should be zero (Figs. 7.3, 7.4), but the standard deviations should be 18.5 (Figs. 7.5, 7.6) because there are 64 counts that span the interval. A standard deviation of velocity counts lower than 18.5 usually signifies a dc offset that could, if present during data collection, bias velocity estimates.

The method for determining radar system timing or ranging is different this year. Instead of measurement of the individual delays (such as initial delay, receiver delay, etc.) the range associated with a particular gate is derived from range of known ground targets. A description of the technique is given in Appendix G.

Orientation and ranging adjustments to the raw data are tabulated in Appendix H, results of Sun flux measurements are given in Appendix I, and spurious velocities due to the Doppler receiver AGC compensation in regions of large reflectivity gradients are shown in Appendix J.

7.2 Mesonet

Several changes in field operations, equipment design, and quality control procedures had been implemented for the 1980 stationary automated mesonetwork (SAM) in an effort to increase the amount of usable data collected and more efficiently evaluate collected data quality.

Field operation changes consisted of servicing each site on a schedule that (1) always allowed at least one workday after a site visit for quality control review and (2) always allowed a site to be serviced at no greater than a six-day interval. This reduced potential problems due to inclement weather forcing personnel to skip a site. Typically, data cassettes ran out of tape after 7-1/2 days meaning that on a seven-day site service schedule a "missed" site was very likely to have an out-of-tape cassette before it could be reached. (3) Data quality control procedures were modified in an attempt to shorten the quality control "loop" so that any problems indicated by raw data analysis could be acted upon quickly.

In the laboratory after site servicing, each data cassette was read by a Motorola EXORciser Microcomputer and plotted on a Tektronix 4051 Graphics Display CRT. Each plot consisted of about 80 percent (~110,000 points) of the raw data from one cassette and took about 30 minutes to produce. A hard copy of the 4051 CRT display resulted in the ability to quickly determine the quality of the data and allowed for good turnaround times for any maintenance necessary. At this point, because the scale of the CRT plot was rather small for very detailed analysis (24 hours worth of data per inch on a time axis) and because there was still about 20 percent of the raw data from each cassette not viewed owing to the CRT space available, further graphic analysis was done. Fortran software was developed to produce a plot on the Calcomp plotter similar in format to the Tektronix CRT Display, but which included the remaining ungraphed data and which had roughly twice as large a time and vertical-axis scale. This second data plot

[3] Berger, M.I. and R.J. Doviak, 1979: An analysis of the clear air planetary boundary layer wind synthesized from NSSL's dual Doppler-radar data. NOAA Tech. Memo ERL NSSL-87, 55 pp.

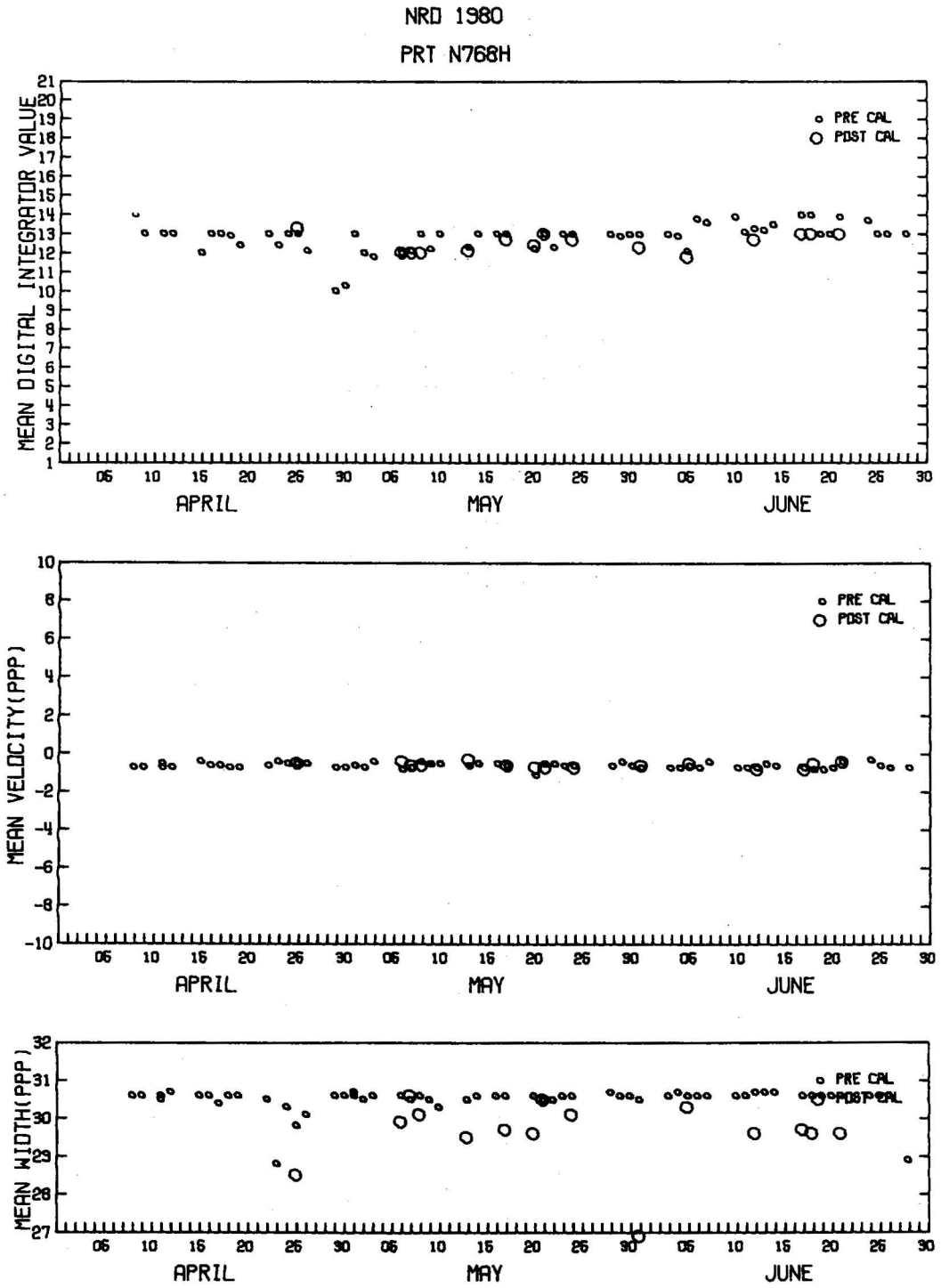

Figure 7.4a. Mean estimates of intensity from the digital integrator and, velocity and width from the pulse pair processor for noise alone at the NRO radar in high gain.

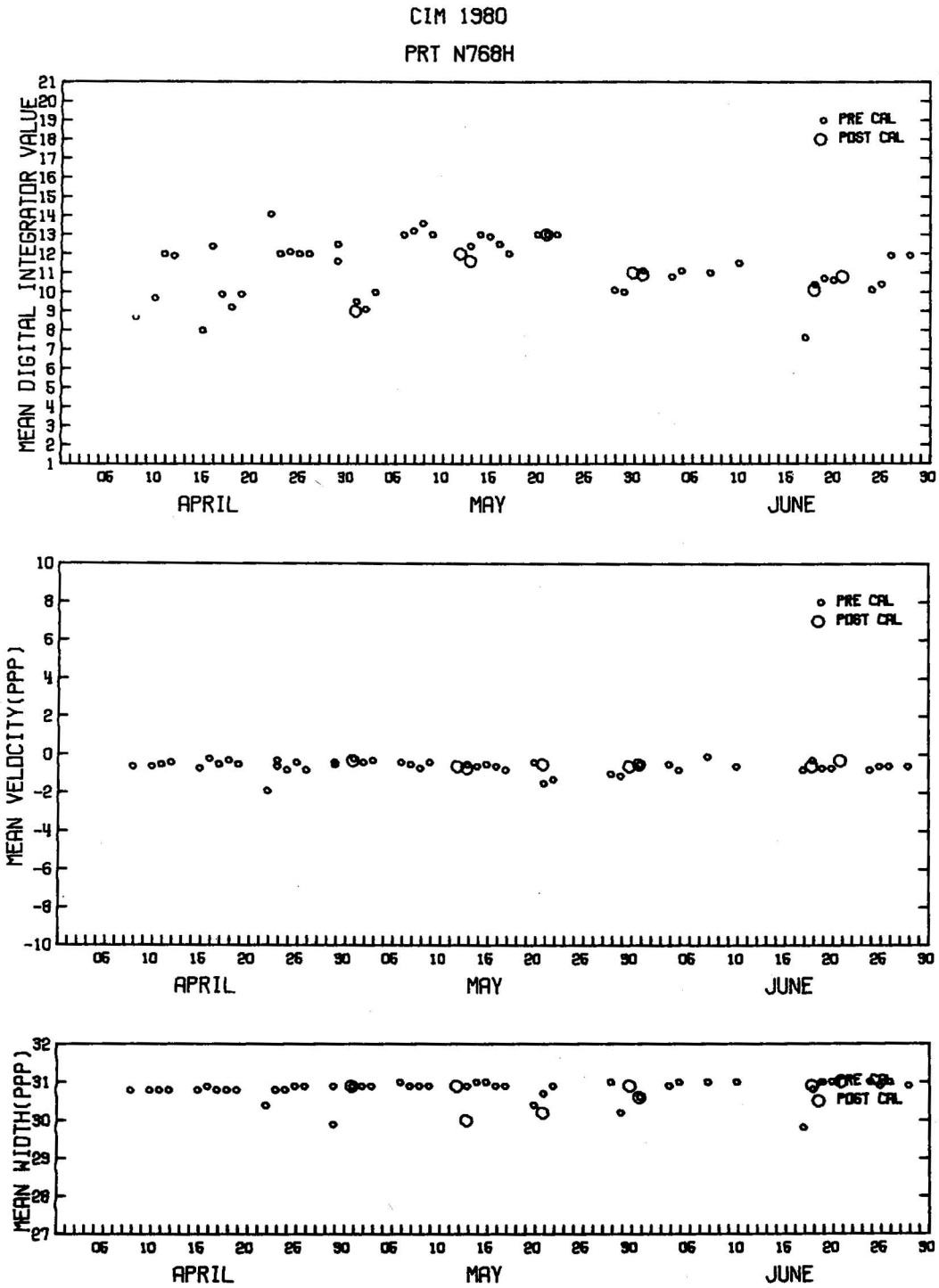

Figure 7.4b. Mean estimates of intensity from the digital integrator, and velocity and width from the pulse pair processor for noise alone at the CIM radar in high gain.

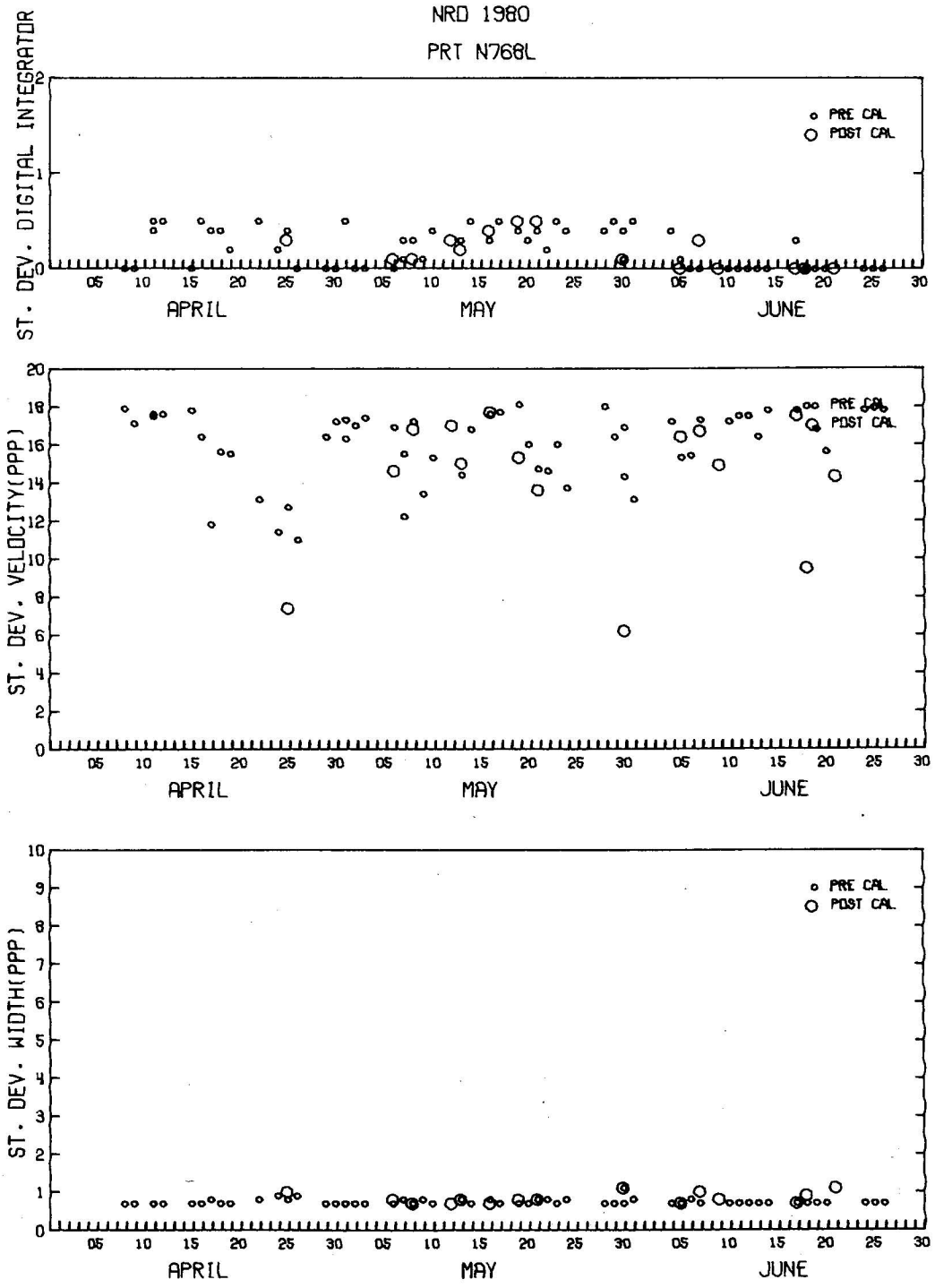

Figure 7.5a. Standard deviation of the digital integrator and pulse pair processor estimated for noise alone at the NRO radar in normal gain.

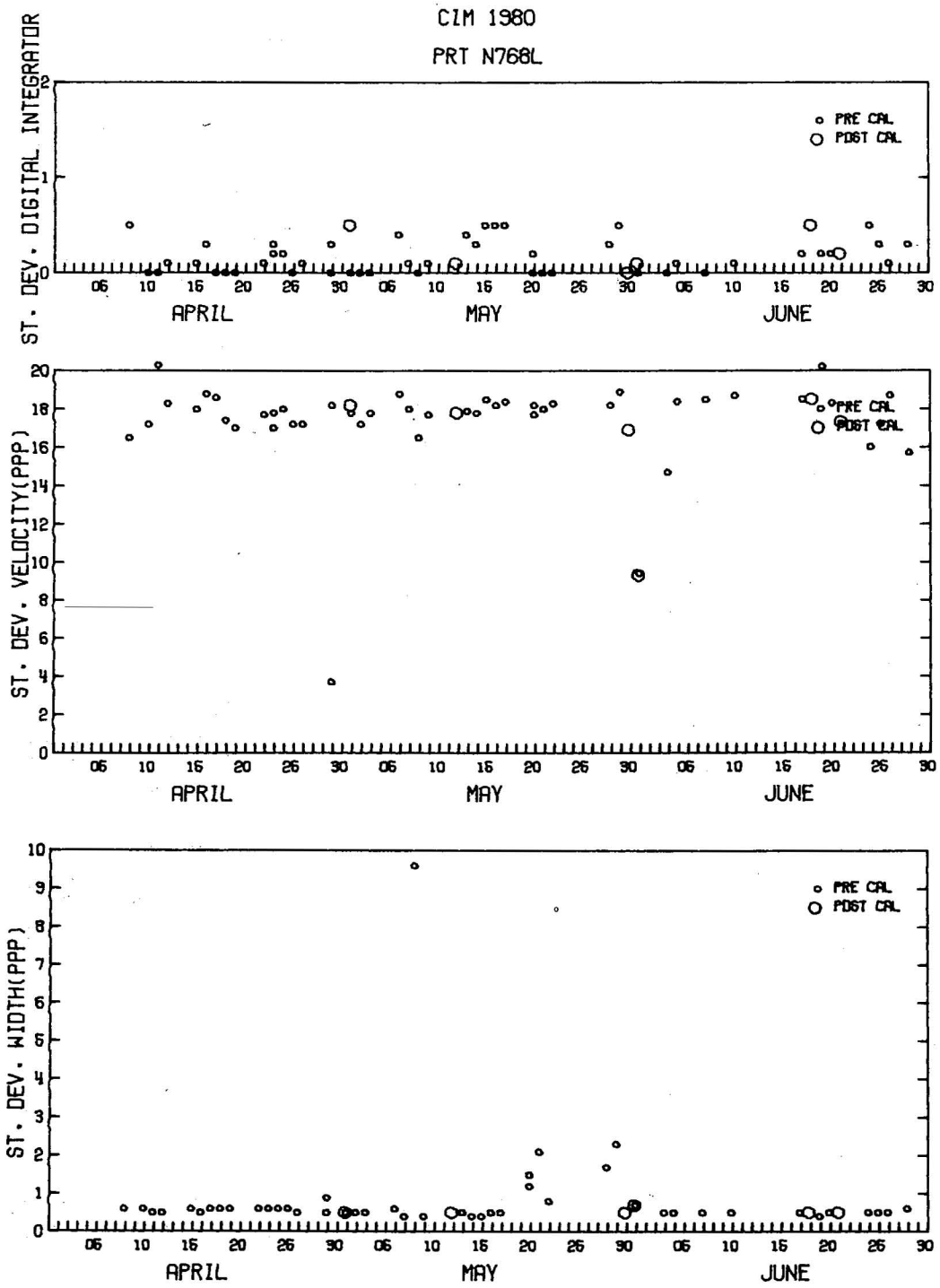

Figure 7.5b. Standard deviation of the digital integrator and pulse pair processor estimates for noise alone at the CIM radar in normal gain.

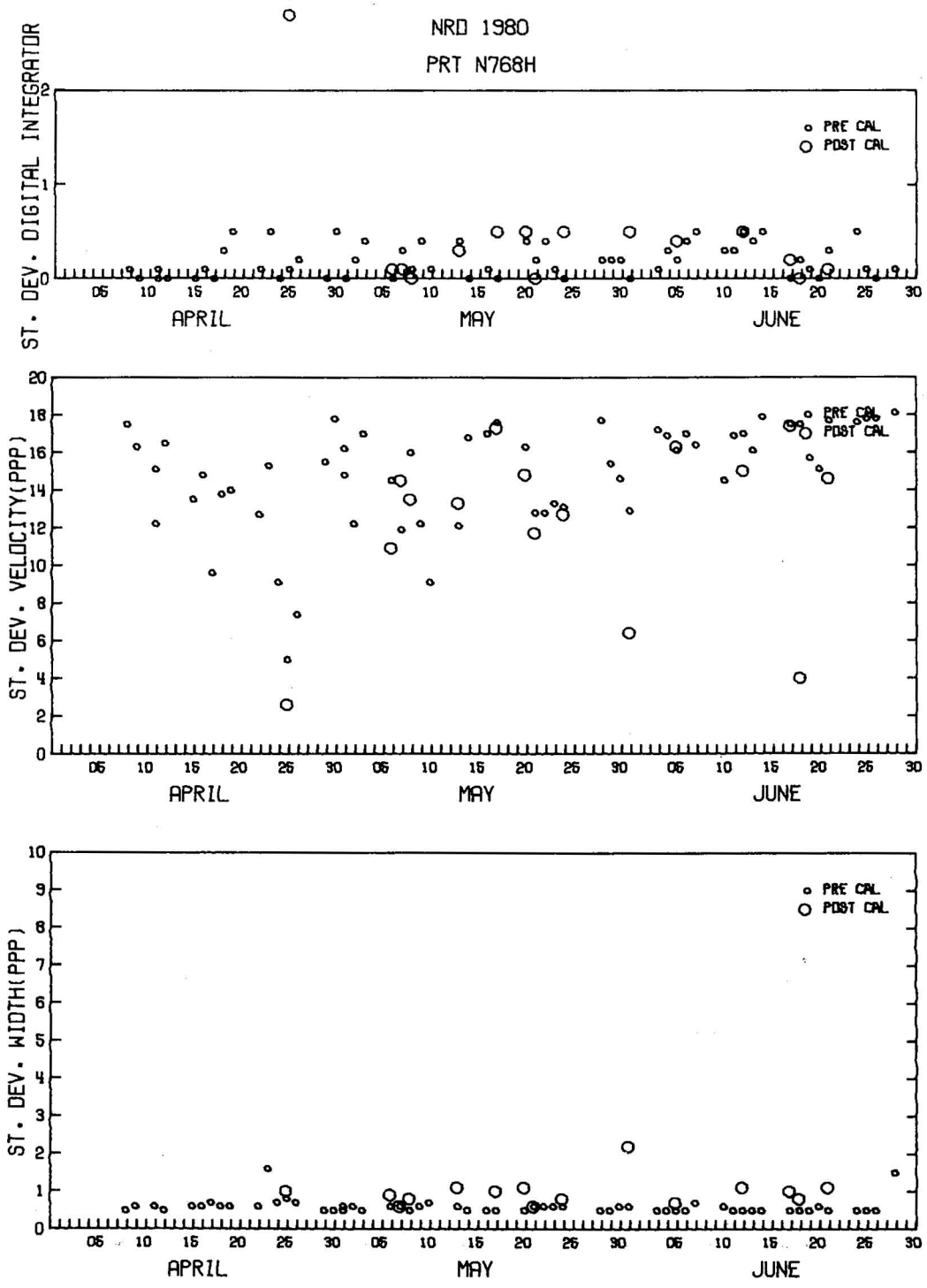

Figure 7.6a. Standard deviation of the digital integrator and pulse pair processor estimates for noise alone at the NRO radar in high gain.

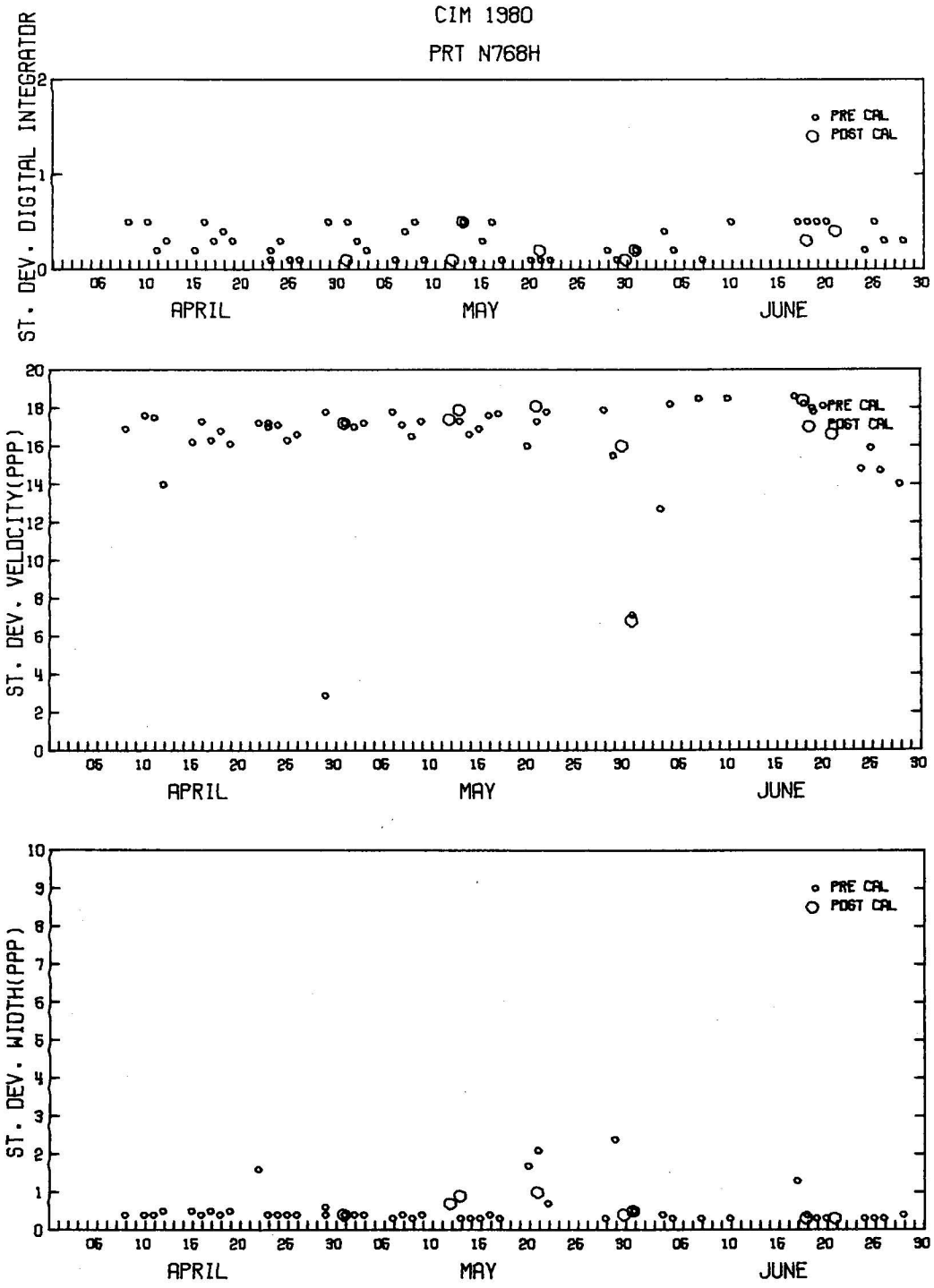

Figure 7.6b. Standard deviation of the digital integrator and pulse pair processor estimates for noise alone at the CIM radar in high gain.

required the transfer of all of the week's cassettes to a 7-track tape via the Motorola EXORciser and Tektronix 4051 before being subject to SEL 8600 data handling.

The data collection period for the 1980 SAM system was scheduled from 10 May to 23 June. On Figure 7.7, the shaded areas depict those times when usable data were collected. Blank areas represent data either not usable or not available. 1 April to 10 May was a shakedown period for some equipment modifications.

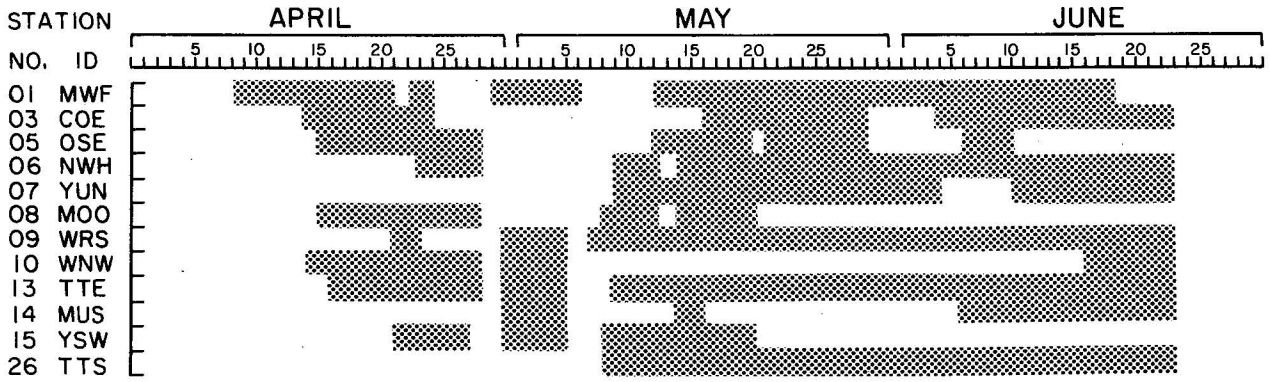

Figure 7.7. Operation periods (shaded areas) of SAM.

7.3 Rawinsonde

General Information. When all data have been received and entered in the minicomputer data files, a check program is called and begins to read pressure and input data from the rawinsonde site. The program converts pressure contact point readings to pressure levels. It then performs tests on the input data to determine the following:

1) Whether consecutive items of raob data increase or decrease as they should.

2) Whether the difference in certain consecutive items of data fall within given limits.

3) Whether the number allowed for each type of data item is not exceeded.

Appropriate error messages are typed with the data item in question, and all errors indicated by the check program messages must be corrected before processing a complete sounding.

Further quality control processing will be done at a later date and is outlined in NSSL Tech Memo ERL NSSL-53.

7.4 Tower

Nearly continuous time series data were collected from the tower facility during the period April 15 - June 25, 1980. A brief schematic of the meteorological parameters collected from the multi-level tower is shown in Figure 7.8. These parameters are amenable to quality control software based on a basic

knowledge of boundary layer behavior. Therefore, each data tape (2- or 3-day sample) is initially edited for record length, character, and physical errors, then converted to meteorological units where tower layer means and profiles are computed in addition to frequency distributions of several parameters which assist in the detection of equipment malfunction or data bias. The quality control techniques used employ a simple computer program that allows quick processing of large quantities of data. The data user is encouraged to refer to NOAA Tech Memo ERL NSSL-68 for a better understanding of NSSL's quality control logic for data collected by the KTVY tower facility. Figures 7.9, 7.10, and 7.11 represent a summary of the data collected during the 1980 season.

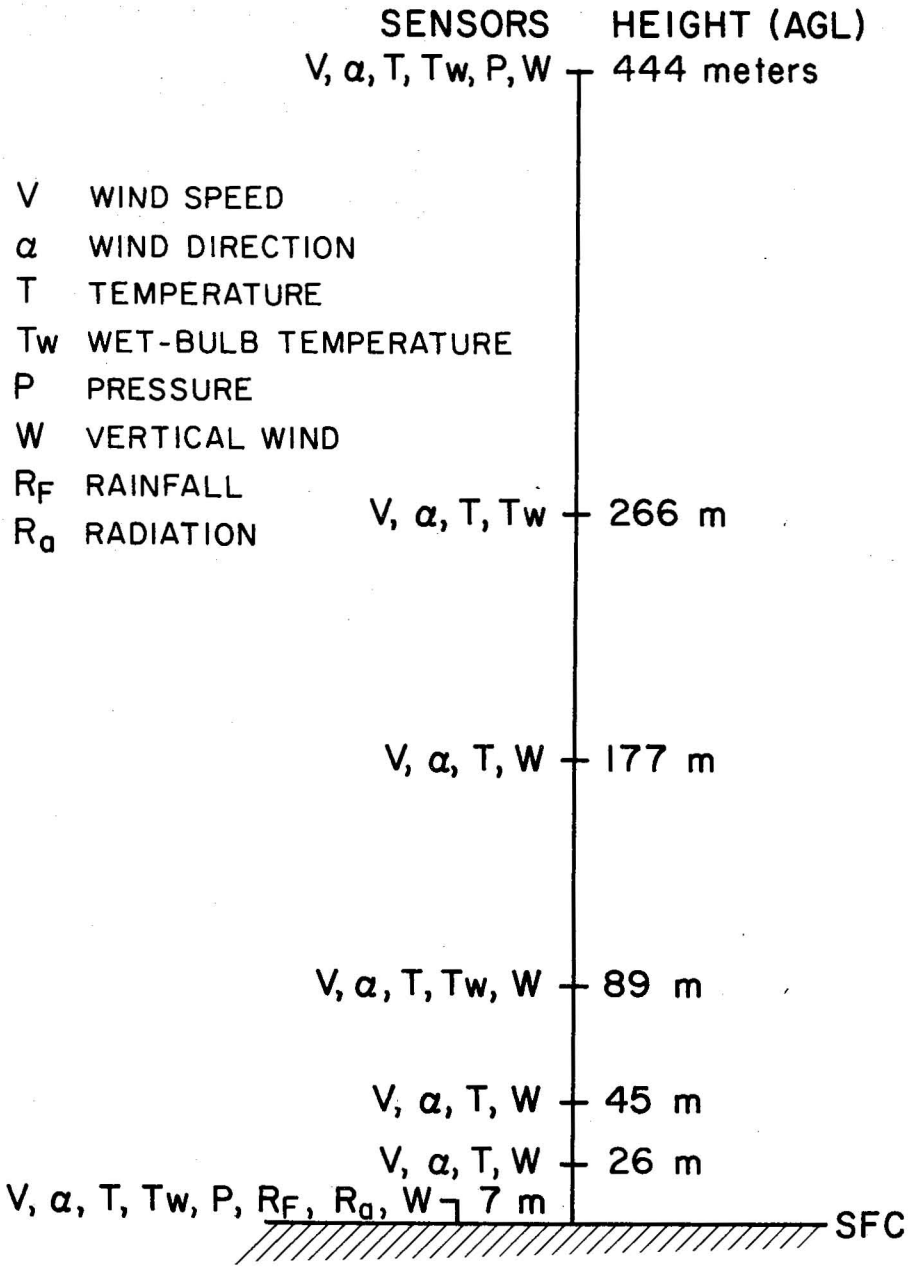

Figure 7.8 Tower sensor configuration.

APRIL 1980 KTVY TOWER

NUMBER OF OBSERVATIONS PER HOUR

DATE \ HOUR	00	01	02	03	04	05	06	07	08	09	10	11	12	13	14	15	16	17	18	19	20	21	22	23
1																								
2																								
3																								
4																								
5																								
6																								
7																								
8																								
9																								
10																								
11																								
12																								
13																								
14																								
15														178	367	367	367	366	367	367	367	367	367	367
16	367	367	368	367	368	367	367	368	366	367	367	366	367	367	367	367	367	366	367	367	367	367	366	366
17	366	366	367	368	367	367	367	367	367	367	367	367	367	367	367	366	367	367	367	367	367	366	367	369
18	367	367	367	367	366	367	367	367	367	366	367	367	315	367	367	367	367	367	367	367	367	367	366	367
19	367	367	367	367	367	367	367	367	367	367	367	367	367	367	367	367	367	367	366	367	367	366	367	367
20	367	367	367	367	367	348	368	367	367	366	367	366	367	366	367	366	366	366	366	367	367	366	367	367
21	367	367	367	367	367	365	366	367	367	366	366	330	366	367	365	367	366	366	367	366	366	367	366	367
22	367	366	367	367	367	366	367	367	367	366	367	366	366	37		268	366	367	366	366	366	367	367	367
23	367	367	367	367	163																			
24													152	366	367	366	370	366	366	367	59	101	367	366
25	367	367	367	367	367	367	367	367	286						88	367	366	367	367	366	367	367	367	367
26	366	367	367	367	366	367	366	367	367	367	366	367	367	367	368	367	367	367	367	367	367	367	367	367
27	367	367	367	367	367	367	367	367	367	367	367	366	367	367	367	367	367	367	367	367	367	367	367	367
28	367	367	367	367	367	367	367	367	367	367	366	282	365	367	367	366	366	363	367	367	367	368	367	367
29	368	366	367	368	366	368	367	367	370	372	367	367	366	366	367	366	367	367	366	367	367	367	367	366
30	367	367	367	367	367	368	367	367	367	367	367	367	367	366	367	367	366	367	367	367	366	367	366	16

Figure 7.9

MAY 1980 KTVY TOWER

NUMBER OF OBSERVATIONS PER HOUR

DATE \ HOUR	00	01	02	03	04	05	06	07	08	09	10	11	12	13	14	15	16	17	18	19	20	21	22	23
1	366	367	367	367	368	367	367	337	74	367	366	368	367	367	368	367	367	367	367	367	367	366	368	367
2	366	367	367	368	367	367	368	368	367	368	367	123	245	367	368	367	367	367	367	367	367	368	366	367
3	368	367	368	366	368	367	368	367	368	367	367	367	367	367	367	367	367	367	366	367	367	366	367	367
4	367	367	367	367	367	368	367	367	367	367	367	364	366	367	366	367	366	367	367	367	367	367	367	367
5	367	367	367	367	368	366	367	367	367	367	367	325	367	367	367	365	366	367	366	367	367	367	367	368
6	366	367	367	368	367	368	366	60																
7												2	349	367	366	367	366	366	367	367	367	367	367	256
8	368	367	368	368	368	367	367	367	367	368	367	368	367	367	368	367	368	367	368	368	367	367	367	367
9	367	367	367	367	368	367	367	367	366	367	367	160	276	366	367	366	367	367	366	366	367	367	366	367
10	367	367	366	367	367	367	367	366	367	366	366	366	320	367	367	366	366	367	366	367	366	367	366	339
11	230	366	366	367	366	367	367	335	366	366	367	366	366	366	366	366	366	366	366	367	366	367	366	366
12	367	367	367	366	367	367	366	367	366	31	306	366	367	366	367	367	366	367	366	366	367	366	366	367
13	366	366	366	367	367	366	367	367	367	367	366	367	367	366	367	366	366	366	366	367	367	366	367	367
14	367	367	367	367	368	367	367	368	366	367	367	367	332	367	367	367	367	366	366	367	367	366	367	367
15	366	367	367	366	367	367	367	367	366	366	368	367	367	367	368	367	368	367	368	367	367	367	367	367
16	367	367	367	368	367	367	367	368	367	367	368	333	367	366	367	367	367	367	366	367	367	366	367	367
17	366	367	367	367	367	309	348	367	368	367	367	366	367	367	366	367	309	366	328	367	366	367	367	1721
18	512	367	367	367	367	367	367	367	366	367	367	367	366	367	367	366	365	367	367	367	367	367	366	367
19	366	366	367	366	367	368	367	367	366	367	367	366	367	367	367	366	367	367	366	366	367	367	366	367
20	366	367	367	367	367	61		183	366	367	367	367	367	367	367	367	367	366	367	367	367	366	367	366
21	367	367	367	367	367	367	366	367	367	367	366	367	367	367	367	366	367	367	367	367	367	367	367	367
22	367	367	368	367	367	368	13			184	366	366	365	366	367	366	366	366	366	366	366	366	366	366
23	366	367	365	366	366	366	367	366	366	366	366	366	366	366	366	365	366	366	366	366	366	366	364	366
24	366	365	366	366	350	352	317	366	365	365	366	366	365	366	337	365	366	366	365	366	101	28	41	10
25	15	366	366	366	365	365	366	366	366	365	366	366	365	366	366	365	366	365	366	365	366	365	366	365
26	366	365	366	366	366	365	366	366	365	366	365	366	365	365	366	365	365	365	366	365	365	366	365	366
27	366	365	365	366	365	366	366	366	366	365	366	365	1	342	360	366	366	365	366	366	365	366	366	366
28	366	366	366	364	366	366	366	365	366	366	365	366	365	366	366	366	365	366	366	365	366	366	366	364
29	366	366	366	366	366	366	480	2466	2467	2466	2264	308	365	366	366	366	365	366	366	366	366	365	366	366
30	366	366	366	367	366	366	366	366	366	366	366	366	105	239	366	365	366	366	365	366	366	366	365	366
31	366	366	366	365	366	366	366	365	365	366	366	364	366	366	365	366	365	366	366	365	366	366	365	366

Figure 7.10

JUNE 1980 KTVY TOWER

NUMBER OF OBSERVATIONS PER HOUR

DATE \ HOUR	00	01	02	03	04	05	06	07	08	09	10	11	12	13	14	15	16	17	18	19	20	21	22	23
1	366	365	24	366	365	366	365	366	366	366	364	366	365	366	366	365	366	366	365	366	366	365	366	366
2	365	366	366	365	366	366	366	366	365	366	366	365	365	331	364	366	366	365	366	366	365	366	366	365
3	366	366	366	365	366	366	366	366	364	366	344	365	366	366	365	366	366	366	365	366	365	366	366	366
4	365	366	366	366	365	366	366	365	366	366	365	336	365	366	366	365	366	365	365	366	365	366	365	366
5	365	366	366	365	365	366	366	366	366	365	366	366	366	365	366	365	366	365	366	365	366	365	366	365
6	366	366	365	366	366	365	366	366	366	365	366	365	1325	2466	344	365	365	365	366	365	365	365	366	365
7	366	365	366	365	366	365	366	366	365	366	365	365	366	365	365	365	365	365	365	365	366	365	365	365
8	366	366	365	366	366	365	366	366	366	365	366	366	365	366	366	365	366	366	366	366	365	366	366	366
9	365	366	366	366	366	366	366	365	366	366	366	366	122	215	366	367	364	366	366	366	365	366	366	366
10	366	366	365	366	366	366	366	365	366	366	366	365	366	366	366	365	365	366	366	365	366	341	358	365
11	366	366	366	365	365	366	365	366	365	366	366	336	366	365	365	366	365	366	365	366	365	366	366	365
12	366	366	365	366	366	366	365	366	365	365	365	365	365	365	364	364	365	365	365	365	366	365	365	366
13	365	366	365	366	365	366	366	365	365	365	364	337	365	365	365	365	365	364	365	365	365	365	365	365
14	365	366	365	366	365	366	365	366	365	362	365	365	365	365	365	365	365	365	365	365	365	365	366	365
15	365	366	366	365	366	366	366	365	366	365	365	365	365	365	365	365	365	365	365	365	365	364	364	365
16	366	365	362	365	365	366	365	365		183	1642	2467	342	365	365	365	365	365	365	365	365	366	365	237
17	210	150	365	365	366	365	366	365	365	1602	1281	366	365	365	366	365	365	365	364	365	365	365	366	365
18	366	365	365	366	365	366	366	73	366	366	365	365	365	365	365	365	365	365	365	365	364	365	365	365
19	365	366	365	365	366	366	365	366	362	365	365	365	365	365	365	365	365	365	365	365	365	365	365	366
20	366	366	365	366	366	366	365	366	365	366	299	365	365	365	365	365	365	365	365	366	366	365	365	366
21	366	365	366	365	366	366	365	366	366	365	365	365	366	364	366	365	365	365	366	365	365	365	365	366
22	365	366	365	366	366	365	366	366	365	366	366	365	365	365	365	365	365	365	366	364	366	365	366	366
23	365	366	365	365	366	365	365	365	365	365	323	365	365	365	365	365	364	365	365	365	364	363	365	365
24	365	365	365	365	365	366	365	365	365	366	366	364	365	365	365	364	365	365	364	365	365	364	365	365
25	365	364	365	365	365	364	365	365	366	365	364	57												
26																								
27																								
28																								
29																								
30																								

Figure 7.11

APPENDICES A-K

DETAILED CHARACTERISTICS OF NSSL OPERATED EQUIPMENT

APPENDIX A

Doppler Radars

Basic radar system characteristics are given in Table A.1 and represent systems configuration during the 1980 data acquisition season. Certain radar parameters such as transmitter power and receiver noise level are subject to variation and are supplied for the particular data set of interest as part of the daily calibration. Other parameters such as initial delays, timing, and gate alignment are provided to the user by NSSL's Computer and Data Processing Group (CDP). It is recommended that the status of the integrator and hardwired velocity calculator for a data set of interest be determined prior to analysis by utilizing available quality control routines. Experience suggests that with as much data as we have, some hardware errors, previously undetected, will show up in data analysis. Therefore, as a result of user feedback these quality control routines represent not only basic hardware checks but logic that is designed to detect those errors that are infrequent and erratic in nature.

This year the radar PRT was selectable at both the NRO and CIM sites, as shown in Table A.1. This option allows the meteorologist flexibility in selecting parameters for data acquisition.

The option of a dual sampling mode was available at all PRT's at NRO and CIM. This acquisition mode retains the selected Nyquist velocity and unambiguous radial range for velocity measurements but allows intensity measurement to an unambiguous range of four times the Doppler unambiguous range (Table A.1). The advantage is that the long-range intensity measurement can be used to detect range aliasing in the velocity field data. Other options included high gain and wide pulse at both sites and high PRF at NRO. The high-gain and wide-pulse modes improve the radar's detection capabilities in that the radar's sensitivity is enhanced by the wide pulse and weak reflectivity spatial variations are accented by high gain, thus allowing improved mapping of clear-air returns. The high-PRF mode has a maximum unambiguous range of 43 km and Nyquist velocity of 91 $m \cdot s^{-1}$ and is designed for the detection of maximum winds in or near tornadoes.

Table A.1 NSSL Doppler Radar Characteristics - Spring 1980

PARAMETER	CIMARRON (CIM)	NORMAN (NRO)	NRO HI PRF
Antenna			
Shape	Parabolic	Parabolic	Parabolic
Diameter	9.15 m	9.15 m	9.15 m
Half-Power Beam Width	0.85 deg.	0.81 deg.	0.81 deg.
Gain	46 dB	46.8 dB	46.8 dB
First Side Lobe Level	21 dB	21 dB	21 dB
Polarization	Vertical	Vertical	Vertical
RMS Surface Deviation	2.5 mm	2.8 mm	2.8 mm
Transmitter			
Wavelength	10.94 cm	10.52 cm	10.52 cm
Frequency	2735 MHz	2850 MHz	2850 MHz
Peak Power	750 kW	750 kW	200 kW
Pulse Width	1 μs (150 m)**	1 μs (150 m)**	0.30 μs (52 m)
Pulse Repetition Time	See below	See below	288 μs
Receiver			
System Noise Figure	4 dB	4 dB	4 dB
Transfer Function	Doppler - linear Intensity - logarithmic	Doppler - linear Intensity - logarithmic	Doppler - linear Intensity - logarithmic
Dynamic Range	80 dB	80 dB	80 dB
Band Width: 3 dB; 6 dB	.6; .85 MHz	.6; .85 MHz	.45; .63 MHz
Receiver Noise Level	-105 dBM	-108 dBM	-107 dBM

Basic PRT	Unambiguous Velocity	Velocity Range	Velocity Range Increment	Intensity Max Range*	Intensity Range Increment*	Digital Tape Density
768 μs	34.2 ms^{-1}	115 km	150 m	460 km	600 m	744 bpi
922 μs	28.5 ms^{-1}	138 km	180 m	552 km	720 m	620 bpi
1075 μs	24.5 ms^{-1}	161 km	210 m	644 km	840 m	531 bpi
1229 μs	21.4 ms^{-1}	184 km	240 m	736 km	960 m	465 bpi

* Values given are for batch; in equi-spaced mode the intensity range coverage is same as velocity.
** In wide-pulse mode, pulse width is 3 μs or 5 μs; PRT is three times one of above four basic PRT's (usually 768 μs). Equispaced pulses only.

APPENDIX B

VHF Mapper

The VHF space-time mapping instrumentation consists of several basic components -- antennas, bandpass filters, directional logic, time encoders, real-time monitor, and magnetic tape recorder. The antenna array is composed of twelve 2-m-long monopoles equally spaced on the ground in a circle of 7.93 m radius, one 2-m-long monopole at the center of this circle and one 2-m-long dipole located 13.74 m directly above the antenna in the center. Elevation and azimuth are determined, respectively, from this pair of vertically spaced antennas and from a pair of antennas on the circle, e.g., numbers 1 and 5, 2 and 6, etc., also spaced 13.74 m apart. The antennas are coupled to coax cables by wideband emitter followers.

All other instrumentation is located about 60 m from the antennas. Coax cable lengths are adjusted to maintain less than ±0.2 ns variation in signal arrival times. Bandpass filters and associated amplifiers are adjusted to give frequency response characteristics that are 6 dB down in amplitude at 30 and 80 MHz. Directional logic circuits select impulses above an adjustable amplitude threshold that arrive from within preset elevation-azimuth directional limits. These limits are nominally set for 0° to 45° in elevation and for a 60° wide azimuthal sector selectable in 30° increments.

Time encoders determine the time difference of arrival for each pair of antennas to ±0.4 ns. This is converted to binary form and presented to a dual buffered, phase encoded, 9-track tape recorder together with timing and impulse amplitude information. The system can resolve 16,000 impulses per second.

Antenna spacing of 13.74 m produces a measured 0.4 ns time difference of arrival of signal when the impulse source is displaced 0.5° from a bearing perpendicular to the line connecting either pair of antennas. The observed azimuth, elevation, and arrival times of impulses are recorded at Norman and Cimarron (separation about 42 km) and used in post analysis to determine the three-dimensional location of each lightning element producing an impulse detected by the system. Formulations for obtaining azimuth and elevation angles from the measured time differences of arrival and for computing the space-time structure of lightning impulse sources were previously presented by Taylor (1978). The arrival times, measured to 16 μs relative accuracy between stations, are used to identify and select impulses observed at each station as having been produced by a common source, and also to obtain the temporal structure and progression speeds of the lightning processes.

APPENDIX C

Instrumentation at the SEB

The following list describes the characteristics of instruments used to acquire electrical data on storms. All analog data are recorded on a 14-track (plus voice), wide band tape recorder. Time is logged on all recorders and is derived from a time code generator (producing IRIBG and DC code time outputs) synchronized with WWV.

1. Slow antenna: The SA measures the electrostatic field change (ΔE) associated with lightning. The instrument has a transient response of $\simeq 1$ μs and an RC decay time of 10 s. Instrument sensitivity is changed by an operator at the SEB to insure that all electric field changes are being recorded at nearly full scale during the periods when events are also recorded by the VHF mapper or L-band radar systems. Flashes at ranges of ~100 km produce detectable ΔE change. ΔEdata are recorded in analog form using an FM channel (with DC to 50 kHz response).

A 3-ms differentiated ΔE is also obtained and recorded from the slow antenna output.

2. Fast antenna: The FA is identical to the SA except that the instrument decay is 100 μs. Analog ΔE data are recorded with FM (DC - 250 kHz) and direct record (D.R.) electronics (250 Hz - 1 MHz).

3. Optical detector: Silicon photodiodes are used in several circuit configurations to record the luminosity from lightning, both outside and inside the cloud. The "fast" detector, with <5 μs rise time and omnidirectional capabilities, is recorded on a D.R. channel. Other optical detector outputs are recorded on the audio track of the television systems.

4. TV video:

a. Omnidirectional: A silicon target tube video camera is mounted above a parabolic reflector for whole sky photography of lightning. The device has been placed on a tower near the SEB for good visibility.

b. Sector: During some storms a TV camera with a NUVICON tube is used at the SEB to record lightning in a particular sector of interest.

Data from (a) are on 1/2-inch wide video tape reels (7-inch diameter) and (b) on 1/2-inch VHS format video cassettes.

5. Field mill: Electric field at the ground is measured continuously with an upward-facing, rotating-vane field mill. The mill is centered in a ground screen $\simeq 2$ m on a side and 0.15 m above ground so that the nearly undistorted field at the earth's surface is obtained. Data are recorded on the SEB strip chart and a digital cassette at the SEB SAM site.

6. Corona current: Stainless-steel points are mounted atop a 7-m tower and connected to a current amplifier to measure corona current. The amplifier circuit smooths transients from lightning to help prevent saturation. The output is recorded on a digital cassette (same as the field mill).

7. Electric current associated with precipitation: A shielded "Faraday funnel" is connected to a charge amplifier with a 10-s time constant to measure the flux of charge arriving on precipitation at the earth. Data are recorded on the SEB strip chart and a digital cassette (same as field mill) during several, but not all, storms.

8. S-band lightning echo: The NRO log video trigger and antenna position are transmitted to the SEB where they are formatted and recorded on a D.R. channel of the 14-track recorder and occasionally also on a video cassette recorder (VHS format), which has been modified to have a manual gain control. The I and Q Doppler data were recorded on an FM channel of the 14-track tape recorder.

9. 35-mm slides: During selected times, color slides of lightning and cloud features are made.

10. Thunder microphone: A Globe microphone is mounted beneath a wind screen on the ground to record thunder from flashes. The data are recorded on an FM channel of the tape.

APPENDIX D

L-Band Radar

The L-band (≃ 23 cm) radar is an aircraft tracking system that has been modified to observe lightning echoes using both linear or circular polarization. The sensitivity of the radar is -111 dBm. The radar antenna has a cosecant squared pattern with a 3-dB beamwidth of 2.5° and is typically pointed at a region of interest and held fixed for a period of time. The log video and trigger are combined and recorded on a direct record channel and a video cassette recorder (VHS format) modified to have manual gain control. The data are analyzed by 1) displaying and photographing an A scope display with an open-shutter camera that has film continually moving in a direction perpendicular to the horizontal scope sweep, or 2) using a digitizing scheme and transient recorder to capture and display a plot of radar echo intensity at a particular range-time.

APPENDIX E

Stationary Automated Mesonetwork (SAM)

E.1 Station Locations

The following is a list of the stations used for the 1980 mesonetwork. Figure 1.2 shows the location of each site. The first two station digits indicate the year; the second pair indicate the station number. Site 8026 was activated to provide data at a point colocated with a rawinsonde site.

1980 Mesonetwork

I.D.	No.	Name	Lat. N.	Long. W.	MSL Elev Ft[1]	County
MWF	8001	NSSL	35°14'13"	97°27'43"	1175	Cleveland
COE	8003	Coltrane Road	35°29'45"	97°26'32"	1245	Oklahoma
OSE	8005	OKC SE	35°26'24"	97°29'42"	1240	Oklahoma
NWH	8006	NW Highway	35°31'36"	97°33'36"	1278	Oklahoma
YUN	8007	Yukon N	35°33'48"	97°43'37"	1340	Canadian
MOO	8008	Moore	35°18'46"	97°30'43"	1205	Cleveland
WRS	8009	Will Rogers S	35°21'50"	97°36'02"	1243	Cleveland
WNW	8010	Will Rogers NW	35°26'07"	97°40'35"	1280	Canadian
TTE	8013	Tuttle E	35°18'18"	97°40'45"	1292	Grady
MUS	8014	Mustang	35°23'30"	97°45'29"	1360	Canadian
YSW	8015	Yukon SW	35°27'51"	97°48'38"	1337	Canadian
TTS	8026	Tuttle S	35°13'38"	97°51'12"	1273	Grady

[1] Sensors are four feet above the surface.

E.2 Description of Sensor and Recording System Used in the 1980 SAM System Parameters

1. Wind speed: Specially calibrated weather service F-420-C rotating cup DC generator.

2. Wind direction: Weather service F-420-C splayed tail wind vane with direction transmitter modified to provide direction dependent DC output.

3. Dry bulb temperature/wet bulb temperature: Linearized Yellow Spring Model 44202 Thermistors with a self-wetting wet bulb. Aspiration is provided by a vertical axis fan at not less than 2.5 meters/second and is not significantly influenced by ambient winds. A standard weather service Stevenson screen houses the entire system and provides solar radiation shielding.

4. Station pressure: Texas Electronics Aneroid/LVDT Unit (Linear Variable Differential Transformer): a precision aneroid cell having electrical but no direct mechanical connection (a virtually frictionless coupling).

5. Rainfall: A Belfort Model 5-780 weighing bucket raingage with the spring and balance mechanism replaced by a weight sensing load cell.

6. Corona probe: The SAM sites have also been instrumented with probes for determining the corona current that flows beneath storms.

The resolution of each of the above is basically determined by the data logger's analog-to-digital converter and is as follows:

Parameter	Recorded Quantization Increment	Recording Range
1. Wind Speed	0.4 m/s	0-50 m/s
2. Wind Direction	1.4°degrees	0°-360°
3. Dry Bulb Temperature	0.2° C	0°-50° C
4. Wet Bulb Temperature	0.2° C	0°-50° C
5. Pressure	0.5 mb	870-998 mb
6. Rainfall	0.6 mm	0-200 mm
7. Corona Current	0.1 μA	± 1.25 μA

The data collection/logging specifications are as follows:

1) Number of analog channels -- 16.

2) Analog sample and hold aperture ≈ 4 μs

3) A/D conversion

   Quantization - 8 bits
   Speed ≈ 100 μs

4) Sampling rate 1 sample per parameter per second.

5) Signal averaging - 60 1-s samples forming 1-minute means

6) Data storage medium - magnetic cassette tape CNRZ format, 600 bpi density.

APPENDIX F

Lightning Strike Locator

The CG lightning location system consists of three remote direction finders and a central position analyzer. The DF's provide azimuth angle of the return stroke channel to the position analyzer which computes the intersection point of the bearings to determine the flash location. Both devices are described below.

F.1 Direction Finder

The principles of operation of the DF are described in detail by Krider et al. (1976) and Krider et al. (1980). Essentially, the DF determines the azimuth angle to each ground flash by sensing the wideband magnetic field (100 Hz - 1 MHz) through a pair of orthogonal loop antennas. The voltage induced in each loop is proportional to the time derivative of the external magnetic flux density, dB/dt, and a geometrical factor dependent on loop area and angle of incidence (Krider and Noggle, 1975). The output of each loop antenna is integrated, and the integral of the wave up to the initial peak value is digitized. The azimuth angle to the discharge is computed by taking the arc tangent of the ratio of the peak value in loops. Since signal polarity is maintained, there is no 180° azimuth ambiguity. Since the initial peak radiation field for return strokes usually occurs within 5 μs, the calculated azimuth angle corresponds to a point on the channel within several hundred meters of the ground. This technique minimizes horizontal polarization errors, allowing accurate fixes at distances from 20 km to 200 + km (Uman et al. 1980). At these distances single-station random azimuth error is normally distributed around zero with a standard deviation of 0.5° → 0.8°. For distances <20 km, the random error increases to several degrees.

Each waveform that crosses a threshold is evaluated in terms of stringent criteria, which reject all waveforms not indicative of return strokes lowering negative charge:

1. Presence of pre-trigger disturbances
2. Time of first peak
3. Time to half peak
4. Pulse width
5. Presence of subsequent peaks
6. Magnitude of overshoot
7. Electric field polarity

Essentially all intracloud flashes, ignition, CB, or other forms of noise are eliminated. The selection criteria occasionally reject CG flashes with atypical waveforms. Detection efficiency is 90 percent (±5 percent) for distances out to 70 km. Beyond 70 km detection efficiency decreases to 50 percent at 220 km and 30 percent at 550 km.

F.2 Position Analyzer

The position analyzer (PA) consists of a communications card which receives data from up to four input ports (DF's), single board computer with 16 K bytes of magnetic memory, and multifunction boards. As messages are received from each DF, the PA computes time of event by subtracting the transmitted time tag from the time the message is received. This eliminates the need for absolute time

at each DF. The PA then searches for other DF events within 50 ms. Should two or more events occur within 50 ms, the PA computes flash position by triangulation using the two azimuths associated with the largest field changes. Should these two azimuths be on or near the baseline, the third azimuth is used in the calculation. Should only two azimuths be available on the baseline the PA uses the ratio of the two signal strengths to determine the range of the flash.

The position analyzer formats the data, time, computed position, range normalized signal strength and number of return strokes for storage on magnetic tape. During the 1980 field program the tape format was changed to include all raw data. Real-time printouts of first-guess flash location are available.

F.3 Configuration

Antenna location coordinates for the Spring '80 configuration are given below:

	Relative to Base (at NSSL)				
	x (km)	y (km)	Latitude(°)	Longitude(°)	Elevation
Origin	0	0	35.2381	97.4619	358
DF 1	+ 0.07	- 0.05	35.2377	97.4604	358
DF 2	-49.33	+24.96	35.4698	97.9991	428
DF 3	-45.49	-15.82	35.1014	97.9566	350

$$\tau_p = (n_p-1)\,\Delta\tau; \qquad \Delta\tau = \frac{PRT(\mu s)}{768}\ \mu s \tag{G.1}$$

where $\Delta\tau$ is the gate spacing. If the range to the known target is r_t then the true time delay between the transmitter start and echo response start is

$$\tau_t = \frac{2r_t}{c} \tag{G.2}$$

Therefore the radar delay time τ_R, which is due to delays in transmitter start, delays in transmission lines from antenna to the transmitter and receiver, and receiver delay due to finite receiver bandwidth, is

$$\tau_R = \tau_p - \tau_t = (n_p-1)\Delta\tau - 2r_t/c \tag{G.3}$$

The radar delay τ_R needs to be substracted from the range time position of any sample gate. Thus given a weather signal voltage, sampled with the k^{th} gate, the precipitation targets (i.e., drops) that contribute most to the k^{th} sample are at range

$$r(k) = \frac{c}{2}\left\{(k-1)\Delta\tau - \tau_R\right\} \tag{G.4}$$

Substituting we obtain

$$r(k) = r_t - \frac{c\Delta\tau}{2}(n_p-k) \tag{G.5}$$

For reference purposes we tabulate in Table G.1 the range of meteorological targets that contribute most to the echo sampled at Gate #1.

An example of the computer output plot is shown on Figure G.2 where two towers are identified on the D.I. output and their true range r_t is given. The apparent range r_a is equal to $C\Delta\tau(k-1)/2$. This figure also shows the PPP Doppler velocity and spectrum width estimate vs. gate number. In these data we have echo returns from the region surrounding the towers that have a positive velocity and relatively high spectrum width, characteristic of clear air returns.

We expect, that when ground clutter echo intensity is strongest, velocity and spectrum width estimate is biased closest to zero. Thus we see in Figure G.2 that minimum width is displaced three gates to the right of the maximum echo intensity returned from the KTVY tower. A similar analysis shows that the velocity gates are also displaced by three from the digital integrator gate positions. Table G.1 lists the gate shift corrections that need to be made in order to align the gates of intensity, velocity, and spectrum width. The most ideal targets for gate alignment are birds or other point targets moving in a field of clear-air returns.

APPENDIX G

Ground Target Method to Determine Radar System Timing

Normally, it is necessary to measure several delays associated with radar system timing (i.e., Tx pulse, Rx delay, etc.) in order to calculate slant range to the first integrator gate. Considerable time and care are required to make these measurements if a ranging uncertainty small compared with radar sample volume is to be achieved (see Part II, Section 5a and 5b of 1975 Summary). The various contributions to the composite delay are of little or no interest to most data users, and prone to misinterpretation. Use of a known range target is a quick objective technique to determine the slant range to the first gate. It is especially adaptable to the integrator and works equally well for all nine data acquisition composite modes for both the Norman and Cimarron Doppler radars. The technique is applied to echoes from isolated, tall television towers near (within 60 km) NSSL. Data are acquired in all modes by pointing the antenna at each tower and collecting fifty sample echoes at all ranges along the beam. These data are then processed by computer, and the output is plotted for visual examination.

A sketch of echo return from a point target is given in Figure G.1 to demonstrate the technique. We select the zero reference for apparent range time τ_a to be at Gate #1. In the following procedure it is not important to know the exact location of the transmitter start time. The delay between Gate #1 and transmitter start is part of a total radar delay τ_R which we now compute. The measured time delay τ_p from Gate #1 to the peak response of an echo from a known point target is

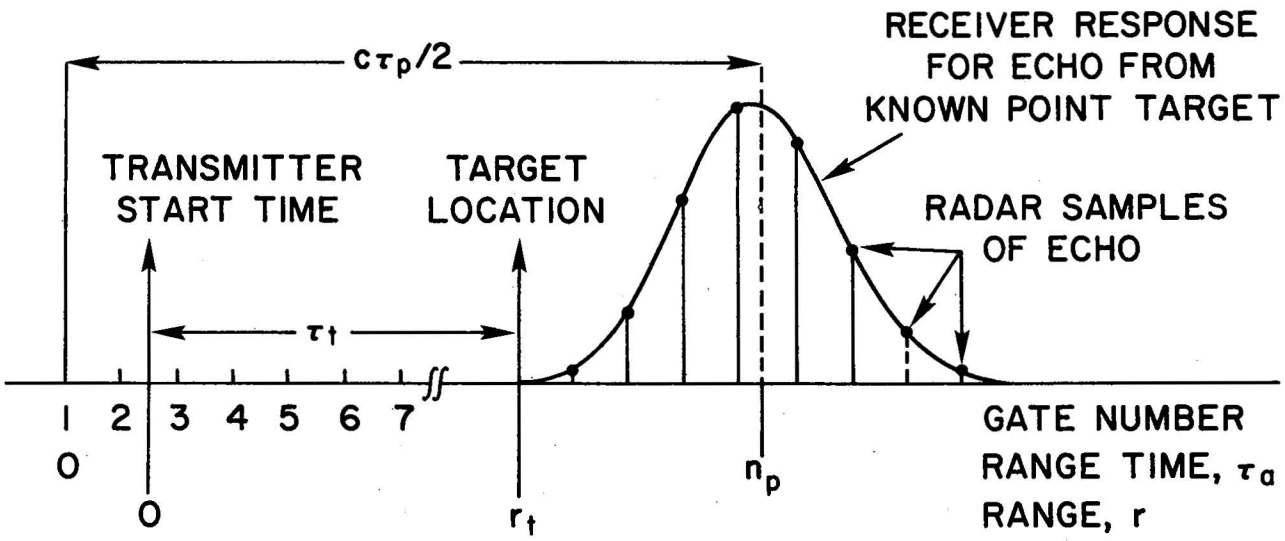

Figure G.1 Schematic of digital integrator output versus range or gate number for an isolated point target.

TABLE G.1

1980 DOPPLER RANGING INFORMATION

RANGE OF TARGET IN GATE #1

PRT	Gate Spacing	NRO Range to Gate 1	CIM Range to Gate 1
768 N	150 m	-310 m	-1010 m
922 N	180 m	-190 m	-1130 m
1075 N	210 m	-130 m	-1100 m
1229 N	240 m	-130 m	-1250 m
768 E	600 m	-310 m	-1300 m
922 E	720 m	-310 m	-1480 m
1075 E	840 m	-180 m	-1730 m
1229 E	960 m	-160 m	-2450 m
768 W3-5	450 m	-200 m	-1750 m

N = Normal Mode
E = Expanded Integrator
W3-5 = Wide Pulse 3 μs

GATE SHIFT CORRECTIONS

NRO - NORMAL
INT(1) = INT(1)
VEL(1) = VEL(3)
STD(1) = STD(3)

NRO - Wide Pulse 3-5
INT(1) = INT(1)
VEL(1) = VEL(3)
STD(1) = STD(4)

CIM - NORMAL
INT(1) = INT(1)
VEL(1) = VEL(3)
STD(1) = STD(4)

CIM - Wide Pulse 3-5
INT(1) = INT(1)
VEL(1) = VEL(2)
STD(1) = STD(3)

Where INT = INTEGRATOR
VEL = PP VELOCITY
STD = PP WIDTH ESTIMATOR

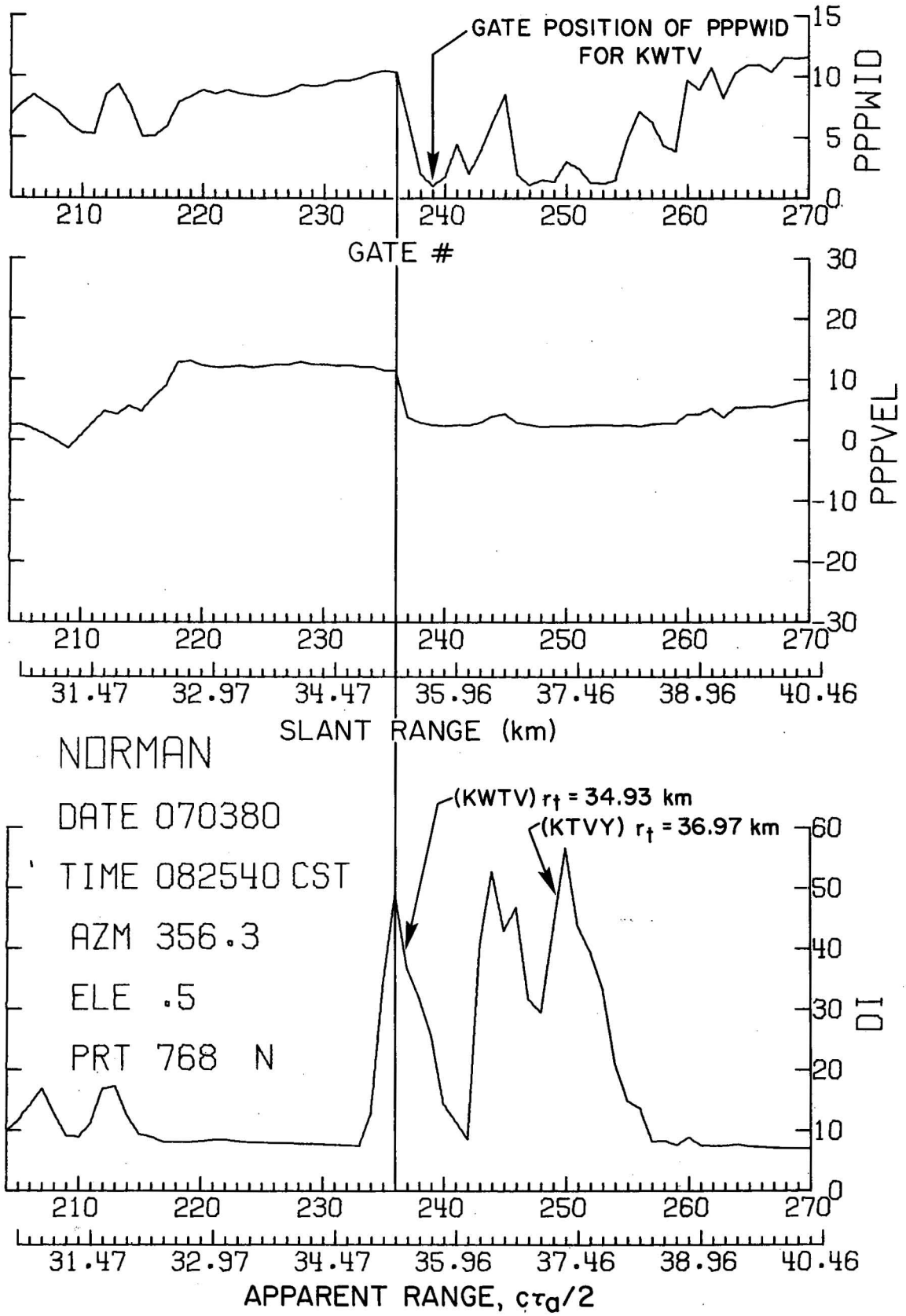

Figure G.2 Plots of average values of the Digital Integrator (DI), PPP Velocity, and the PPP Width Estimator versus Slant Range and Gate Number. Peak DI values represent returns from isolated tall television towers.

APPENDIX H

Antenna Beam Pointing Corrections for NRO/CIM Doppler Radars

The following are recommended 1980 antenna pointing error correcting functions for the NRO/CIM radars. The beam direction error function is derived from sun scan data.

1980 Beam Direction Error Functions

CIM

Elevation Error = $-0.7 \cos \theta + 0.52$ degrees

Azimuth Error = $-0.75 [\cos (\phi + 23°)] - 0.55$ degrees

NRO

Elevation Error = $-0.5 \sin \theta$ degrees

Before 5/13/80

Azimuth Error = $-0.67 [\cos (\phi + 5°)] - 0.25$ degrees

After 5/13/80

Azimuth Error = $-1.15 [\cos (\phi + 5°)] - 0.42$ degrees

where ϕ and θ are the indicated (recorded) azimuth and elevation angles. A negative error indicates the recorded elevation angle is less than the true elevation angle and the recorded azimuth is CCW from (less than) the true azimuth.

APPENDIX I

Solar Flux Measurements

Three measurements of solar power at a wavelength of 10 cm were made during the 1980 Spring Season. The power is calculated from sun flux, F, data measured at the Algonquin Radio Observatory in Ottawa, Canada. The value issued by the Observatory is the sum of both horizontal and vertical polarization and is reduced by one-half for comparison with the single polarization measurement of the radars. The Observatory measures the vertically polarized component and multiplies by two for total power. Results are summarized in the following table.

Date: 4/22/80 Sun Flux = $197(10^{-22})$ watts/m^2/Hz

Station	D.I. Digit	Time	Pr Measured	Pr Estimated	Difference
NRO	27.4	1259:38 CST	-99.2 dBm	-97.8 dBm	-1.4 dB
CIM	24.8	1300:29 CST	-100.7 dBm	-99.1 dBm	-1.6 dB
Date: 5/8/80		Sun Flux = $191(10^{-22})$ watts/m^2/Hz			
NRO	26.4	1200:02 CST	-98.9 dBm	-97.9 dBm	-1.0 dB
CIM	26.0	1200:28 CST	-99.7 dBm	-99.2 dBm	-0.5 dB
Date: 6/27/80		Sun Flux = $209(10^{-22})$ watts/m^2/Hz			
NRO	25.7	6:59:00 CST	-99.4 dBm	-97.5 dBm	-1.9 dB
CIM	21.7	6:59:30 CST	-98.4 dBm	-98.8 dBm	+0.4 dB
WSR-57	9.7	7:02:30 CST	-102.3 dBm	-103.2 dBm	+0.9 dB

The general agreement between the Observatory and radar measured flux is within the calibration uncertainty of the radars. Details of the power calibration and radar system characteristics are given below. Estimated power is referenced to the radar receiver calibration port and is calculated by:

$$Pr\ (dBm) = 10 \log [F\ Aeff\ BW_n] - L_{wg} - L_r + 30 \qquad (I.1)$$

where

- Pr = receiver input power (dBm)
- F = sun flux (watts/m^2/Hz)
- Aeff = effective area of antenna aperture (m^2)
- BW_n = receiver noise bandwidth (Hz)
- L_{wg} = waveguide loss from calibration port to aperture
- L_r = radome transmission loss (dB)

Individual system parameters:

Site	Aeff	BW_n	L_{wg}	L_r
WSR-57	5.72 m^2	0.795 (10^6) Hz	0 dB	0 dB
CIM	38.1 m^2	0.636 (10^6) Hz	1.8 dB	1 dB
NRO	42.1 m^2	0.636 (10^6) Hz	1 dB	1 dB

APPENDIX J

Effects of Doppler Radar Receiver's AGC in Regions of Large Reflectivity Gradient

J.1 Hardware Functional Description

The receiver Automatic Gain Control (AGC) scheme in the Doppler radars is a "look ahead" method. Echo power is measured by integrating logarithmic receiver samples weighted with an exponential time window having a time constant compatible with time required to collect samples for velocity estimation. Echo power, estimated at the beginning of the velocity sample acquisition period, is used to control receiver gain for the entire period over which the velocity and spectrum width estimate is made. Receiver gain is not allowed to vary during this estimate period because a modulation of the complex signal would result in velocity and spectrum width errors.

The tacit assumption in this technique is that reflectivity during the velocity estimation period does not vary and does not differ from its previous value by more than that which can be accommodated by the digital word size used in the PPP. The AGC is not adjusted for trends in reflectivity. If the antenna is moving from low to high reflectivity, the AGC will undercompensate, i.e., allow the signal amplitude presented to the processing chain to increase above the quiescent value. If moving from high to low reflectivity, the AGC will overcompensate, i.e., allow the signal amplitude to fall below the quiescent value.

The Analog-to-Digital Converter (ADC) word length is eight bits (2's complement). Normally, the complex video is set such that signal rms amplitude is about 1/3 of the ADC conversion range (about digital 40 on a scale of 0-127). This allows signal amplitude to increase about a factor of three (10 dB) before significant clipping occurs. Severe clipping after phase demodulation (i.e., by the ADC) results in both mean velocity bias and increased uncertainty in velocity estimates. The extreme case of hard limiting also causes an error in signal correlation resulting in a width estimate bias proportional to true width.

However, this effect would probably not be detectable in practice unless the signal rms exceeded the AGC maximum range by about a factor of 4, i.e., AGC undercompensation by about 13 dB. Saturation prior to phase demodulation (at RF or IF), as can only occur in NSSL's radars, does not result in a bias of the mean velocity estimate but does result in an increase in apparent spectrum width (increases by $\sqrt{2}$).

AGC overcompensation is a more serious problem than undercompensation. Reduction of the input signal rms amplitude to a level comparable with the digital quantization interval results in loss of detection and zero amplitude samples in the estimate. Quantization effects become appreciable when signal rms is less than about digial eight.

J.2 Examples of Problem Areas

An example of reflectivity gradient effect on AGC performance is shown in the attached plots of intensity, velocity, and spectrum width (Figures J.1, CW antenna rotation, J.2 CCW antenna rotation). Enclosed areas are regions where the reflectivity azimuthal gradient is greater than 13 dB per azimuth increment (ΔAZ). Direction of antenna beam motion is indicated by arrow. Of particular interest in

Figure J.1 is the region centered about -51 km, -40 km where the beam is moving from high to low reflectivity. The gradient in this region has an average of 18.4 dB/ΔAz and a standard deviation of gradient 3.5 dB/ΔAz. Note the low velocities along the upper radials with magnitude inconsistent with surrounding radials. This anomaly is attributed to coarse quantization by the ADC because of AGC overcompensation.

Note also the region centered at -42 km where the antenna is moving from a region of low to high reflectivity. Average gradient in this region is 16 dB/ΔAz with standard deviation of 2 dB/ΔAz. A signal increase of 16 dB is well beyond the range that can be absorbed by the ADC for normal AGC setup and should result in significant clipping. However, this effect is not readily apparent in the velocity field.

An example of signal quantization and clipping at the next lower elevation angle is shown in Figure J.2. The region centered at -49 km, -40 km has average gradient of 18.5 dB/ΔAz with a standard deviation of 2.7 dB/ΔAz, and the beam moves from a region of low to high reflectivity. As in Figure J.1, the effects of clipping are not obvious. However, in the region of J.2 centered at -45 km, -45 km, the average gradient is 16 dB/ΔAz with a standard deviation of 3 dB/ΔAz, and the beam sweeps from high to low power. Here the effects of signal quantization are evident in the magnitude of the velocity estimate as in Figure J.1. Comparison of Figures J.1 and J.2 adds credence to the interpretation that anomalous velocities can be due to large gradients and to low gain of the AGC for much of the acquisition period.

Biases are not readily apparent in the width fields shown in Figures J.1 and J.2. However, there is a hint of anomalously large widths in J.2 where the AGC overcompensation may cause signal rms level to be small compared with the ADC quantization interval.

J.3 Estimation of Gradient Magnitudes That Cause Trouble

The magnitude of gradient resulting in significant problems with mean velocity estimate appears to be about 15 dB/(ΔAz per radial) provided that samples for velocity estimation are acquired during at least 70 percent of the time between radial updates. Theory and simulation predict the influence to become significant at a signal rms of 8 which is about 14 dB below the usual quiescent value of about 40. As illustrated in the blocked regions of Figs. J.1 and J.2, the quantization effect is apparent at gradient values of 16 dB/ΔAz and larger. Effects are not obvious at gradient of 10 dB/ΔAz and smaller.

The same theory predicts the effects of clipping to become significant at gradients greater than about 10 dB/ΔAz. However, clipping effects are more subtle than quantization. As mentioned previously, clipping at RF or IF results in an increase in apparent spectrum width, causing an increase in standard deviation of mean velocity estimate, but not a bias. In the extreme (hard limiting), spectrum width increase is about 40 percent (about 1.6 m s^{-1} for a true width of 4 m s^{-1}). Generally, this would probably be obscured by the inherent variation of a field width estimate standard diviation of about 1 m s^{-1}.

J.4 Summary

Velocity and spectrum width data taken in regions where the intensity change is 15 dB/ΔAz or larger between adjacent azimuthally spaced estimates (or radially

spaced estimates for data collected in the expanded model) may have significant bias, particularly in the velocity estimate. Data recovery by correction of mean velocity estimate according to the gradient is not recommended. Instead, it is recommended that data in regions where the gradient exceeds 13 dB to 15 dB/ΔAz (or per radial increment ΔR = 600 m) be flagged as potentially erroenous and subjectively edited.

This gradient problem can be minimized by increasing the azimuthal (or radial) sampling density. However, in extreme cases, as illustrated in Figures J.1 and J.2, this would require sampling at a small fraction (about 1/4) of the antenna beamwidth and a slow through-put rate which may not be compatible with experimental objectives.

A better solution would be expansion of the hardware to accommodate a larger signal dynamic range. This is planned as part of the long-range engineering for upgrading of the Doppler radars (in conjunction with conversion from 7-track to 9-track recording) but obviously this does not help with data already acquired.

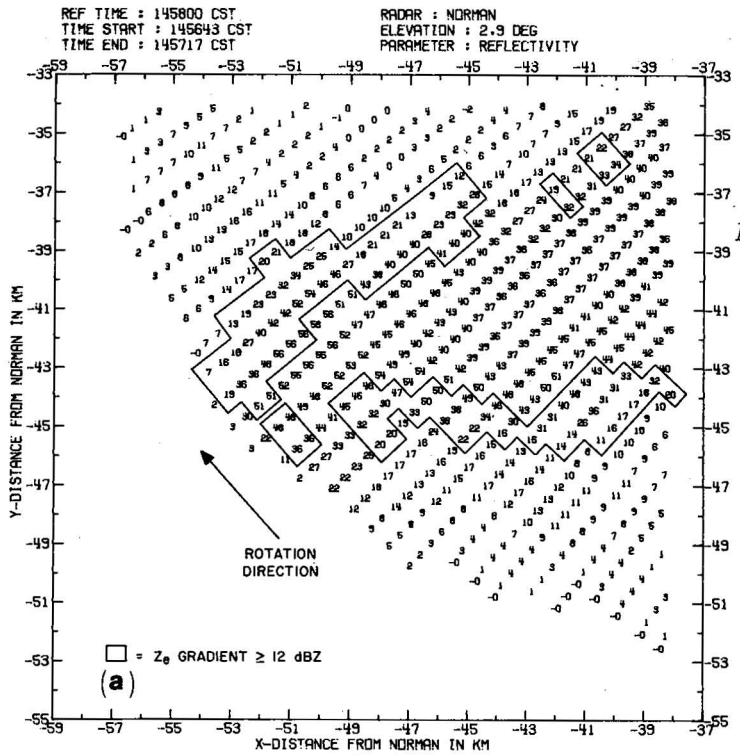

Figure J.1 Intensity (a), velocity (b) and spectrum width (c) from Norman Doppler radar at 2.9° elevation angle. Boxed regions indicate intensity gradients greater than 12 dB/ΔAz. Circled velocity values are the most obvious anomalous values.

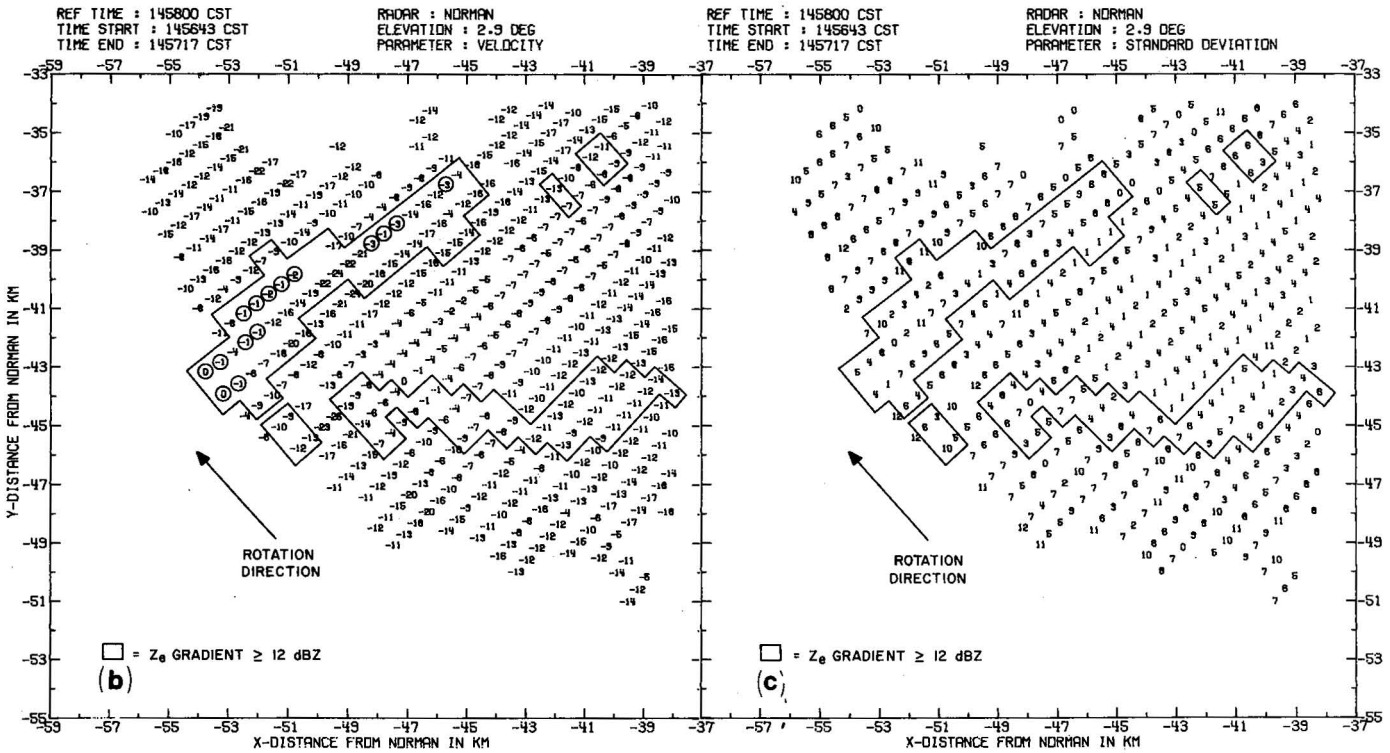

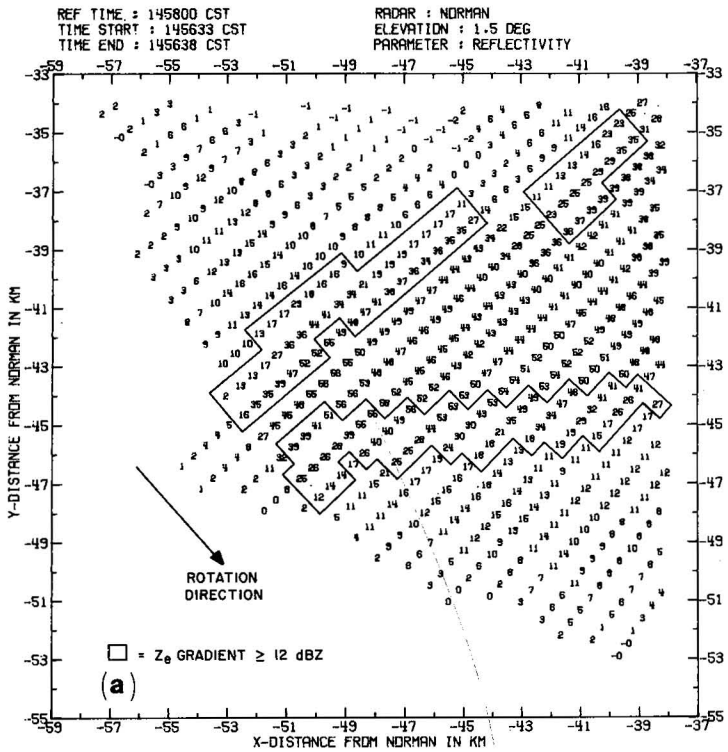

Figure J.2 Same as Figure J.1 except for adjacent elevation angle (1.5°) where radar antenna rotation is in the opposite direction.

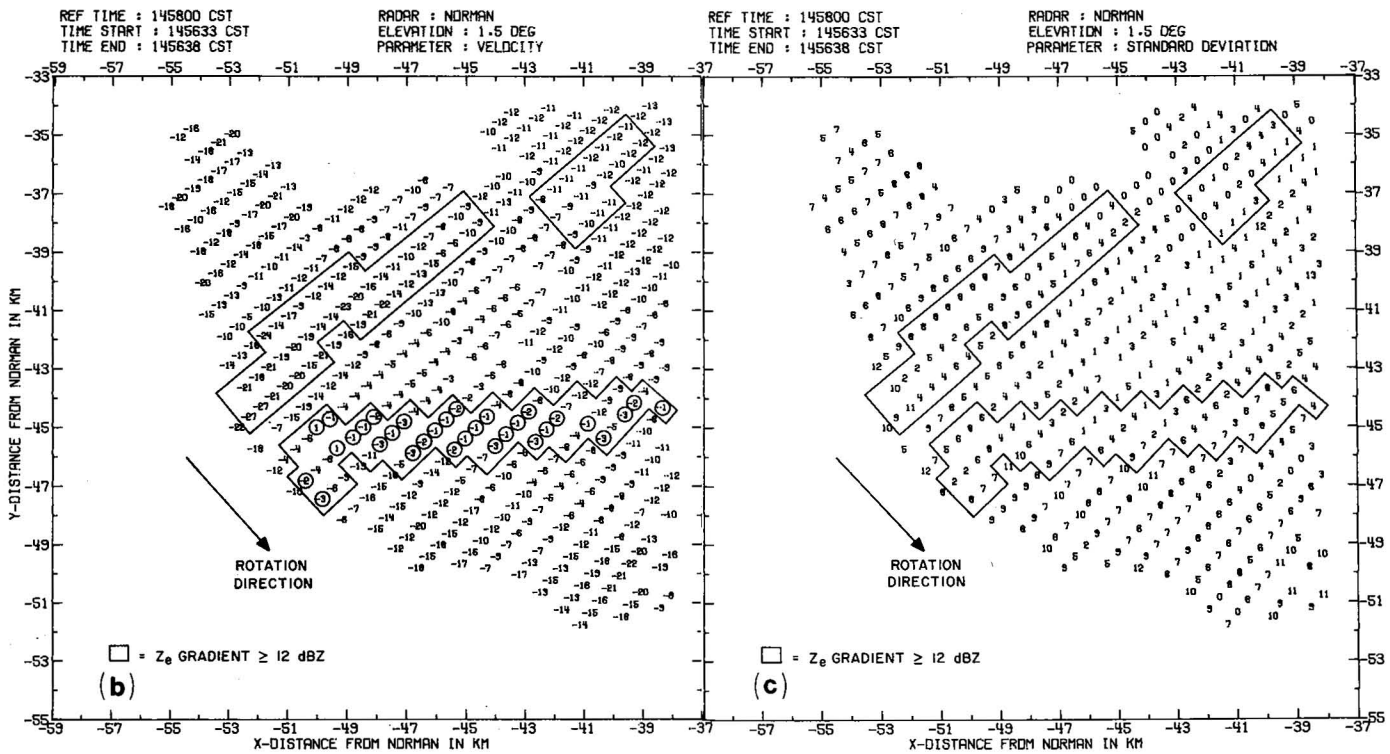

APPENDIX K

Aircraft Data Instrumentation

K.1 Information recorded by the T-28 instrumentation system

A. State parameters and position keeping

1. Time
2. Altitude
3. Temperature

    a. Rosemount resistance
    b. WSI reverse flow
    c. Barnes IR

4. VOR
5. DME

B. Updrafts

1. Rate-of-climb
2. Manifold pressure
3. Indicated airspeed
4. Vertical accelerations

C. Composition of high reflectivity zone

1. Liquid

    a. Rain rate 40
    b. J. W. liquid water
    c. Kyle total water
    d. Rosemount ice rate

2. Solid

    a. Hail sound on windshield
    b. Hail sensor
    c. Hail camera

3. Liquid and solid

    a. Foil impactor
    b. Precipitation sampler

D. General

1. Regulated 5 volts
2. Event code
3. Voice comments (pilots observations)
4. Radio conversations

Table K.1 - F-106B Measurements on Aircraft Instrumentation System for Storm Hazards '80

Measurement	Range	Required Flat to Freq. Resp., Hz	σ Error Accuracy	Resolution	Notes
Stormscope dots	-	-	-	-	Serial PCM
Stormscope clear	-	-	-	-	Discrete
Stormscope range buttons	-	-	-	-	Discrete
Pilot event	-	-	-	-	Pilot's control stick-discrete
Copilot event	-	-	-	-	AIS panel-discrete
Static pressure	0-15 psia	3	0.07 psia	0.0004 psia	Quartz transducer-under-nose pitot-static head
Dynamic pressure	0-3 psid	6	0.03 psid	0.0004 psid	Quartz transducer-gust boom for p_t
Angle of attack	±15°	10	0.09°	0.015°	Flow vane on gust boom
Angle of side-slip	±15	10	0.09°	0.015°	Flow vane on gust boom
Pitch rate	±1 s^{-1}	5	0.01s^{-1}	0.004s^{-1}	Mounted in weapons bay
Roll rate	±1 s^{-1}	5	0.01s^{-1}	0.004s^{-1}	Mounted in weapons bay
Yaw rate	±1 s^{-1}	5	0.01s^{-1}	0.004s^{-1}	Mounted in weapons bay
Long. accel.	±1g	10	0.01g	0.004g	Mounted at CG - no good
Lat. accel.	±1g	10	0.01g	0.004g	Mounted at CG - no good
Norm. accel.	4 to -2g abs	10	0.01g	0.012g	Mounted at CG

Table K.1 - Continued

Measurement	Range	Required Flat to Freq. Resp., Hz	σ Error Accuracy	Resolution	Notes
Total air temperature	35° to -75°C	0.5	0.3°C	0.205°C	Probe beneath nose
Stick-Lateral	Full travel	N/A	-	-	Pilot's control stick
Stick-Long.	Full travel	N/A	-	-	Pilot's control stick
Pitch attitude	±15°	5	0.03°	0.015°	INS platform-contin. synchro.
Roll attitude	±30°	5	0.1°	0.03°	INS platform-contin. synchro.
True Heading	0°-360°	-	-	0.18°	INS platform-contin. synchro.
Vertical accel.	3 to -1g	5	0.005g	0.008g	INS platform-accel.
N-S ground speed	±4096ft/s	50 ms	3ft/s	0.001ft/s	INS platform-digital
E-W ground speed	±4096ft/s	50 ms	3ft/s	.001ft/s	INS platform-digital
Latitude	±90°	600 ms	1nmi/h	0.14arcsec	INS platform-digital
Longitude	±180°	600 ms	1nmi/h	0.14arcsec	INS platform-digital
Track angle	±(0°-180°)	600 ms	-	0.14arcsec	INS platform-digital
Dist. to go	$64x10^6$ ft	600 ms	-	16 ft	INS platform-digital
True heading	0° - 360°	50 ms	-	0.14arcsec	INS platform-digital-should be used for data
Bearing to dest.	0° - 360°	600 ms	-	0.14arcsec	INS platform-digital
ACE events	-	-	-	-	24 ACE bottles-discretes
Audio	-	-	-	-	Transmit, receive and intercom
Rudder pedals	Full range	-	-	-	Pilot's pedals

Table K.1 - Concluded

Measurement	Range	Required Flat to Freq. Resp., Hz	σ Error Accuracy	Resolution	Notes
Ship's altitude	-	-	-	-	From ship's computer-ref. use only
Ship's airspeed	-	-	-	-	From ship's computer-ref. use only

ACKNOWLEDGMENTS

The authors are indebted to Ms. J. Walton for her meticulous and accurate typing and management of the typing efforts of Mss. B. Franklin, C. Carter, S. Mudd and M. Tyo. Drafting support of Messrs. C. Clark and R. Goldsmith and Ms. J. Kimpel is greatly appreciated. R. Brown's diligent observations resulted in Appendix J.

REFERENCES

Krider, E. P., and R. C. Noggle, 1975: Broadband antenna systems for lightning magnetic fields, J. Appl. Meteor., 14, 252-256.

_____, R. C. Noggle, and M. A. Uman, 1976: A gated, wideband magnetic direction finder for lightning return strokes, J. Appl. Meteor., 15, 301-306.

_____, R. C. Noggle, A. E. Pifer, and D. L. Vance, 1980: Lightning direction-finding systems for forest fire detection, Bull. Amer. Meteor. Soc., 61, 980-986.

Taylor, W. L., 1978: A VHF technique for space-time mapping of lightning discharge processes, J. Geophys. Res., 83, 3575-3583.

Uman, M. A., Y. T. Lin, and E. P. Krider, 1980: Errors in magnetic direction finding due to non-vertical lightning channels, Radio Sci., 15, 35-39.

Vonnegut, B., and R. E. Passarelli, Jr., 1978: Modified cine sound camera for photographing thunderstorms and recording lightning, J. Appl. Meteor., 17, 1079-1081.

NATIONAL SEVERE STORMS LABORATORY

The NSSL Technical Memorandum, beginning with No. 28, continue the sequence established by the U. S. Weather Bureau National Severe Storms Project, Kansas City, Missouri. Numbers 1-22 were designated NSSP Reports. Numbers 23-27 were NSSL Reports, and 24-27 appeared as subseries of Weather Bureau Technical Notes. These reports are available from the National Technical Information Service, Operations Division, Springfield, Virginia 22151, a microfiche version for $3.50 or a hard copy, cost depending upon the number of pages. NTIS numbers are given below in parenthesis.

No. 1 National Severe Storms Project Objectives and Basic Design. Staff, NSSP. March 1961, 16 p. (PB-168207)

No. 2 The Development of Aircraft Investigations of Squall Lines from 1956-1960. B. B. Goddard. 34 p. (PB-168208)

No. 3 Instability Lines and Their Environments as Shown by Aircraft Soundings and Quasi-Horizontal Traverses. D. T. Williams. February 1962. 15 p. (PB-168209)

No. 4 On the Mechanics of the Tornado. J. R. Fulks. February 1962. 33 p. (PB-168210)

No. 5 A Summary of Field Operations and Data Collection by the National Severe Storms Project in Spring 1961. J. T. Lee. March 1962. 47 p. (PB-165095)

No. 6 Index to the NSSP Surface Network. T. Fujita. April 1962. 32 p. (PB-168212)

No. 7 The vertical structure of Three Dry Lines as Revealed by Aircraft Traverses. E. L. McGuire. April 1962. 10 p. (PB-168213)

No. 8 Radar Observations of a Tornado Thunderstorm in Vertical Section. Ralph J. Donaldson, Jr. April 1962. 21 p. (PB-174859)

No. 9 Dynamics of Severe Convective Storms. Chester W. Newton. July 1962. 44 p. (PB-163319)

No. 10 Some Measured Characteristics of Severe Storms Turbulence. Roy Steiner and Richard H. Rhyne. July 1962. 17 p. (N62-16401)

No. 11 A Study of the Kinematic Properties of Certain Small-Scale Systems. D. T. Williams. October 1962. 22 p. (PB-168216)

No. 12 Analysis of the Severe Weather Factor in Automatic Control of Air Route Traffic. W. Boynton Beckwith. December 1962. 67 p. (PB-168217)

No. 13 500-Kc./Sec. Sferics Studies in Severe Storms. Douglas A. Kohl and John E. Miller. April 1963. 36 p. (PB-168218)

No. 14 Field Operations of the National Severe Storms Project in Spring 1962. L. D. Sanders. May 1963. 71 p. (PB-168219)

No. 15 Penetrations of Thunderstorms by an Aircraft Flying at Supersonic Speeds. G. P. Roys. Radar Photographs and Gust Loads in Three Storms of 1961 Rough Rider. Paul W. J. Schumacher. May 1963. 19 p. (PB-168220)

No. 16 Analysis of Selected Aircraft Data from NSSP Operations, 1962. T. Fujita. May 1963. 29 p. (PB-168221)

No. 17 Analysis of Methods for Small-Scale Surface Network Data. D. T. Williams. August 1963. 20 p. (PB-168222)

No. 18 The Thunderstorm Wake of May 4, 1961. D. T. Williams. August 1963. 23 p. (PB-168223)

No. 19 Measurements by Aircraft of Condensed Water in Great Plains Thunderstorms. George P. Roys and Edwin Kessler. July 1966. 17 p. (PB-173048)

No. 20 Field Operations of the National Severe Storms Project in Spring 1963. J. T. Lee, L. D. Sanders, and D. T. Williams. January 1964. 68 p. (PB-168224)

No. 21 On the Motion and Predictability of Convective Systems as Related to the Upper Winds in a Case of Small Turning of Wind with Height. James C. Fankhauser. January 1964. 36 p. (PB-168225)

No. 22 Movement and Development Patterns of Convective Storms and Forecasting the Probability of Storm Passage at a Given Location. Chester W. Newton and James C. Fankhauser. January 1964. 53 p. (PB-168226)

No. 23 Purposes and Programs of the National Severe Storms Laboratory, Norman, Oklahoma. Edwin Kessler. December 1964. 17 p. (PB-166675)

No. 24 Papers on Weather Radar, Atmospheric Turbulence, Sferics and Data Processing. August 1965. 139 p. (AD-621586)

No. 25 A Comparison of Kinematically Computed Precipitation with Observed Convective Rainfall. James C. Fankhauser. September 1965. 28 p. (PB-168445)

No. 26 Probing Air Motion by Doppler Analysis of Radar Clear Air Returns. Roger M. Lhermitte. May 1966. 37 p. (PB-170636)

No. 27 Statistical Properties of Radar Echo Patterns and the Radar Echo Process. Larry Armijo. May 1966. The Role of the Kutta-Joukowski Force in Cloud Systems with Circulation. J. L. Goldman. May 1966. 34 p. (PB-170756)

No. 28 Movement and Predictability of Radar Echoes. James Warren Wilson. November 1966. 30 p. (PB-173972)

No. 29 Notes on Thunderstorm Motions, Heights, and Circulations. T. W. Harrold, W. T. Roach, and Kenneth E. Wilk. November 1966. 51 p. (AD-644899)

No. 30 Turbulence in Clear Air Near Thunderstorms. Anne Burns, Terence W. Harrold, Jack Burnham, and Clifford S. Spavins. December 1966. 20 p. (PB-173992)

No. 31 Study of a Left-Moving Thunderstorm of 23 April 1964. George R. Hammond. April 1967. 75 p. (PB-174681)

No. 32 Thunderstorm Circulations and Turbulence from Aircraft and Radar Data. James C. Fankhauser and J. T. Lee. April 1967. 32 p. (PB-174860)

No. 33 On the Continuity of Water Substance. Edwin Kessler. April 1967. 125 p. (PB-175840)

No. 34 Note on the Probing Balloon Motion by Doppler Radar. Roger M. Lhermitte. July 1967. 14 p. (PB-175930)

No. 35 A Theory for the Determination of Wind and Precipitation Velocities with Doppler Radars. Larry Armijo. August 1967. 20 p. (PB-176376)

No. 36 A Preliminary Evaluation of the F-100 Rough Rider Turbulence Measurement System. U. O. Lappe. October 1967. 25 p. (PB-177037)

No. 37 Preliminary Quantitative Analysis of Airborne Weather Radar. Lester P. Merritt. December 1967. 32 p. (PB-177188)

No. 38 On the Source of Thunderstorm Rotation. Stanley L. Barnes. March 1968. 28 p. (PB-178990)

No. 39 Thunderstorm - Environment Interactions Revealed by Chaff Trajectories in the Mid-Troposphere. James C. Fankhauser. June 1968. 14 p. (PB-179659)

No. 40 Objective Detection and Correction of Errors in Radiosonde Data. Rex L. Inman. June 1968. 50 p. (PB-180284)

No. 41 Structure and Movement of the Severe Thunderstorms of 3 April 1964 as Revealed from Radar and Surface Mesonetwork Data Analysis. Jess Charba and Yoshikazu Sasaki. October 1968. 47 p. (PB-183310)

No. 42 A Rainfall Rate Sensor. Brian E. Morgan. November 1968. 10 p. (PB-183979)

No. 43 Detection and Presentation of Severe Thunderstorms by Airborne and Ground-based Radars: A Comprehensive Study. Kenneth E. Wilk, John K. Carter, and J. T. Dooley. February 1969. 56 p. (PB-183572)

No. 44 A Study of a Severe Local Storm of 16 April 1967. George Thomas Haglund. May 1969. 54 p. (PB-184970)

No. 45 On the Relationship Between Horizontal Moisture Convergence and Convective Cloud Formation. Horace R. Hudson. March 1970. 29 p. (PB-191720)

No. 46 Severe Thunderstorm Radar Echo Motion and Related Weather Events Hazardous to Aviation Operations. Peter A. Barclay and Kenneth E. Wilk. June 1970. 63 p. (PB-192498)

No. 47 Evaluation of Roughness Lengths at the NSSL-WKY Meteorological Tower. Leslie D. Sanders and Allen H. Weber. August 1970. 24 p. (PB-194587)

No. 48 Behavior of Winds in the Lowest 1500 ft in Central Oklahoma: June 1966-May 1967. Kenneth C. Crawford and Horace R. Hudson. August 1970. 57 p. (N71-10615)

No. 49 Tornado Incidence Maps. Arnold Court. August 1970. 76 p. (COM-71-00019)

No. 50 The Meteorologically Instrumented WKY-TV Tower Facility. John K. Carter. September 1970. 18 p. (COM-71-00108)

No. 51 Papers on Operational Objective Analysis Schemes at the National Severe Storms Forecast Center. Rex L. Inman. November 1970. 91 p. (COM-71-00136)

No. 52 The Exploration of Certain Features of Tornado Dynamics Using a Laboratory Model. Neil B. Ward. November 1970. 22 p. (COM-71-00139)

No. 53 Rawinsonde Observation and Processing Techniques at the National Severe Storms Laboratory. Stanley L. Barnes, James H. Henderson and Robert J. Ketchum. April 1971. 245 p. (COM-71-00707)

No. 54 Model of Precipitation and Vertical Air Currents. Edwin Kessler and William C. Bumgarner. June 1971. 93 p. (COM-71-00911)

No. 55 The NSSL Surface Network and Observations of Hazardous Wind Gusts. Operations Staff. June 1971. 20 p. (COM-71-00910)

No. 56 Pilot Chaff Project at the National Severe Storms Laboratory. Edward A. Jessup. November 1971. 36 p. (COM-72-10106)

No. 57 Numerical Simulation of Convective Vortices. Robert P. Davies-Jones and Glenn T. Vickers. November 1971. 27 p. (COM-72-10269).

No. 58 The Thermal Structure of the Lowest Half Kilometer in Central Oklahoma: December 9, 1966-May 31, 1967. R. Craig Goff and Horace R. Hudson. July 1972. 53 p. (COM-72-11281)

No. 59 Cloud-to-Ground Lightning Versus Radar Reflectivity in Oklahoma Thunderstorms. Gilbert D. Kinzer. September 1972. 24 p. (COM-73-10050)

No. 60 Simulated Real Time Displays of Velocity Fields by Doppler Radar. L. D. Hennington and G. B. Walker. November 1972. 10 p. (COM-73-10515)

No. 61 Gravity Current Model Applied to Analysis of Squall-Line Gust Front. Jess Charba. November 1972. 58 p. (COM-73-10410)

No. 62 Mesoscale Objective Map Analysis Using Weighted Time-Series Observations. Stanley L. Barnes. March 1973. 60 p. (COM-73-10781)

No. 63 Observations of Severe Storms on 26 and 28 April 1971. Charles L. Vlcek. April 1973. 19 p. (COM-73-11200)

No. 64 Meteorological Radar Signal Intensity Estimation. Dale Sirmans and R. J. Doviak. September 1973. 80 p. (COM-73-11923/2AS)

No. 65 Radisonde Altitude Measurement Using Double Radiotheodolite Techniques. Stephan P. Nelson. September 1973. 20 p. (COM-73-11932/9AS)

No. 66 The Motion and Morphology of the Dryline. Joseph T. Schaefer. September 1973. 81 p. (COM-74-10043)

No. 67 Radar Rainfall Pattern Optimizing Technique. Edward A. Brandes. March 1974. 16 p. (COM-74-10906/AS)

No. 68 The NSSL/WKY-TV Tower Data Collection Program: April-July 1972. R. Craig Goff and W. David Zittel. May 1974. 45 p. (COM-74-11334/AS)

No. 69 Papers on Oklahoma Thunderstorms, April 29-30, 1970. Stanley L. Barnes, Editor. May 1974. 147 p. (COM-74-11474/AS)

No. 70 Life Cycle of Florida Key's Waterspouts. Joseph H. Golden. June 1974. 147 p. (COM-74-11477/AS)

No. 71 Interaction of Two Convective Scales Within a Severe Thunderstorm: A Case Study and Thunderstorm Wake Vortex Structure and Aerodynamic Origin. Leslie R. Lemon. June 1974. 43 p. (COM-74-11642/AS)

No. 72 Updraft Properties Deduced from Rawinsoundings. Robert P. Davies-Jones and James H. Henderson. October 1974. 117 p. (COM-75-10583/AS)

No. 73 Severe Rainstorm at Enid, Oklahoma - October 10, 1973. L. P. Merritt, K. E. Wilk, and M. L. Weible. November 1974. 50 p. (COM-75-10583/AS)

No. 74 Mesonetwork Array: Its Effect on Thunderstorm Flow Resolution. Stanley L. Barnes. October 1974. 16 p. (COM-75-10248/AS)

No. 75 Thunderstorm-Outflow Kinematics and Dynamics. R. Craig Goff. December 1975. 63 p. (PB-250808/AS)

No. 76 An Analysis of Weather Spectra Variance in a Tornadic Storm. Philippe Waldteufel. May 1976. 80 p. (PB-258456/AS)

No. 77 Normalized Indices of Destruction and Deaths by Tornadoes. Edwin Kessler and J. T. Lee. June 1976. 47 p. (PB-260923/AS)

No. 78 Objectives and Accomplishments of the NSSL 1975 Spring Program. K. Wilk, K. Gray, C. Clark, D. Sirmans, J. Dooley, J. Carter, and W. Bumgarner. July 1976. 47 p. (PB-263813/AS)

No. 79 Subsynoptic Scale Dynamics As Revealed By The Use Of Filtered Surface Data. Charles A. Doswell III. December 1976. 40 p. (PB-265433/AS)

No. 80 The Union City, Oklahoma Tornado of 24 May 1973. Rodger A. Brown, Editor. December 1976. 235 p. (PB-269443/AS)

No. 81 Mesocyclone Evolution and Tornado Generation Within the Harrah, Oklahoma Storm. Edward A. Brandes. May 1977 28 p. (PB-271675/AS)

No. 82 The Tornado: An Engineering-Oriented Perspective. Joseph E. Minor, James R. McDonald, and Kishor C. Mehta. December 1977. 196 p. (PB-281860/AS)

No. 83 Spring Program '76. R. L. Alberty, J. F. Weaver, D. Sirmans, J. T. Dooley, and B. Bumgarner. December 1977. 130 p. (PB280745/AS)

No. 84 Spring Program '77. P. S. Ray, J. Weaver, and NSSL Staff. December 1977. 173 p. (PB-284953/AS)

No. 85 A Dual-Doppler Variational Objective Analysis as Applied to Studies of Convective Storms. Conrad L. Ziegler. November 1978. 116 p. (PB-293581/AS)

No. 86 Final Report on the Joint Doppler Operational Project (JDOP) 1976-78. Prepared by Staff of the National Severe Storms Laboratory, Environmental Research Laboratories; Weather Radar Branch, Air Force Geophysics Laboratory; Equipment Development Laboratory, National Weather Service; and Air Weather Service, United States Air Force. March 1979. 84 p. (PB80-107188/AS)

No. 87 An Analysis of the Clear Air Planetary Boundary Layer Wind Synthesized from NSSL's Dual Doppler-Radar Data. Myron I. Berger and R. J. Doviak. June 1979. 55 p. (PB-300865/AS)

No. 88 The Relationship of the 300-mb Jet Stream to Tornado Occurrence. Carolyn M. Kloth and Robert P. Davies-Jones. July 1980. 62 p.

No. 89 A Study of Hail Production in a Supercell Storm Using a Doppler Derived Wind Field and a Numerical Hail Growth Model. Stephan P. Nelson. December 1980. 90 p.

☆ U. S. GOVERNMENT PRINTING OFFICE 1980 - 777-002/1235 Reg. 8